PRACA DOKTORSKA

Institute of Physical Chemistry
Polish Academy of Sciences
Kasprzaka 44/52
01-224 Warsaw, Poland

Langmuir monolayers of ferroelectric and bolaamphiphilic liquid crystals at the air–water interface

Ph.D. Thesis

(prepared within the International Ph.D. in Chemistry Studies at the Institute of Physical Chemistry of the Polish Academy of Sciences)

Patrycja Nitoń

Supervisor:
Prof. dr hab. Robert Hołyst

Warsaw, July 2012

Most importantly, I would like to sincerely thank my Supervisor, Prof. dr hab. Robert Hołyst, for his guidance, immense knowledge, enthusiasm and patience during my PhD studies.

Special thanks to dr Andrzej Żywociński for his scientific assistance, many useful advice and crucial contribution to this research , which makes him a backbone of this thesis.

Also I would like to thank my colleagues from Department of Soft Condensed Matter for their help and friendly atmosphere at work. In particular, thanks to Natalia Ziębacz for her great assistance over the last years.

I would like to thank my Family, especially my Husband, Mother and Parents-in-law for their help, support and understanding. Finally, I would like to thank Wojtuś for being an inexhaustible source of motivation.

Acknowledgments

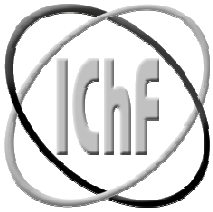

Institute of Physical Chemistry,

Polish Academy of Sciences

European Union within the European Regional Development Fund, through grant Innovative Economy (POIG.01.01.02-00-008/08)

Polish Ministry of Science and Higher Education under programme “Iuventus Plus”, project 2010-2011 (IP2010 028270)

Foundation for Polish Science Parent-Bridge programme under support for women conducting research projects during pregnancy, co-financed by the EU European Regional Development Fund (POMOST_C/43)

List of publications from PhD research

1. Patrycja Nitoń, Andrzej Żywociński, Jan Paczesny, Marcin Fiałkowski, Robert Hołyst, Benjamin Glettner, Robert Kieffer, Carsten Tschierske, Damian Pociecha and Ewa Górecka, "Aggregation and Layering Transitions in Thin Films of X-, T-, and Anchor-Shaped Bolaamphiphiles at the Air–Water Interface", *Chemistry – A European Journal*, **2011**, *17*, 5861-5873.
2. Patrycja Nitoń, Andrzej Żywociński, Robert Hołyst, Robert Kieffer, Carsten Tschierske, Jan Paczesny, Damian Pociecha and Ewa Górecka, "Reversible aggregation of X-Shaped bolaamphiphiles with partially fluorinated lateral chains at the air/water interface" *Chem. Commun*., **2010**, *46*, 1896 – 1898.
3. Patrycja Milczarczyk – Piwowarczyk, Andrzej Żywociński, Krzysztof Noworyta and Robert Hołyst, "Collective rotations of ferroelectric liquid crystals at the air/water interface", *Langmuir*, **2008**, *24*, 12354–12363.

List of other publications

4. Jan Paczesny, Patrycja Nitoń, Andrzej Żywociński, Krzysztof Sozański, Robert Hołyst, Marcin Fiałkowski, Robert Kieffer, Benjamin Glettner, Carsten Tschierske, Damian Pociecha and Ewa Górecka, "Stable, ordered multilayers of partially fluorinated bolaamphiphiles at the air–water interface", *Soft Matter*, **2012**, DOI: 10.1039/C2SM00022A
5. Hongguang Li, Xia Xin, Tomasz Kalwarczyk, Ewelina Kalwarczyk, Patrycja Nitoń, Robert Hołyst and Jingcheng Hao, "Reverse Vesicles from a Salt-Free Catanionic Surfactant System: A Confocal Fluorescence Microscopy Study" *Langmuir*, **2010**, *26*, 15210-15218.

List of publications in preparation from PhD research

6. Patrycja Nitoń, Andrzej Żywociński, Marcin Fiałkowski and Robert Hołyst, "Extremely slow rotations of chiral liquid crystalline monolayer at the air/water interface".
7. Patrycja Nitoń, Andrzej Żywociński, Marcin Fiałkowski and Robert Hołyst, "Thermodynamics of phase transition in Langmuir monolayer of ferroelectric liquid crystal"
8. Patrycja Nitoń, Andrzej Żywociński, Jan Paczesny, Marcin Fiałkowski, Robert Hołyst, Benjamin Glettner, Carsten Tschierske, "Comparative studies of fluorinated and hydrogenated molecules of different shape in monolayers at the air/water interface".

Contents

Abbreviations

BAM	Brewster angle microscopy
Col_{hex}	columnar hexagonal phase
Col_{ob}	columnar oblique phase
Col_{rec}	columnar rectangular phase
Col_{squ}	columnar square phase
Cr	crystal phase
FLC	ferroelectric liquid crystal
G	gas phase
Iso	isotropic phase
LC	liquid condensed phase
LE	liquid expanded phase
LB	Langmuir-Blodgett technique
LS	Langmuir-Schaefer technique
MLM	monolayer lipid membrane
N	nematic phase
N*	chiral nematic (cholesteric) phase
N_D	nematic discotic phase
S	solid phase
SAM	self-assembled monolayer
SmA	smectic A phase
SmB	smectic B phase
SmC	smectic C phase
SmC*	chiral smectic C phase
TR	transfer ratio

XRR X-ray reflectivity technique

Symbols

A area per molecule, nm^2

A_0 area per molecule obtained by extrapolating the slope of isotherm to zero pressure, nm^2

A_1, A_2 area per molecule at the beginning and at the end of the plateau, respectively, nm^2

A_c area per molecule at which the collapse of the monolayer occurs, nm^2

C_s two-dimensional compressibility

γ surface tension of pure water, mN/m

γ^* surface tension of water covered with monolayer, mN/m

γ_1, γ_s rotational viscosity and surface viscosity, respectively, Pa s

ε_0 electric permittivity of vacuum, F/m

ε_r electric permittivity of the monolayer

κ compressional modulus, m/mN

μ electric dipole moment of molecule in Langmuir monolayer, D

$\mu_\perp$ vertical component of dipole moment of molecule in Langmuir monolayer, D

p_{sat} pressure of saturated water vapour, Pa

π surface pressure, mN/m

π_c surface pressure of the collapse of the monolayer, mN/m

T_c experimentally established temperature of phase transition to solid state, K

T_g hypothetic glass transition, K

ΔH enthalpy of water vaporization, J/mol

ΔV surface potential, mV

1. Introduction

For over a century, Langmuir films have served as excellent two-dimensional model systems for studying the conformation and ordering of amphiphilic molecules at the air-water interface. There are many reasons to study Langmuir monolayers. Langmuir monolayers are used for studies of chemical and biological reactions in two dimensions. They are excellent model systems for membrane biophysics, since a biological membrane can be considered as two weakly coupled monolayars. Formation of monomolecular films insoluble in water provide much useful information on molecular scale which is useful for understanding many industrial and biological phenomena in chemical, pharmaceutical, medical and food science applications. For instance information obtained from lipid and biopolymer monolayer studies has been useful in determining the forces that are known to stabilize emulsions and biological cell membranes.[1] Langmuir monolayers also are necessary for the fabrication of Langmuir-Blodgett films, which are multilayers transferred from the liquid surface to a solid support.[2] Investigations of Langmuir films have provided a bridge between physics, chemistry, biology and electronics. With Wilhelmy plate technique, Brewster angle microscopy (BAM), and surface potential measurements, the interfacial phase and rheological behavior of Langmuir films can be investigated. In my dissertation, these techniques are employed to examine Langmuir films of ferroelectric and bolaamphiphilic liquid crystals.

In the first part of my experiment work I present the results of the monolayers behavior of four ferroelectric liquid crystals spread on water surface. The chiral molecules with tilted orientation to the surface create textures of circular stripe. These patterns arise from collective rotation of molecules driven by water evaporation through the monolayer. The rate of rotation was examined under variety of water temperatures. As it is shown, the rotation frequency depends on subphase temperature and at low temperature, when the

driving force for rotation is reduced, the speed of collective rotation decreases. Typical time of rotation of a single molecule is in the range 10^{-12} – 10^{-9} s.[3] *I observed in Langmuir monolayer the time of rotation up to 500 seconds, fourteen orders of magnitude slower than the one for a single molecule*.

In the second part of my work I present the studies of 11 compounds from the group of specific surfactants known as bolaamphiphiles. The molecules of different shape (X-, T-, and anchor shaped) were studied. Some of these compounds have a fluorinated lateral chains and some are non-fluorinated. The research shows that the bolaamphiphiles create on water surface stable and well organized Langmuir monolayers and multilayers. *The most interesting feature of the compounds is that partially fluorinated bolaamphiphiles exhibit an unusual reversibility and reproducibility of Langmuir isotherms in spite of the compression to complete collapse of the film.*

2. Theoretical part of my thesis

This chapter will be concerned with the theoretical background of the Langmuir technique, substances used for the formation of insoluble monolayers such as ferroelectric and bolaamphiphilic liquid crystals, and a description of experimental tools that have been developed for characterising Langmuir monolayers.

2.1. Liquid crystals

Until the late 1800s, scientists described physical matter as existing in three states (solid, liquid, and gas). The first experimental observations of liquid crystalline state date from the 19th century.[4] At that time, biologists started using the polarizing microscope for studying vegetable and animal tissues. In 1857 the ophthalmologist Mettenheimer, by placing myelin in contact with water observed the growth of tubular objects at the myeline-

water interface. Today we know that these tubes, now called myelin figures, were created by phospholipids arranged in bilayers. These bilayers can take the form of cylinders, which are the main elements of the myeline textures observed by Mettenheimer.[5]

Liquid crystals (LCs) are a state of matter that is intermediate between the isotropic liquids and crystalline solid. From the Greek *mésos,* which means "intermediate", the liquid crystalline phases are called *mesophases*. For the first time the mesophases were observed in aqueous solutions of amphiphilic molecules. They are termed lyotropic liquid crystals, in contrast to thermotropic liquid crystals which do not contain water. For the first time the thermotropic liquid crystals were observed by the biologists Planer in 1861 and Reinitzer in 1888. During examination of cholesterol, a substance extracted from plants, they noticed its opaqueness and the iridescent colours exhibited upon melting from the crystalline phase or upon cooling from the isotropic liquid. In the letter sent to Otto Lehman, Reinitzer presented in details his surprising observations on the properties of cholesteryl esters:

" The substance (cholesteryl benzoate) has two melting points, if one may say so. At about 145.5°C it melts, forming a turbid, but completely fluid liquid, that suddenly becomes completely clear at about 178.5°C." [5]

After systematic study of cholesteryl benzoate, and related compounds which exhibited the double-melting phenomenon, in 1889 Otto Lehmann published a paper entitled "Über fliessende Kristalle" thus coining the name "liquid crystals". What surprised Lehmann the analyzed substances, although fluids, were birefringent, one of the features of solid crystals. The scientists of the 19th and 20th centuries had observed new mesophases, but without understanding that they were dealing with new states of matter, different from the liquid and solid state. The liquid crystal physics began in the early 1920s with the famous French crystallographer Georges Friedel. He was the first to suggest that liquid crystals are states of matter in their own right, intermediates between isotropic liquids and crystals.

Finally, Friedel named, from the Greek language, the new states of matter: nematic, cholesteric and smectic. Since that time liquid crystal physics was inactive by almost half a century. In the early 1970s, under the influence of P.-G. de Gennes, the liquid crystal physics entered a stage of expansion that continues to the present day. [5,6]

Following the idea proposed originally by Friedel, liquid crystals are a state of matter whose molecular structure is intermediate between the crystals and ordinary liquids. The states of matter are different from each other because the molecules in each state create different amounts of order. In the solid state the molecules occupy a certain positions creating molecular crystal. The molecules occupying specific positions are also oriented in a specific way, so we say that the solid state possesses *positional* and *orientational order*. When the temperature is changed and the phase transition from solid to isotropic liquid takes place, both types of order are lost completely. But when a solid melts to a liquid-crystalline phase, the positional order may be lost although some of the orientational order remains. Figure 1 illustrates the order present in the crystalline solid, liquid crystal, and liquid phase.[7]

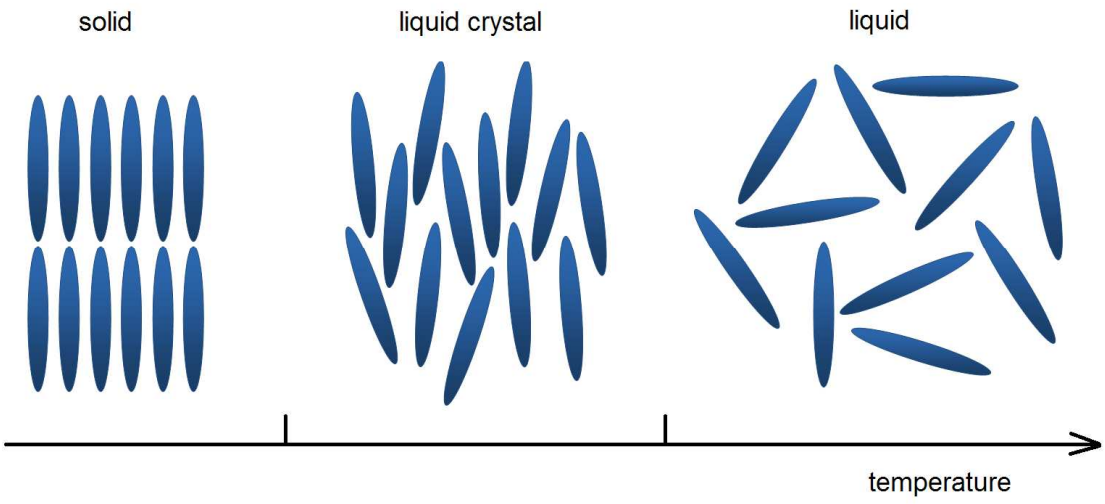

Figure 1 Schematic illustration of the solid, liquid crystal, and liquid phases. The slender "sticks" represent molecules.

An essential requirement for liquid crystalline phase to occur is that the molecule must be highly geometrically anisotropic, usually long and relatively narrow. The most common liquid crystal phases are formed by rod – like molecules, but also disc – like and banana – like molecules form liquid crystal phases. These shapes of molecules are presented in Figure 2.

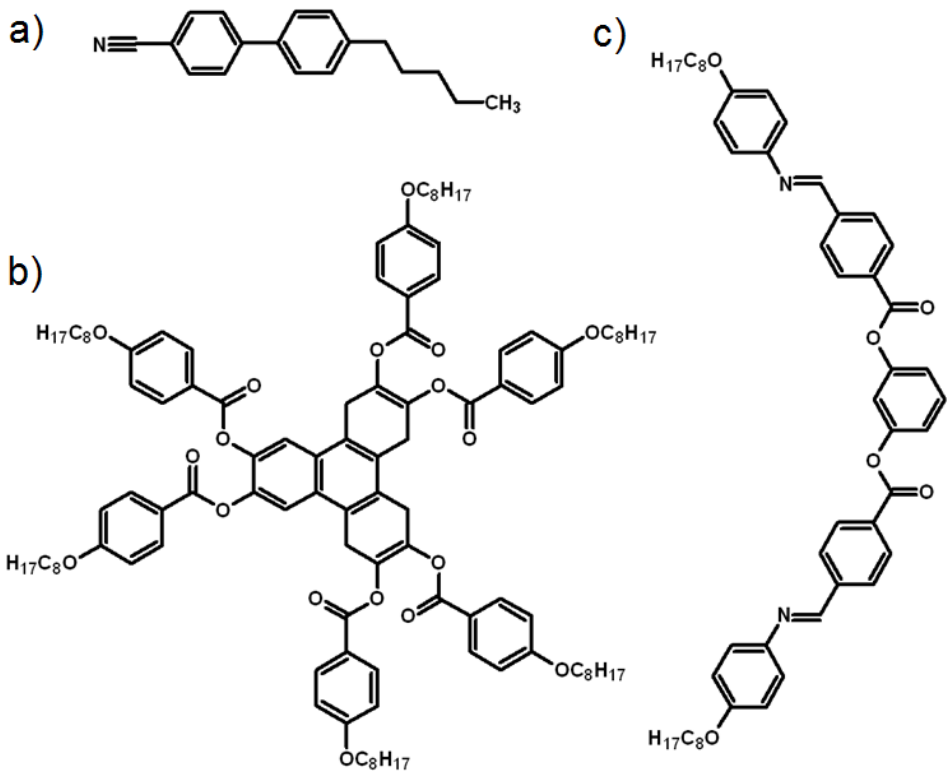

Figure 2 Different shapes of liquid crystal molecules: a) typical rod – like molecule, b) discotic liquid crystal molecule, c) banana shape molecule

The system may pass through one or more intermediate states before it is transformed into the isotropic liquid. Transitions to these mesophases may be caused by temperature change (thermotropic liquid crystals) or by the change of concentration (lyotropic liquid crystals).[6]

2.1.1. Thermotropic liquid crystals

Thermotropic liquid crystals are those in which the order is determined or changed by temperature (mesophases occur in a certain temperature range). One of the most common thermotropic liquid crystal phases is the nematic (N). The word *nematic* comes from the Greek *nema*, which means "thread". This term originates from the “linear discontinuities, winding like threads” observed by Friedel.5 The namatic phase has a high degree of long range orientational order of the molecules, but no long range translational order. The molecules in nematic phase are spontaneously oriented with their long axes approximately parallel but their centre of mass positions are randomly distributed as in a liquid. The direction of preferred orientation in a liquid crystal is called *director* $(\hat{n})$. Alignment of rod – like molecules in a nematic phase additionally with director which is represented by an arrow are presented in Figure 3a. This Figure also schematically presents alignment of molecules in the next mesophase, cholesteric phase (Figure 3b).

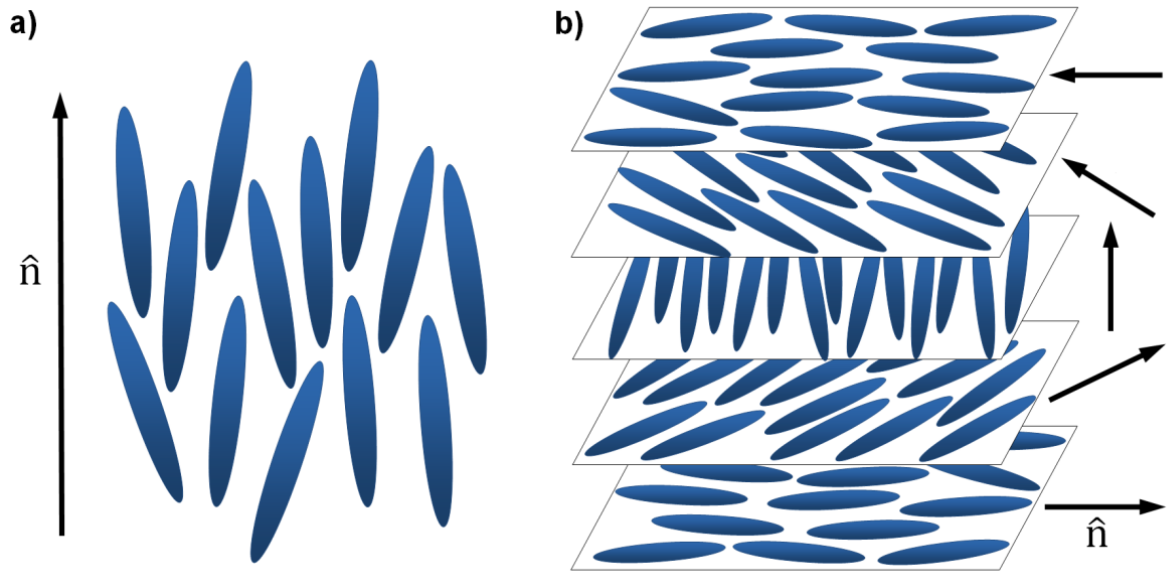

Figure 3 Alignment of rod – like molecules in a) nematic and b) cholesteric phase.

The cholesteric phase is also a nematic type of liquid crystal except that this phase is composed of chiral molecules. Thus, this phase is called the chiral nematic liquid phase (N*). In the cholesteric phase, the director is not fixed in space as in nematic phase, but it rotates throughout the sample (as it is presented in Figure 3b). A substance may possess either the nematic or cholesteric liquid crystal phase, but not both. If a substance is composed of two optically active isomers (enantiomers), the cholesteric phase exists only when there is different proportion of each enantiomer. A mixture of equal parts of an optically active isomer is termed racemic, and do not create a cholesteric but proper nematic phase.[8]

The third liquid crystal phase is called the smectic, from the Greek word for soap. There are many different smectic phases, but all of them form well-defined layers. In the smectic A phase (SmA), the molecules are oriented along the layer normal, the director is perpendicular to the layers . However, in the smectic C phase (SmC) the molecules are tilted away from the layer normal. Figure 4 illustrates arrangement of the molecules in these two types of smectic liquid crystal phases.7

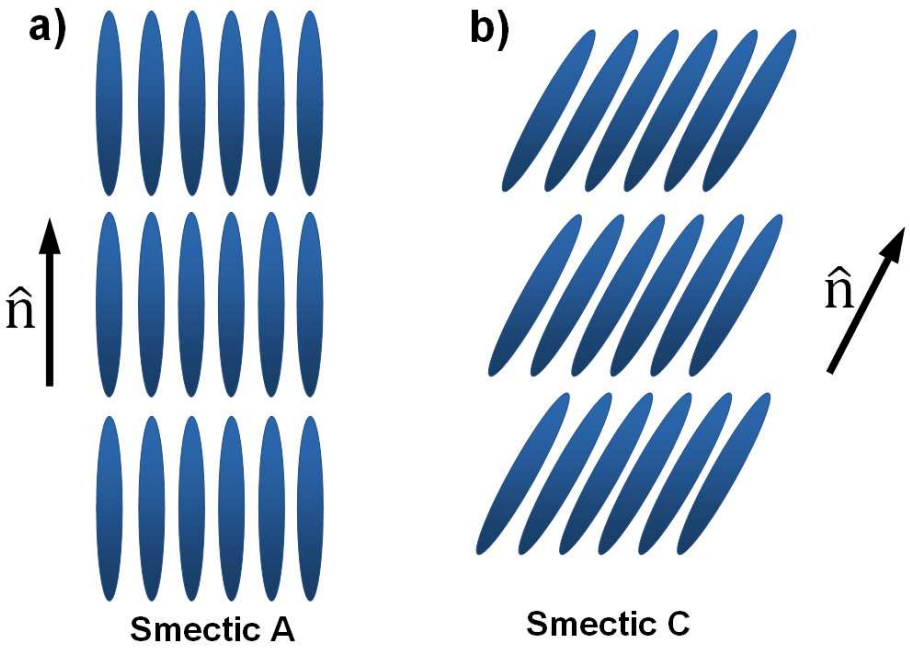

Figure 4 The arrangement of the molecules in a) smectic A phase and b) smectic C phase.

In smectic A (SmA) the molecules are upright in each layer but their centres irregularly spaced in a liquid – like fashion. Smectic B (SmB) differs from A in that the molecular centres in each layer are hexagonal close packed. There are many different smectic phases, all characterized by different types and degrees of positional and orientational order.

Above – mentioned liquid crystal phases are formed by rod – like molecules. However, disc – like molecules also form liquid crystal phases in which the axis perpendicular to the plane of molecule tends to orient along a specific direction. These mesophases are called discotic liquid phases. Disc – like molecules exhibit two distinct classes of phases, the columnar and the discotic nematic phases.[9] In discotic nematic phase (N_D) there is only orientational order but no positional order between the molecules. Such a phase is shown in Figure 5a, where the molecules have been drawn as flat discs.

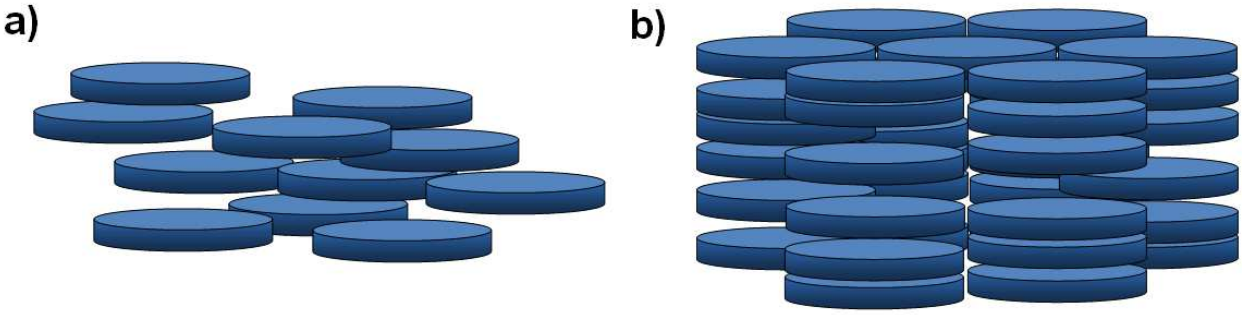

Figure 5 Discotic liquid crystal phases: a) nematic discotic (N_D) and b) columnar hexagonal (Col_{hex}).

In the columnar phases the columns are parallel and form a two – dimensional lattice, that can be hexagonal (Col_{hex}), rectangular (Col_{rec}), oblique (Col_{ob}) or square (Col_{squ}).[5,10-12] Along the axes of the columns long – range order or disorder of the molecules can exist.[9] Figure 5b shows hexagonal columnar phase (with disordered stacking in a column). Some examples of different two-dimensional ordered lattices found in columnar mesophases are shown in Figure 6.

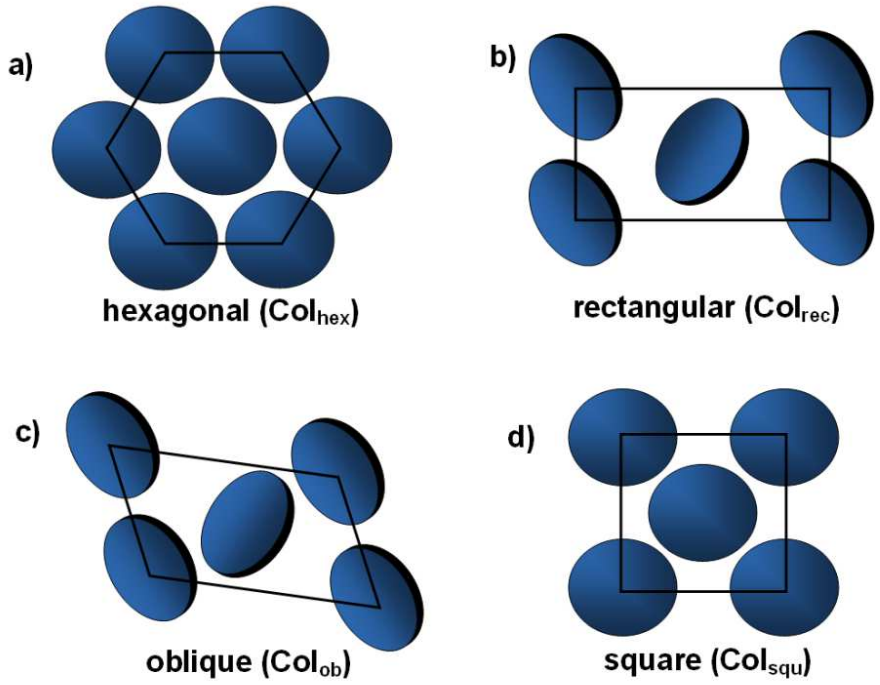

Figure 6 Structures of columnar mesophases. Two-dimensional lattice symmetries: a)hexagonal columnar phase (Col_{hex}) b) rectangular (Col_{rec}), c) oblique (Col_{ob}), d) square (Col_{squ}).

2.1.2. Phenomenon of ferroelectricity and ferroelectric mesophase

Ferroelectricity is defined as a property of some materials to exhibit a permanent electric polarization. The ferroelectric crystals posses a spontaneously polarized dipole domains in zero applied electric field. Under the influence of an external electric field these electric dipole domains arrange in common direction and the material demonstrate a macroscopic polarization. If there is no external electric field ferroelectric materials show ferroelectric behavior only below a critical temperature ,called the Curie temperature T_C. Below temperature T_C electric dipoles align themselves and the ferroelectric crystal undergoes a phase transition from a nonpolar state into a polar state.[13,14] Ferroelectric materials have the property, that the direction of spontaneous electric polarization can be reversed by the application of an external electric field, yielding a hysteresis loop.[15]

Ferroelectricity was discovered by Joseph Valasek in 1920 in Rochelle salt. After this discovery the ferroelectricity was considered as a property of solid crystals. However, in

1974 a physicist Robert Meyer theoretically anticipated that certain liquid crystal phases are ferroelectric.[16-19] He utilized the symmetry arguments to predict that tilted, layered crystal phases of chiral molecules are ferroelectric. Then he asked his organic chemists friends, Lionel Liebert, Leszek Strzelecki and Patrick Keller, to synthesize a compound that (1) might posses a smectic C phase, (2) might be chiral, and (3) might posses a permanent electric dipole moment. The result of their work was the molecule known by the acronym DOBAMBC, shown in Figure 7.

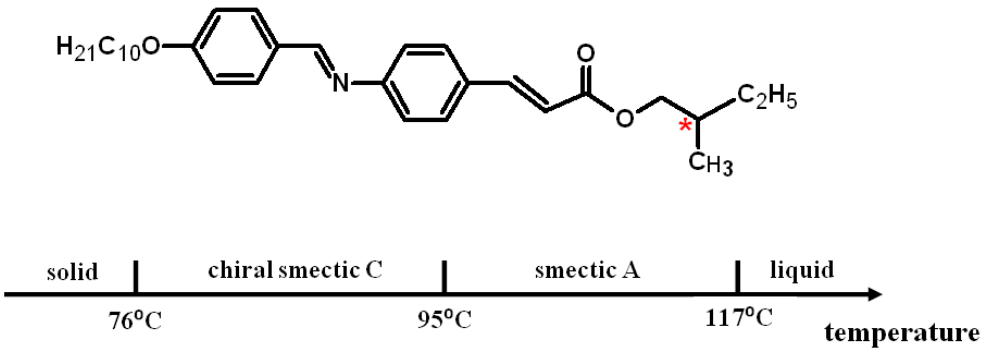

Figure 7 First ferroelectric liquid crystal.

A chiral molecule is a molecule that is not superposable on its mirror image. Human hands, for example, are chiral because they are not superposable on their mirror image. The feature that is most often the cause of chirality in molecules is the presence of an asymmetric carbon atom. An asymmetric carbon atom is a carbon atom that is attached to four different types of atom or four different groups of atoms. The DOBAMBC molecule contains an asymmetric carbon atom near one end of the molecule (denoted by an asterisk in Figure 7) rendering it chiral, and C=O group provides a transverse permanent dipole moment. Meyer, Liebert, Strzelecki and Keller observed that below 95°C the phase sequence of chiral DOBAMBC has a chiral smectic C phase (SmC*) and this phase exhibits very strong rotatory power. The molecular structure of the SmC* phase is presented in Figure 8.

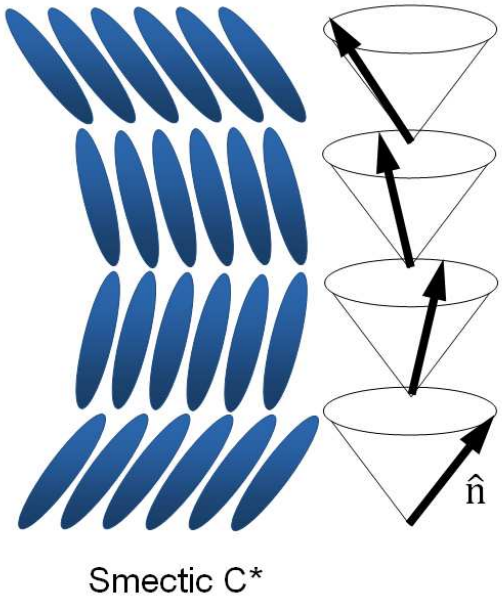

Figure 8 Structure of the chiral smectic C phase (SmC*).

The structure of the SmC* phase is very similar to the usual SmC phase, except that the azimuthal angle φ continuously rotates, the director precesses from layer to layer. In the chiral smectic C phase microscopic electric dipoles formed a spontaneous electric polarization, which lies in the smectic planes, what causes that the SmC* phase is ferroelectric. Ferroelectric liquid crystals (FLCs) can be extremely useful in high-speed, high-resolution electrooptic devices, such as flat panel displays.[20]

2.2. Langmuir technique

2.2.1. Historical background

The first experience with oil films on water took place in ancient times when the calming effect of oil on a rough sea was observed by sailors. But the first scientific investigation of this effect were reported in 1774 by Benjamin Franklin. He described the famous experiment on the pond on Clapham Common, in which he noticed that the teaspoonful of oil pored on water surface produced an instant calm over a space several yards square making the pond smooth as a looking glass.[21] At the end of the nineteenth

century Agnes Pockels described a method for manipulating oil film on water using barriers laid across the top of a trough. Then, Lord Rayleigh quantitatively measured the lowering of the water surface tension due to spreading of olive oil and proposed that the film was only a single molecule in thickness. In 1917 Irving Langmuir put forward evidence for the monomolecular nature of the film. He concluded that not only the films were indeed one molecule thick, but that the molecules were oriented at the water surface with polar group immersed in the water and the long nonpolar chain directed vertically up from the surface.[22] For the measurements he devised the surface balance with which his name is associated.[23] In 1935 Katherine Blodgett showed how to build up multilayers on solid plates by the successive deposition of monomolecular layers.[24] These built-up films are now referred to as Langmuir-Blodgett films.

2.2.2. Substances for insoluble monolayers formation

A Langmuir monolayer is a layer consisting of amphiphilic molecules. Amphiphilic is an attribute which means "loving both" or "having a affinity for both", thus amphiphilic molecules are composed of hydrophilic (water-loving) and hydrophobic (water-hating) parts.[25] The hydrophobic group is typically a large hydrocarbon moiety, such as a long chain of the form $CH_3(CH_2)_n$, and is commonly referred to as the "tail". The hydrophilic part ("head") can be polar or ionic. The examples of such groups are: $-CH_2OH$, $-COOH$, $-CN$, $-CONH_2$. In general, amphiphiles used for monolayer fabrication are long chain fatty acids, phospholipids and alcohols, of which *n*-octadecanoic acid (stearic acid) is the most common one for monolayer studies.

The molecules in Langmuir monolayers are trapped at the interface between two dissimilar phases, either liquid-gas or liquid-liquid, creating a layer of the one–molecule thickness. For air-water interface molecules are arranged in such a way that polar head

group is immersed in the water and the hydrophobic tail points towards the air, as shown in Figure 9.

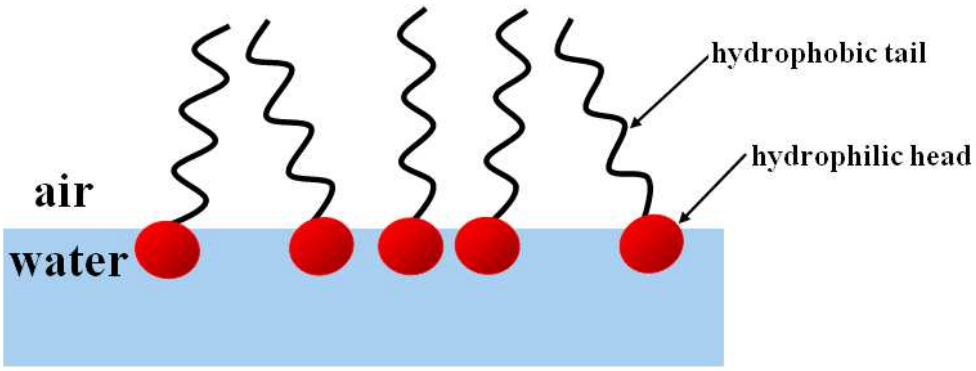

Figure 9 Amphiphilic molecules arranged in Langmuir monolayer at the air-water interface.

It is known that for a monolayer to be obtained at the air-water interface, the molecule should possess at least 12 carbon atoms. Otherwise, solubility in the aqueous subphase causes monolayer loss with a decrease in monolayer area.[26] The solubility of an amphiphilic molecule in water depends on the balance between the alkyl chain length and the strength of its hydrophilic head. For example, while hexadecanoic acid [CH_3–$(CH_2)_{14}$–COOH] forms stable Langmuir film hexadecyltrimethylammonium chloride [CH_3–$(CH_2)_{15}$–$N(CH_3)_3^+Cl^-$] is too soluble in water to allow the formation of a monolayer.[27] The effectiveness of functional groups attached to the hydrocarbon chains in film formation is summarised in the Table 1.

In addition to amphiphilic molecules, bolaamphiphilic molecules also form a Langmuir monolayer. These organic compounds contain hydrophilic groups at both ends of hydrophobic part (see Figure 10). The word *bola* comes from the Spanish and means throwing weapon made of weights at the ends of interconnected chains, designed to capture animals by entangling their legs.[28,29] The original interest in bolaform molecules stems from the bipolar ether lipids of archaebacterial membranes. These natural bolaamphiphiles can form monolayer lipid membranes (MLMs) which are stable at extreme conditions, such as

high temperature. Synthetic bolaamphiphiles are used to reproduce the unusual architecture of monolayered membranes found in archaebacteria. However, they are compared of different building blocks than lipids in archaebacteria.[30-32]

Table 1 The effect of different functional groups on film formation of C_{16}-componds (adapted from reference 27)

Very Weak (no film)	Weak (unstable film)	Strong (stable film with C_{16} chain)	Very Strong (C_{16} compounds dissolve)
Hydrocarbon	$-CH_2OCH_3$	$-CH_2OH$	$-SO_3^-$
$-CH_2I$	$-C_6H_4OCH_3$	$-COOH$	$-OSO_3^-$
$-CH_2Br$	$-COOCH_3$	$-CN$	$-C_6H_4SO_4^-$
$-CH_2Cl$		$-CONH_2$	$-NR_4^+$
$-NO_2$		$-CH=NOH$	
		$-C_6H_4OH$	
		$-CH_2COCH_3$	
		$-NHCONH_2$	
		$-NHCOCH_3$	

Interfacial behaviour of bolaamphiphiles with unusual head-group topology is different from the typical amphiphiles. Generally, three kinds of configurations of the Langmuir monolayers of bolaamphiphile at the air-water interface can be expected, i.e. stretched, flat and U-shaped configurations.[33] In flat configuration, the molecules lie horizontally on the water surface. This situation occurs when there is no compression of the surface layer. When a monolayer is compressed, both head groups remain in contact with water and the single hydrocarbon chain assumes a “U” form or “wicket” conformation.[29, 34-36] In stretched configuration only one polar head group is in contact with water, while the other one extrudes out from water surface. The possible conformations of bolaamphiphiles on aqueous surfaces are shown in Figure 10.

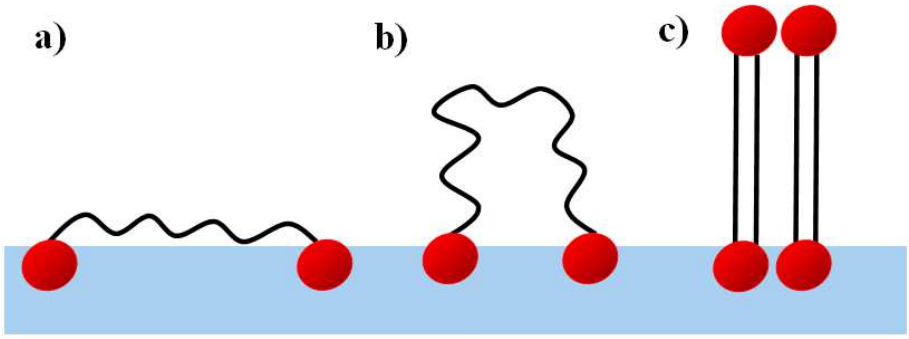

Figure 10 Schematic illustration of the possible conformations of bolaamphiphilic molecules at the air-water interface. A) horizontal conformation of single-chain bolaamphiphile in gas phase b) "U-shaped conformation of single-chain bolaamphiphile at high surface pressure c) vertical (stretched) conformation of rigid-core bolaamphiphile at high surface pressure.

2.2.3. The subphase, film spreading, trough and barriers

The Langmuir films are produced and characterized in an apparatus called the Langmuir trough or the Langmuir film balance.[23] Figure 11 presents a schematic description of the typical Langmuir trough.

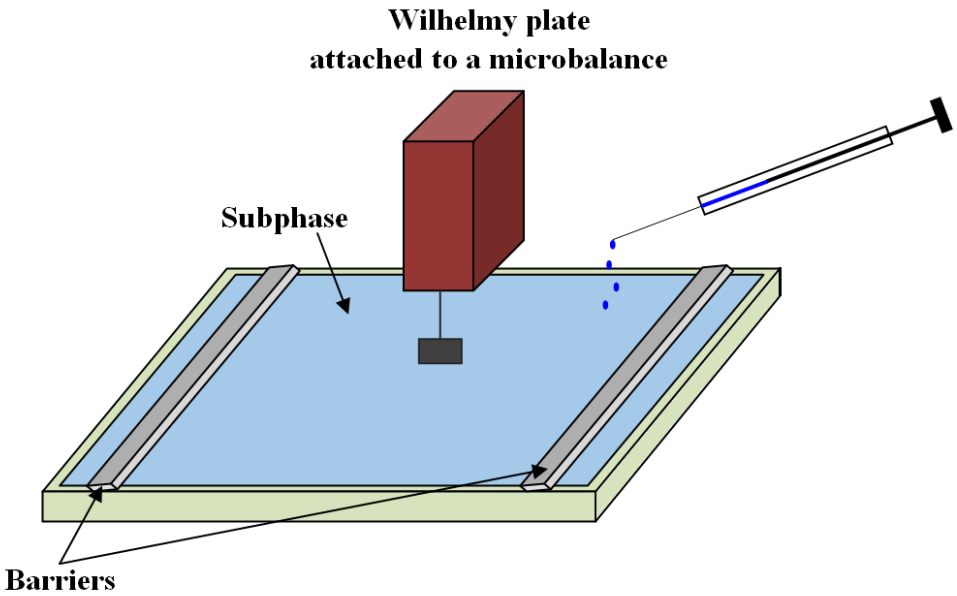

Figure 11 Schematic representation of of the typical Langmuir trough.

The Langmuir trough consists of trough made of hydrophobic material like Teflon (polytetrafluoroethylene), two movable barriers and Wilhelmy plate attached to a very

sensitive electrobalance. The trough is filled to the brim with subphase. The most commonly used subphase for the study of monomolecular films is ultrapure water, because its surface tension value is high and equal to 72.8 mN/m at 25°C. The general rule is that the subphase has to have high surface tension. Therefore, other materials such as mercury and glycerol, also can be used.[37,38]

The monolayer is formed on the surface of the subphase by dissolving the amphiphilic compounds in a suitable solvent. The solvent must be volatile and immiscible with the subphase, for example chloroform is usually placed on the water surface. First small droplets of solution fall from the syringe onto the interface. After evaporation of the solvent, the amphiphilic molecules form a monolayer at the air-water interface. The amount of the amphiphile is calculated so that resulting film is a monomolecular layer. Sweeping barriers over the water surface causes the molecules to come closer together and to form compressed and ordered monolayer, as shown in Figure 12.

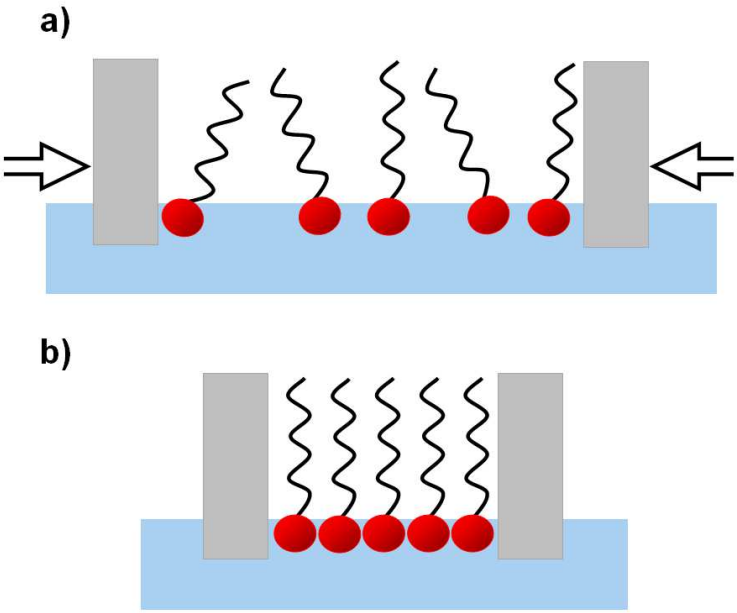

Figure 12 Expanded and compressed monolayers at the air-water interface.

During the motion of the barriers and compression of the molecules the area per molecule and surface pressure are recorded. The surface pressure π is the difference between

the surface tension of pure water γ, and that of the water covered with a monolayer γ^*: $\pi = \gamma - \gamma^*$.[39] The main method of the surface pressure measurement is the Wilhelmy plate method. The Wilhelmy plate is a thin plate, usually made of platinum or filter paper, which when suspended at air-water interface is pulled into the bulk of subphase. In this method such forces acting on the plate as gravity, surface tension and buoyancy due to displacement of water are measured using a microbalance. If the plate is completely wetted by water and has the width l and the thickness t then the net force downwards F is described by the equation: $F = 2(l + t)\pi$. Therefore, the surface pressure is given by: $\pi = F/perimeter$, where surface tension is in mN/m.

2.3. Characterization of Langmuir monolayers

This chapter contains the description of experimental methods that were used in my work to obtain information on molecular ordering and structures of the monolayer phases. To examine Langmuir films I used the surface pressure and surface potential measurement simultaneously with Brewster angle microscopy (BAM). They are described in the following paragraphs.

2.3.1. Surface pressure measurement

One of the most important indicator of the monolayer formation is the plot of surface pressure as a function of the area of water surface per molecule. This is carried out at constant temperature and therefore it is known as a surface pressure-area per molecule isotherm (π-A). An example of the simplest π-A isotherm obtained for stearic acid $C_{17}H_{35}COOH$ is shown in Figure 13.

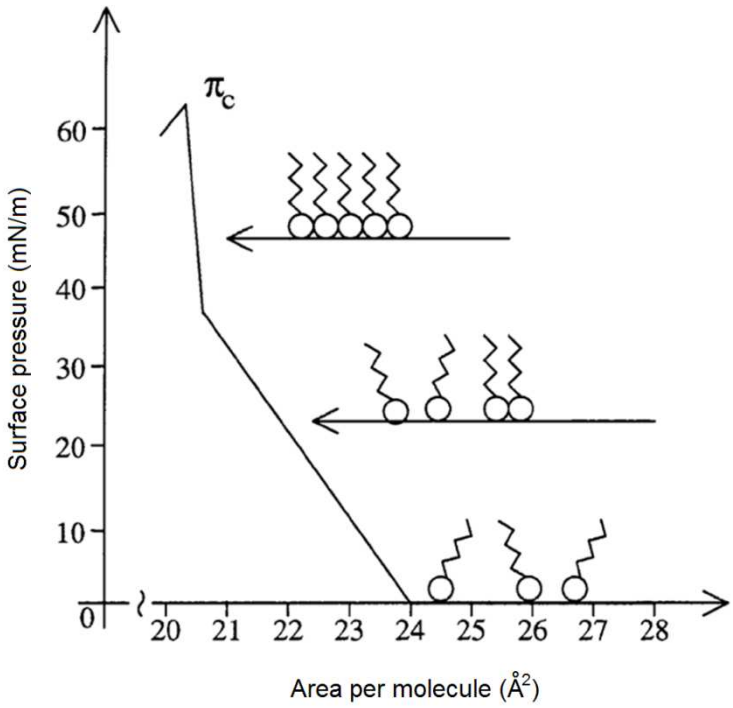

Figure 13 A scheme of the surface pressure-area per molecule isotherm of stearic acid on pure water.

At very large *A* values, when the available area per molecule is much larger than the cross-sectional area of an isolated molecule, the molecules are far apart and do not interact with each other. At this stage the surface pressure is very low (<1 mN/m) and the monolayer behaves as a two-dimensional gas (G). For the ideal two-dimensional gas the following equation should be satisfied:

$$\pi A = kT \qquad (1)$$

where *A* is the area per molecule, π is the surface pressure, *T* is the absolute temperature and *k* is the Boltzmann constant.

As the barrier moves, the intermolecular distance decreases and the molecules start to interact. Then the surface pressure increases and the phase transition is observed. The singularities, plateaus, kinks, etc, in the isotherm are signatures of different phase transitions occurring in the monolayer. This first phase transition is assigned to a transition from the gas to the liquid state. Further compression leads to an increase in π and to second phase

transition, from the liquid to the solid state. The zero-pressure molecular area (A_0) obtained by extrapolating the slope of the second linear portion of the isotherm is ~20 Å^2. Such an area corresponds to the cross-sectional area of a hydrocarbon chain, suggesting that at this stage monolayer consists of close packed vertically oriented molecules. If pressure is further applied by the compression of barriers the monolayer collapse occurs and a sharp decrease in the pressure is observed. The collapse pressure π_c at which the film loses its monomolecular form and disordered aggregates are formed depends on experimental conditions, i.e. the temperature and the rate at which the film is compressed.

For other substances, phases such as liquid expanded (LE) or liquid condensed (LC) can occur. An example is the naturally occurring phospholipid dimyristoylphosphatidylethanolamine (L-α-DMPE). Its surface isotherm is depicted in Figure 14.[40] At a very low surface pressure the coexistence of gas (G) and liquid expanded (LE) phase takes place. In practice, at very dilute monolayer states, above 2 nm^2 per molecule the homogeneous gas phase is not observed. The equation $\pi A = kT$ shows that reduction in area per molecule to A<4 nm^2 should result in a measurable increase in surface pressure up to 1 mN/m. Usually experiments starts at the area per molecule A=2 nm^2 and the surface pressure is close to zero. It fallows that for large area per molecule we have a coexistence of G and LE phase (region LE/G in Figure 14). In LE phase the tilted molecules are in contact although lacking long range correlations. On further compression the isotherm exhibits a plateau at which a phase transition from the LE phase to the liquid condensed (LC) phase takes place. The LC phase of L-α-DMPE is characterized by a short-range translational order of the headgroup positions. Simultaneously, the alkyl chains of the hydrophobic molecular part show a long-range order in their orientation.[40]

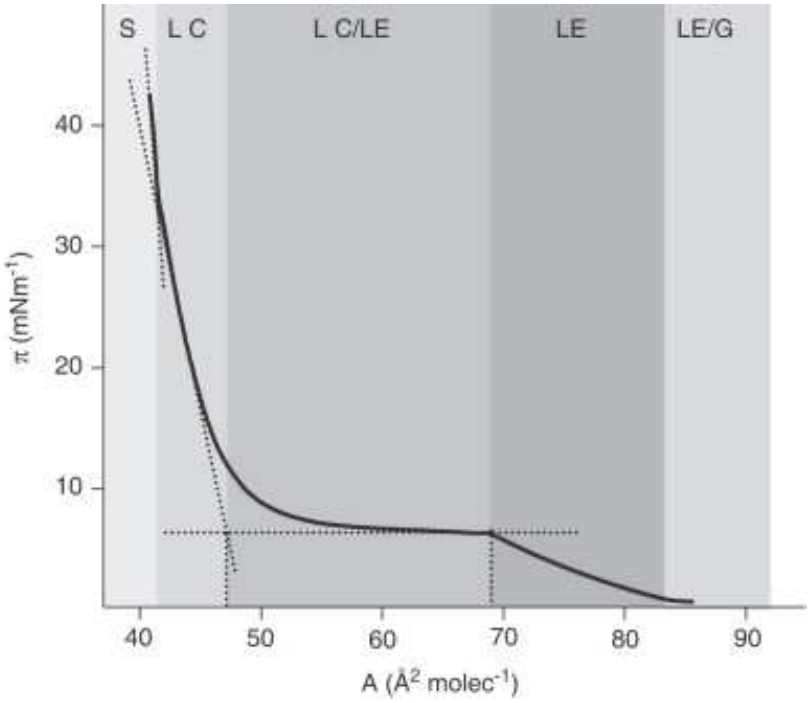

Figure 14 Isotherm of Langmuir monolayer of the phospholipid L-α-DMPE at 20°C (adapted from reference 40).

An insoluble monolayers can be characterized by two-dimensional compressibility (C_s). This parameter corresponds to the slope of the compression isotherm and can be calculated by the following equation:[23,41]

$$C_S = C_s = -\frac{1}{A}\left(\frac{\partial A}{\partial \pi}\right)_T \qquad (2)$$

The reciprocal quantity of C_s, denoted as compressional modulus is also often used to describe monolayer properties:[23,42]

$$\kappa = -A\left(\frac{\partial \pi}{\partial A}\right)_T \qquad (3)$$

According to the terminology for the monolayer phases their compressibility is different in each phase from the sequence G>LE>LC>S. Table 2 presents the values of the compressional modulus for the different phases.[43]

Table 2 The approximate values of the compressional modulus, κ, for different monolayer phases.[43]

Monolayer phase	The approximate values of the compressional modulus, κ, m/mN
Gas (G)	$0{,}04 \geq \kappa$
Liquid expanded (LE)	$0{,}02 \leq \kappa \leq 0{,}07$
Liquid condensed (LC)	$0{,}005 \leq \kappa \leq 0{,}01$
Solid (S)	$0{,}0005 \leq \kappa \leq 0{,}001$

2.3.2. Surface electrostatic potential measurement

Surface electrostatic potential (for short surface potential) measurements are used as an additional source of information on the arrangement of molecules on the water surface. The monolayer surface potential ΔV is defined as a difference between the potential of a clean subphase and a monolayer-covered subphase. The surface potential is usually measured with the vibrating capacitor technique also known as the Kelvin vibrating electrode method.[44,45] In this technique the potential difference between two electrodes, one in the aqueous subphase and the other in the air above the surface, is measured. The electrode in the air is moved with respect to the water surface. As a result of its vibration the capacity of the air gap changes. This leads to current flow in the external circuit. The magnitude of the current is proportional to the potential difference across the gap. In practice, the null method is applied in which the current is cancelled by applying an external bias till the potential difference between the electrodes is zero. The bias voltage is measured, that is taken to give the potential difference, i.e. surface potential.[23,26,46] Figure 15 shows the scheme of the surface potential measurement by the vibrating plate method.

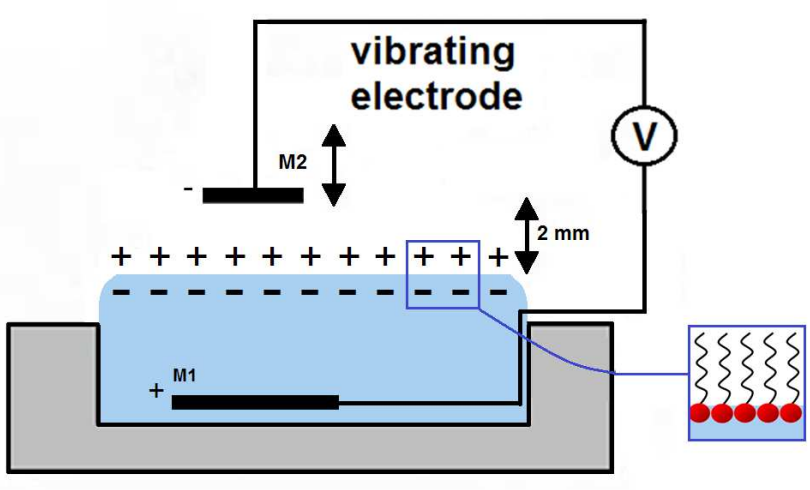

Figure 15 Scheme of the surface potential measurement by the Kelvin vibrating electrode method.

The surface potential ΔV is described by the Helmholtz formula[41]:

$$\Delta V = \frac{\mu_{\perp}}{A\varepsilon_r\varepsilon_0} \qquad (4)$$

where A is the average molecular area, ε_0 is the electric permittivity of vacuum, ε_r is the relative electric permittivity of the monolayer, and $\mu_{\perp}$ is the vertical component of the dipole moment defined as $\mu_{\perp} = \mu\cos\theta$ (where θ is the angle between the surface normal and the dipole axis). The surface potential is measured as a function of the area per molecule, giving the ΔV-A isotherm. Surface potential measurement provides important information on the properties of monomolecular films, in particular on the orientation of the molecules at the interface during compression.

2.3.3. Brewster angle microscopy

Brewster angle microscopy (BAM) is an effective technique to detect subtle morphological changes in the monolayer at the air-water interface. This technique utilizes polarized beam of light incident on the boundary of two media at the Brewster angle. This special angle, also known as the polarization angle, is an angle of incidence at

which unpolarized light is reflected from the surface yielding a particular polarization. The Brewster angle is graphically illustrated in Figure 16.

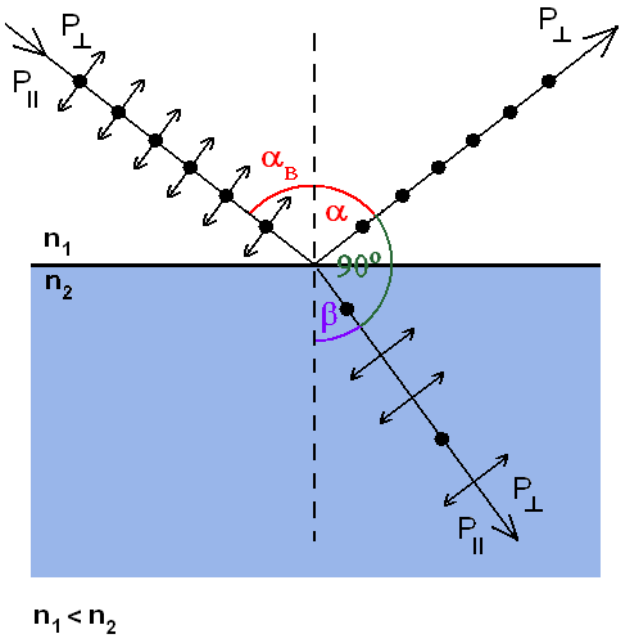

Figure 16 Illustration of unpolarized light that is incident on an interface at the Brewster angle.

When the beam of light is falling at the boundary of two phases, at the Brewster angle there is a 90^o angle between the reflected and refracted rays. The reflected light is linearly polarized and the direction of polarization is perpendicular to the plane of the incidence. Whereas if parallel polarized beam of light is falling on an interface then for the Brewster angle of incidence the light is completely refracted. Brewster angle depends on the refractive indices of the medium in the system and can be written as follows:

$$\alpha + \beta = 90° \qquad (5)$$

$$\tan \alpha_B = \frac{n_2}{n_1}$$

where α is the angle of reflection, β is the angle of refraction, n_1 is the refractive index of the initial medium through which the light propagates (the "incident medium"), and n_2 is the refractive index of the other medium. For an air-water interface (n_1 = 1, n_2 = 1.33) Brewster

angle for visible light is approximately 53°, while for air-glass ($n_2 \approx 1.5$) interface it is approximately 56°.

The operating principle of BAM is based on the fact that at the Brewster angle of incidence a parallel (p) polarised laser beam is perfectly transmitted through a transparent dielectric surface, with no reflection. Under this condition the image of a pure water surface appears black. Addition of a monolayer to the air-water interface modifies the local refractive index, and hence, a small amount of light is reflected.[47-49] This phenomenon is illustrated in Figure 17.

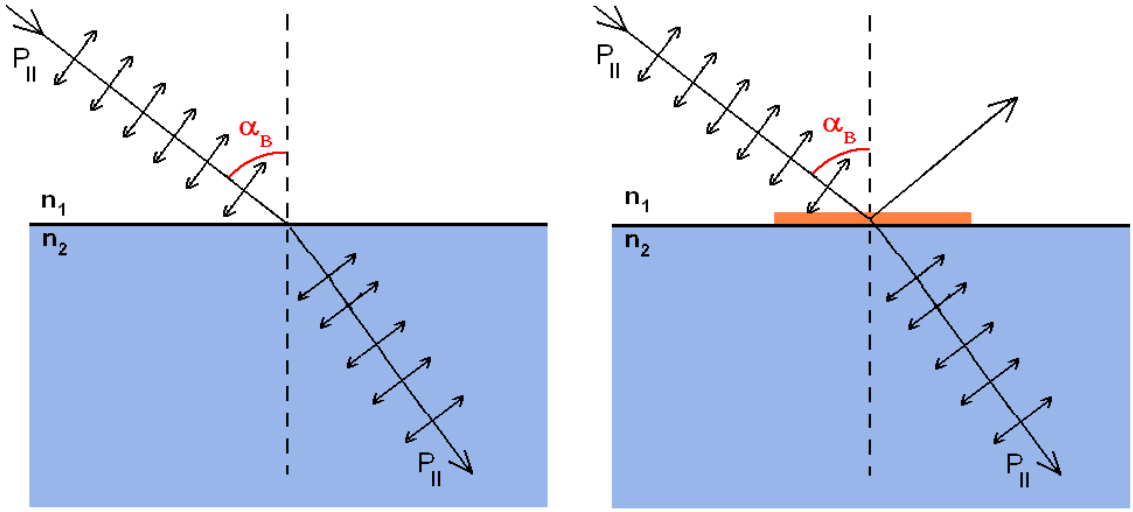

Figure 17 Principle of Brewster angle microscopy

The reflected beam is analyzed by a CCD camera, as a result we can observe the contrast between the water surface and monolayer, and the contrast from the difference in thickness of the monolayer and multilayer. Both the shape of the condensed phase domains and their inner texture can be visualised.

2.4. Transfer of monomolecular films onto solid substrates

Ordered organic films with thickness of molecular dimension assembled on appropriate solid surface have attracted considerable attention over the last few decades. A reason for this interest is a wide potential application of these systems, in catalyst, sensors[27,50] and modified electrodes.[51,52] Amphiphilic compounds can be deposited onto solid substrate in two different ways. The first method involves the formation of organic monomolecular layers by plunging a solid plate directly into an amphiphile solution containing a headgroup, which reacts chemically with the surface of the solid. Film obtained by this process is popularly known as self-assembled monolayers (SAMs). Monolayers of alkanethiolates on gold surface are probably the most frequently studied SAMs to date. [53,54]The second method of preparation ordered monomolecular films onto solid support is based on transfer of Langmuir monolayers. In this case Langmuir film formed at the air-water interface can be transferred by the vertical dipping or by the horizontal touching method. These two techniques, known as Langmuir-Blodgett (LB) and Langmuir-Schaefer (LS) technique are described in the two paragraphs below.

2.4.1. Langmuir – Blodgett technique

A monolayer located at the surface of water can be transferred onto a solid substrate by the vertical dipping method, which was demonstrated first by Blodgett and Langmuir.[55] In this method, also known as the Langmuir-Blodgett (LB) technique, the monomolecular film is deposited onto solid substrate by the displacement of a vertical plate. During this process the surface pressure is kept constant. The monolayer can be transferred onto hydrophilic or hydrophobic solid substrate. The transfer takes place during the motion of the substrate in the upward or downward directions, for the hydrophilic or hydrophobic support respectively. When the solid substrate is hydrophilic (glass, SiO_2) the first layer is deposited

by raising the solid substrate from the subphase through the monolayer, whereas if the solid substrate is hydrophobic (HOPG, silanized SiO_2) the first layer is deposited by lowering the substrate into the subphase through the monolayer. The deposition process is schematically shown in Figure 18.

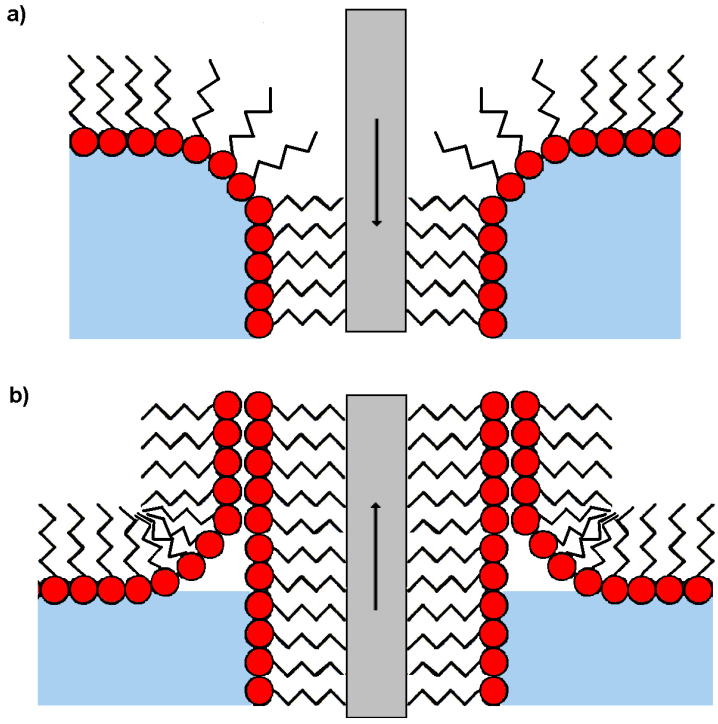

Figure 18 Deposition of the a) first and b) second monolayer onto a hydrophobic substrate.

The quantity and quality of the deposited monolayer on a solid support is measured by a so called transfer ratio, TR. TR is defined as the ration between the area of monolayer removed from subphase at constant pressure and the area of substrate immersed in water. For ideal transfer the TR is equal to 1.[56]

Depending on the behaviour of molecules the solid substrate can be dipped through the film until the desired thickness of the film is achieved. By successive deposition of monolayers on the same substrate different kinds of LB multilayers can be produced. The most common one is the Y-type multilayer, which is produced when the monolayer deposits

to the solid substrate in both up and down directions. When the monolayer deposits only in the up or down direction the multilayer structure is called either Z-type or X-type. Figure 19 presents Y-, X-, and Z-types of deposition of LB multilayers. Intermediate structures are sometimes observed for some LB multilayers and they are often referred to be XY-type multilayers.

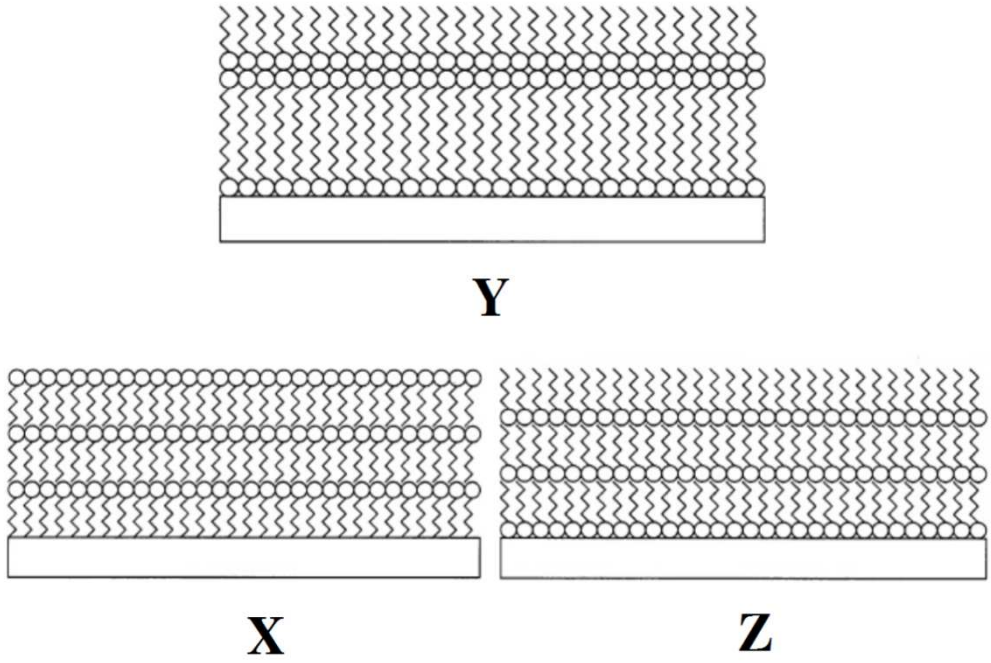

Figure 19 Structures of multilayers in different deposition types.

2.4.2. Langmuir – Schaefer technique

Another way of building multilayer structures onto solid substrate is the Shaefer's method (horizontal lifting method), which was introduced by Langmuir and Schaefer in 1938.[57] In this method a solid substrate is placed horizontally on the monolayer. The hydrophobic tails of amphiphilic molecules attach to a hydrophobic substrate and when the substrate is lifted and separated from the water surface, the monolayer is transferred. Figure 20 presents schematic illustration of the Langmuir-Schaefer method. It is interesting that

sometimes the Langmuir-Schaefer method produces not an expected X-type multilayer, but a Y-type film.[58]

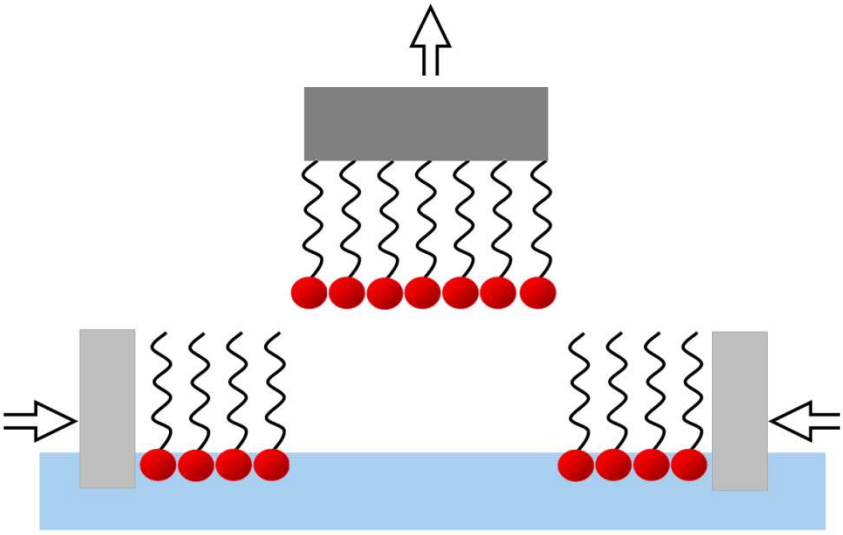

Figure 20 The Langmuir-Schaefer method of transfer.

3. Detailed description of experimental methods used in the PhD thesis

3.1. Experimental procedures and substances

Water, used as a Langmuir film subphase, was distilled and further purified with Millipore. The water was characterized by surface tension of 72.75 mN/m at 20°C and resistivity of 18.3 MΩ/m. The subphase surface was cleaned by repeated compressing, aspirating of traces of surface active compounds and expanding before a sample of the investigated solution was spread. Investigated compounds were dissolved in pure chloroform. All solutions for the monolayer spreading were prepared with a typical concentration of ca. 1mg/ml. A 10-20 μl sample was spread on the water surface, than the chloroform was allowed to evaporate for about 15 min and after that the isotherms were recorded. Films were compressed and decompressed at approximately the same rate close to

2 cm^2min^{-1} unless otherwise stated. Ethanol 95% (Merck) used for cleaning the trough and the barriers as well as the other solvents were of analytical grade.

3.2. Equipment

Experiments were carried out using the equipment from Nima Technology: a Teflon trough of the size 50 mm × 750 mm × 10 mm equipped with two hydrophobic barriers for symmetric compression and a film balance of resolution 0.01 mN/m for a surface pressure (π) measurements. Surface pressure was measured with the accuracy of ±0.1 mN/m using a Wilhelmy plate made of rectangular piece of analytical filtering paper (20 mm × 10 mm × 0.1 mm) as a pressure sensor.

The trough was also equipped with a surface potential measuring head with vibrating electrode from Treck Inc. (model 320C). The vibrating plate was located ca. 2 mm above the water surface, while the reference electrode made from steel, was placed in the water subphase. Since the surface potential signal is extremely sensitive to a distance between vibrating electrode and water surface, and of course to the surface-active impurities, its stability was checked before each experiment and after cleaning the surface. After the surface potential signal had reached constant value it was calibrated to zero and the compounds were spread from chloroform solutions in proper amounts onto the aqueous subphase. The surface potential measurements were reproducible to ±10 mV.

Morphologies of monolayers at the air – water interface were observed with Brewster angle microscope (BAM) of resolution 8.3 μm/pixel from NFT – Nanofilm Technology GmbH (Göttingen, Germany). This microscope was used to image surface topography changes during the film compression and expansion. The size of an imaged surface and the Brewster angle adjusted for the air – water interface was 4.8 x 6.4 mm^2 and ca. 50º10', respectively.

The subphase temperature was controlled with accuracy 0.1ºC by circulating thermostated water. Temperature was measured with two Pt100Ω resistance thermometers immersed at two ends of the trough and connected to Keithley multimeter. Whole system was placed on a "home-made" antivibration table and closed in a ventilated Plexiglas box to control temperature and humidity of an atmosphere over the water surface. Some measurements were carried out in an atmosphere of dry argon. For that purpose the box with the Langmuir trough was flushed with argon flowing through a container with drying agent (silica gel) starting 2 hours before the beginning of monolayer compression.

4. Results and discussion

This chapter contains two sections. One of them describes interfacial behaviour of ferroelectric liquid crystals at the air-water interface and the second Langmuir films obtained from bolaamphiphilic compounds.

4.1. Ferroelectric liquid crystals at the air – water interface

The study of the Langmuir monolayers of four different ferroelectric liquid crystals at the air – water interface is given in this part of the thesis. Following chapter contains description of oscillatory patterns formation in Langmuir monolayers of two compounds. These patterns arise from collective rotation of chiral molecules with tilted orientation to the surface. The rotation is driven by the evaporation of water through the monolayer.

The collective rotation driven by water molecules transfer through the Langmuir monolayer doped with chiral additives for the first time was described by Tabe and Yokoyama[59]. The authors examined the monolayer behaviours of chiral compounds spread on glycerol – water mixture surface. The coherent rotary motion gave a characteristic oscillatory pattern observed under a reflected light polarizing microscope. Since the

pioneering work of Tabe and Yokoyama[59] many papers describing spatiotemporal stripe patterns were published.[60-64] The authors[59-61] demonstrated that evaporation of subphase across a chiral liquid crystalline monolayer, in which molecules are coherently tilted from the surface normal, can drive collective molecular precession. This collective motion opens a new route to design synthetic molecular motors, which have received considerable interest in recent years due to the fact that they perform similar functions as natural motor proteins. [65-67]

The chemical structures of four ferroelectric liquid crystals under investigation are shown in Figure 21. In a following work I use the symbols **A, B, C,** and **D** in place of the long names of the compounds given below:

Compound **A:** (S) 4-nonanoyloxy-4'-(2-methylbutyloxycarbonyl)biphenyl, also known as MBOBC

Compound **B:** (S) 4-[4-(1-methylheptyloxycarbonyl)phenyl]-4'-[6(propanoyloxy) hexyloxy] biphenyl-4-carboxylate

Compound **C:** (S) 4-[4-(1-methylheptyloxycarbonyl)phenyl]-4'-[6-(cyano-etanoyloxy) hexyloxy]biphenyl-4-carboxylate

Compound **D:** (S) 4-(3-methyl-2-chloropentanoyloxy)-4'-heptyloxybiphenyl

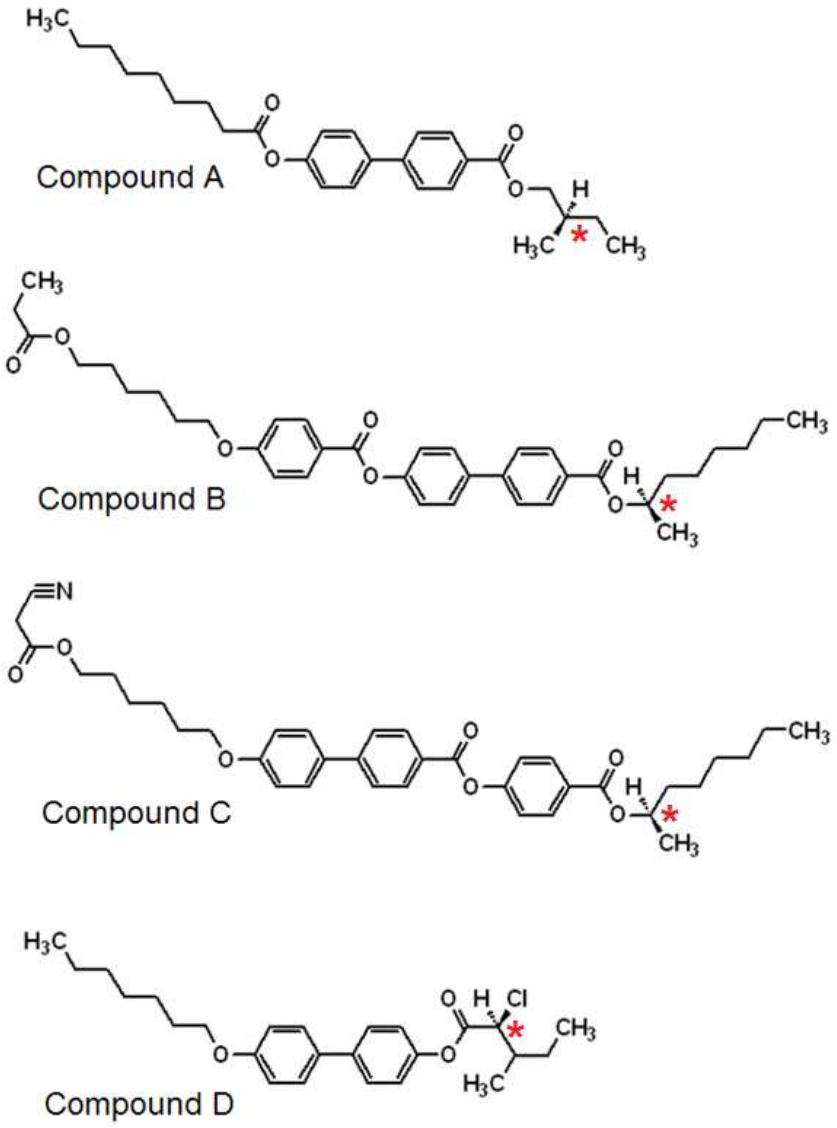

Figure 21 Chemical structures of the ferroelectric liquid – crystalline compounds. Red star shows the location of the chiral centre.

All compounds were synthesized[68,69] in the group of Professor R. Dąbrowski from the Military Academy of Technology, Warsaw, Poland, and were used without further purification. The temperatures of the phase transitions observed for particular compound in bulk phases are collected in Table 3.

Table 3 Polymorphism of pure compound, denoted as A, B, C, and D, in bulk phase: Cr is a crystal, SmC* is a chiral smectic C, SmA is a smectic A, and Iso is an isotropic phase.

Compound	Temperatures of the phase transitions / ºC	References
A	$Cr \xrightarrow{39.0^{\circ}C} SmC^{*} \xrightarrow{41.5^{\circ}C} SmA \xrightarrow{59.5^{\circ}C} Iso$	69
B	$Cr \xrightarrow{54.1^{\circ}C} SmC^{*} \xrightarrow{74.4^{\circ}C} SmA \xrightarrow{95.8^{\circ}C} Iso$	68
C	$Cr \xrightarrow{62.2^{\circ}C} SmC^{*} \xrightarrow{90.5^{\circ}C} SmA \xrightarrow{97.6^{\circ}C} Iso$	70,71
D	$Cr \xrightarrow{42.4^{\circ}C} SmC^{*} \xrightarrow{54.0^{\circ}C} SmA \xrightarrow{61.3^{\circ}C} Iso$	72

It is important that each of the compounds has the same chiral configuration (S) and all of them, in spite of different chemical structure, show the same sequence of liquid crystalline phases in bulk. However, the structural differences cause big changes in a behaviour of these compounds in monomolecular layer spread on water surface. The behaviour of the compounds in monolayers will be demonstrated and discussed in the next four sections.

4.1.1. Langmuir isotherms of ferroelectric liquid crystal A

The isotherms of surface pressure π as a function of average area per molecule *A*, was measured at temperature 23ºC. The results recorded during compression and decompression are shown in Figure 22.

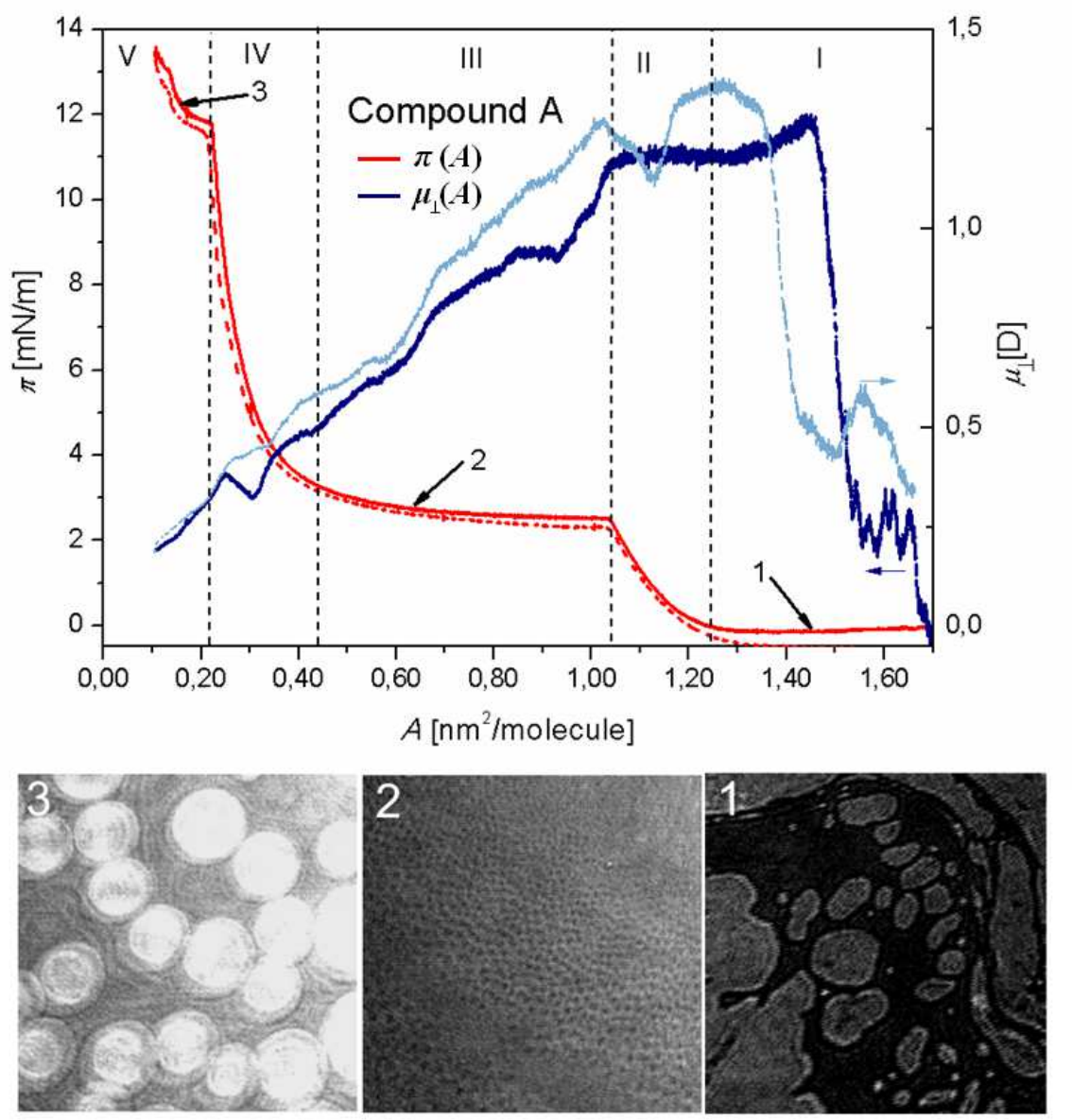

Figure 22 Surface pressure and effective dipole moment as a function of average molecular area for compound A measured at 23ºC during compression and decompression. Dotted lines represent the experimental data. The arrows with numbers show, at which surface pressure-area values the BAM images, were taken. The images show the areas (1.66 × 1.66) mm^2.

The curves of $\pi - A$ in both directions almost overlap what means that compound A has no tendency for aggregation and observed phase transitions are reversible. The most important feature of $\pi(A)$ curve is that the first increase of surface pressure ("take-off" point and the range of molecular area marked as II) occurs at a very big area per molecule. It

means that the molecules of compound A are lying flat on water attached strongly to the surface with both polar carboxylic groups.

The area range marked as I is a two-phase region of gas phase (single molecules) and two-dimensional drops of expanded liquid with all the molecules in planar orientation. The BAM image 1 in Figure 22 shows the brighter islands of liquid inside the continuous gas phase. A pressure increase in range II is a compression of the planary oriented molecules occupying at the beginning the area *ca.* 1.20 nm^2/molecule. In this region I did not observe any specific pattern which suggest the existence of homogenous monolayer.

The planarly oriented phase looses its stability above π = 2.7 mN/m. A singularity at π = 2.7 mN/m and A = 1.04 nm^2/molecule is a beginning of the first order phase transition visible as a broad plateau (range III). It corresponds to smooth change of molecular orientation from planar to homeotropic. The change of orientation is supported also in ΔV measurements (discussed later in this section). The BAM observations (image 2 in Figure 22) in range III revealed a coexistence of small darker spots of thinner film (molecules still lying flat) in a field of brighter thicker film (raised molecules). It is strange that there is no sign of any singularity between range III (plateau) and range IV (fast pressure increase) that should mark the end of the two-phase transition region (a position of dashed line separating the regions III and IV is a little arbitrary). I suppose that it is caused by a crossover from the 2D system of the planarly oriented molecules to the quasi-2D system of the molecules attached at one end to water surface and changing the tilt angle during compression. The range V with an average molecular area of less than A = 0.22 nm^2/molecule is a building-up of the second layer of the molecules still remaining in the liquid phase as proved by BAM observations shown on an image 3 in Figure 22, in which the circular bright domains (droplets) of thicker bilayer coexist with darker monolayer. This image is similar to image (e) from ref. 73 by Gallani et al., showing also the creation of second layer. Brewster angle

microscopy observations did not reveal any collective rotation of the molecules during compression or decompression.

During surface pressure measurement, surface potential – area per molecule dependences were recorded. The surface potential (ΔV) measurements were converted to the vertical component of a single molecule dipole moment, $\mu_\perp$, according to the Helmholtz equation[41]:

$$\mu_\perp = \Delta V A \varepsilon_r \varepsilon_0 \qquad (6)$$

in which: $\mu_\perp = \mu \cos\theta$ (where θ is the angle between the surface normal and the dipole axis), ΔV is the surface potential, A is the average molecular area, ε_0 is the electric permittivity of vacuum, and ε_r is the relative electric permittivity of the monolayer.

The changes of $\mu_\perp(A)$, shown in Figure 22, give merely an information about the average orientation of the molecules, and for that it is not necessary to know the exact value of ε_r, so I can take $\varepsilon_r = 1$ in my estimation. As can be seen from the curve $\mu_\perp(A)$ the apparent dipole moment remains high until the point A = 1.04 nm^2/molecule. At this point the molecules start to rise from the water surface by detachment the part with hydrocarbon chain (opposite end with carboxylic and chiral groups remains in water). The rising of the molecules causes an increasing tilt of the dipole moment vector and linear decrease of its vertical component, $\mu_\perp$. Such behaviour of $\mu_\perp$ strongly supports the change from planar to homeotropic orientation of the molecules at the plateau of the $\pi(A)$ curve.

Important fluctuations of $\mu_\perp$, observed in the region I before the point A = 1.04 nm^2/molecule is reached, are the result of formation of expanded-liquid phase domains, which are able to move freely under the surface potential sensor during film compression. Taking into account those facts, it is possible to clearly distinguish an increase of $\mu_\perp$ with A during compression between 1.6 and 1.4 nm^2/molecule, as well as linear decrease of $\mu_\perp$ for A<1.04 nm^2/molecule. However, the values of $\mu_\perp$ observed for A between

ca. 1.4 and 1.04 nm^2/molecule are less certain (especially when one compares the curves observed for compression and decompression). Therefore, it seems reasonable to assume that rather an ill-developed plateau on the $\mu_\perp(A)$ curve is observed for A values between 1.4 and 1.04 nm^2/molecule.

4.1.2. Langmuir isotherms of ferroelectric liquid crystal D

The isotherm of surface pressure π, and surface potential ΔV, as a function of area per molecule A, was measured at temperature 23ºC. The results recorded during compression and decompression are depicted in Figure 23.

The BAM observations in region I show that the compound creates big "islands" of 2D solid aggregates on water surface (an example is visible on image 1 of Figure 23). On compression, a pressure increase appears at molecular area A = 0.23 nm^2. The area corresponds to typical value for the molecular core of closely packed rod-like molecules or fatty acids, like stearic or arachidic.[41]

The isothermal compressibility coefficient, κ, in the range (0.011-0.020) $(mN/m)^{-1}$, were obtained for this phase. These values of κ are too high for solid and are rather typical for condensed liquid. An explanation of such behaviour is an aggregation, very slow in this part of isotherm and not-detectable in BAM observations (image 2 of Figure 23 shows rather uniform film).

During further compression (region III) the film collapses at rather low surface pressure π = 5.5 mN/m with further chaotic aggregation. It indicates a very low cohesion of the molecules to water surface. On decompression the aggregates disintegrate when π < 3 mN/m is reached. A behaviour of the dipole moment, $\mu_\perp$, as a function of molecular area supports the above description. No sign of any rotating molecules was observed in compound D.

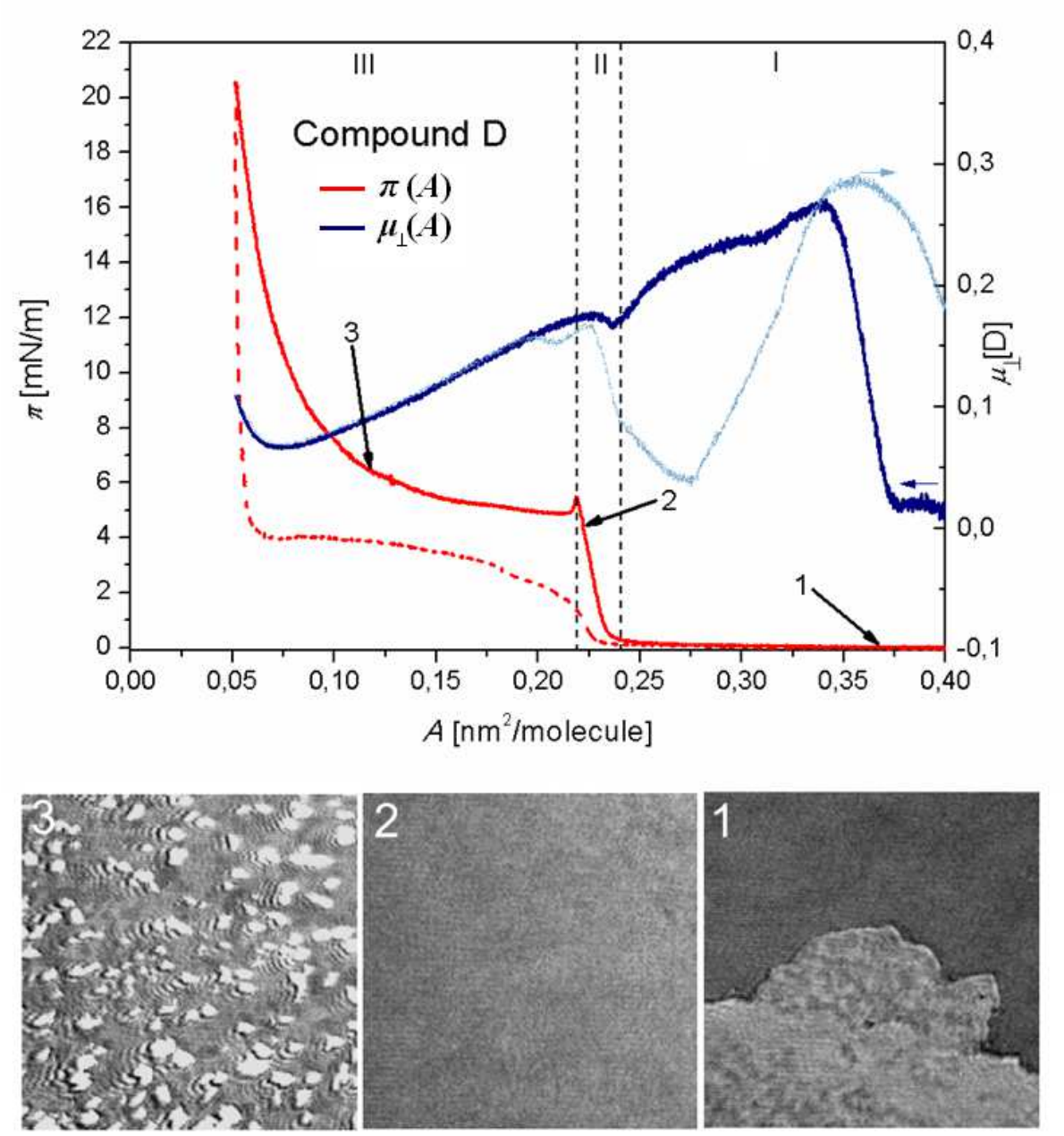

Figure 23 Surface pressure and effective dipole moment as a function of average molecular area for compound D measured at 23ºC during compression and decompression. Surface pressure during compression is represented by solid line, during decompression - by dashed line. The arrows with numbers show, at which surface pressure-area values the BAM images, were taken. The images show the areas (1.66 × 1.66) mm^2.

4.1.3. Langmuir isotherms of ferroelectric liquid crystal B

The isotherm of compound B was recorded at temperature 23ºC. The curve *π(A)* is presented in Figure 24 together with the BAM images of the monolayer in particular stages of compression.

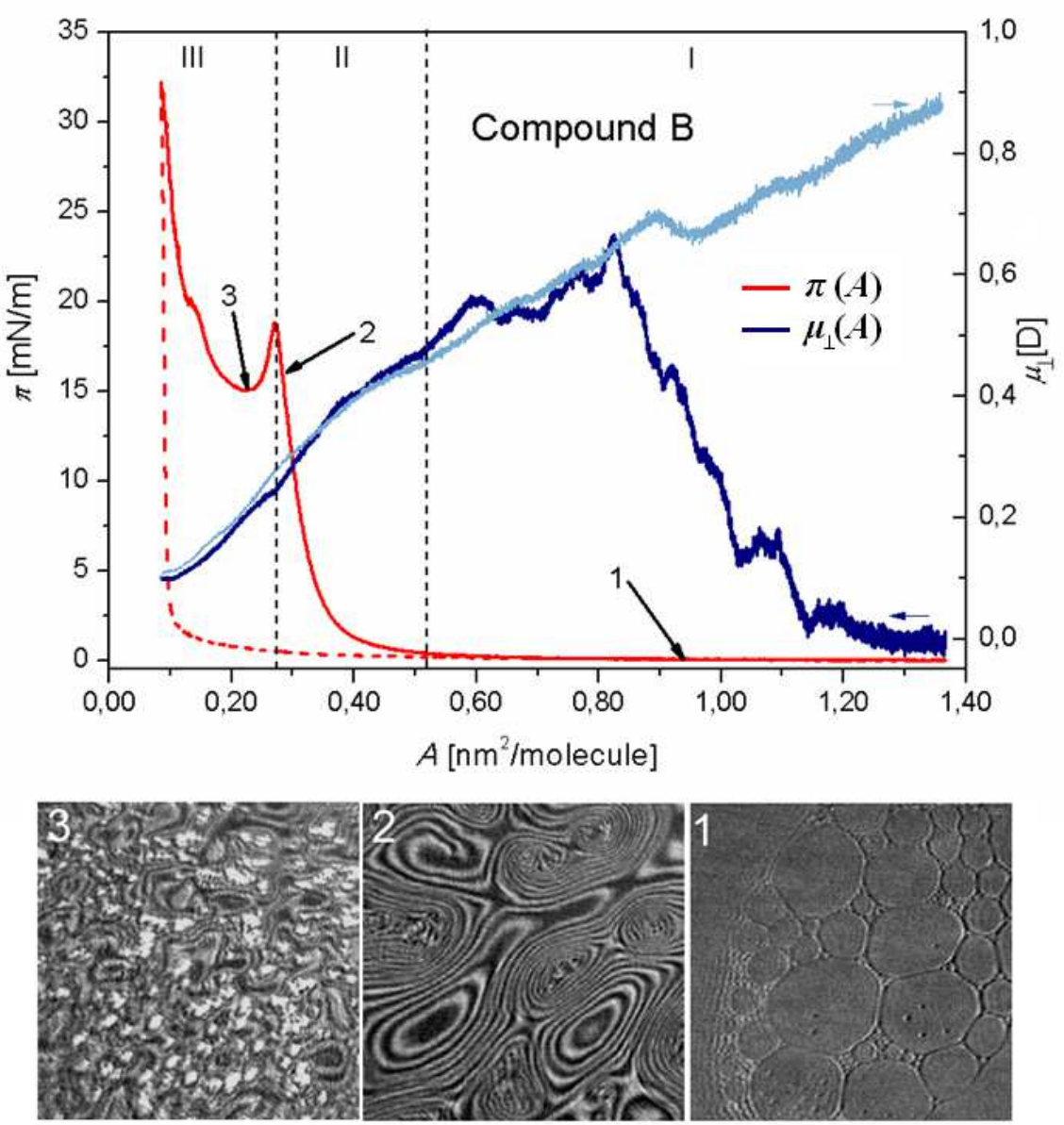

Figure 24 Surface pressure and effective dipole moment as a function of molecular area for compound B measured at 23ºC during compression (dashed lines) and decompression (dotted lines). The arrows with numbers show, at which surface pressure-area values the BAM images, were taken. The images show the areas (1.66×1.66) mm^2.

The transition from 2D-gas to 2D-liquid (region I) is confirmed by a presence of 2D-foam[74] visible on image 1 in Figure 24. This image was recorded in a two-phase region at molecular area of 0.95 nm^2. It is hard to define the end of the two-phase region because it is not manifested as a singularity (typical for most of isotherms), but is strongly rounded-off

showing a smooth change to condensed phase. The image of condensed phase taken at π = 15 mN/m and A = 0.29 nm^2 (image 2 in Figure 24) shows a texture of dark and bright circular stripes. They are created by an organized phase of molecules periodically changing their azimuthal orientation. This texture is continuously changing; that is, dark areas turn bright and opposite, which means that a director of molecular orientation is rotating. A detailed description and analysis of this rotation will be presented in section 4.1.5. Occurrence of the collective molecular rotation proves the existence of ordered liquid phase in region II. The phase was observed also as ordered domains in the two-phase regions I and III. The phase transition in region III is simply a collapse of rotating liquid phase to inhomogeneous multilayered solid phase. The collapse starts from a metastable state (equivalent to overcooling) visible as a peak located around A = 0.27 nm^2. The inhomogeneous, multilayered solid phase is visible on image 3 in Figure 24 as white spots among the domains of rotating liquid phase. The $\pi(A)$ curve shows that the multilayer films do not disintegrate on decompression. The surface pressure π drops to value close to zero immediately after the direction of the barriers movement is reversed.

Extrapolation of the compression curve in range II to π = 0 gives the molecular area A_0 = 0.35 nm^2. This value is greater than area usually occupied by vertically oriented molecule, but much smaller than the molecule lying flat. The observation allows to conclude that the molecules of compound B in the rotating phase are strongly tilted, and this tilt forces the in-plane orientation and ordering. A two-dimensional isothermal compressibility coefficient calculated close to the point A = 0.29 nm^2 at π = 15.0 mN/m is equal to 0.0141 (mN/m)$^{-1}$. This value falls in the range of typical compressibilities between expanded and condensed liquid.[41,43,75]

The curves of a vertical component of the dipole moment, $\mu_\perp$, calculated according to the Helmholtz equation for a temperature of 23ºC are shown in Figure 24. They present a

continuous decrease in the whole measured range during compression with a small but clear change of slope at the molecular area $A \approx 0.40$ nm^2/molecule. This value corresponds to the end of the two – phase region and the beginning of a compression of pure rotating phase. The observation shows that despite the rounded-off $\pi(A)$ curve, the surface potential measurement can be helpful in determination of the phase – transition point.

4.1.4. Langmuir isotherms of ferroelectric liquid crystal C

The compound C has a molecule very similar to the one of compound B. Their terminal polar groups are different (the cyano-group in the compound C is replaced by the methyl group of the compound B), and in the stiff rod-like cores the phenyl and the biphenyl rings are replaced. Also, the isotherms have similar features: in both compounds the first pressure increase corresponding to loosely packed liquid phase appears at the average molecular area ca. 0.40 nm^2/molecule. In both compounds this expanded liquid phase is ordered and able to rotate. The rotation of ordering vector (director) in compound C is presented and discussed in the next section. The isotherm of the compound C recorded at temperature 23ºC is presented in Figure 25.This isotherm two phase transitions. In region I, a coexistence of gas phase with the domains of rotating liquid phase can be observed as shown in image 1 of Figure 25. A compression of the compact rotating liquid phase characterized by typical texture (image 2 of Figure 25) occurs in region II. A slope of the $\pi(A)$ curve in this part is rather small, indicating high compressibility of this phase and proving its similarity to expanded liquid. An isothermal compressibility coefficient varies in the range of the rotating phase. The smallest value calculated close to the point $A =$ 0.35 nm^2/molecule equals $\kappa = 0.0162$ (mN/m)$^{-1}$. This value is very close to the one calculated for the rotating phase of the compound B. At the point $A = 0.35$ nm^2/molecule, the next phase transition to solid phase begins.

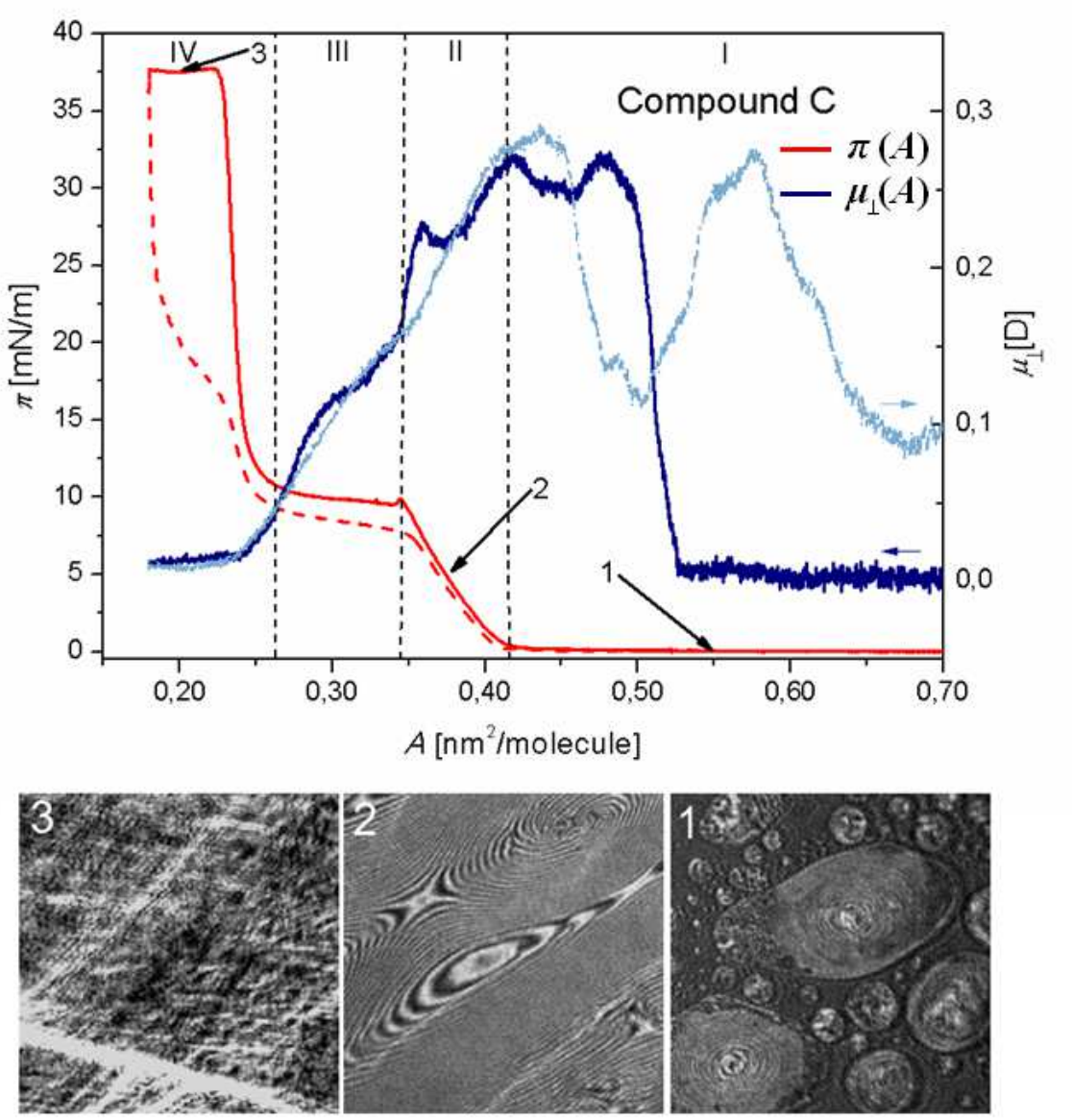

Figure 25 Surface pressure and effective dipole moment as a function of molecular area for compound C measured at 23ºC during compression and decompression. Surface pressure during compression is represented by dotted line, during decompression - by dashed line. The arrows with numbers show, at which surface pressure-area values the BAM images, were taken. The images show the areas (1.66 × 1.66) mm^2.

The plateau in region III is a two – phase region in which the domains of still rotating molecules are visible. I can classify the phase in region IV as a solid because the image 3 in Figure 25 shows a collapse of this phase with the numerous straight lines of breaking structure. These lines are crossing at an angle of ca. 60°. Also, the compressibility coefficient calculated at $\pi = 25$ mN/m (close to an inflection point) equals κ = 0.0011

$(mN/m)^{-1}$. This value is typical for 2D solids, that is, an order of magnitude smaller than κ for 2D condensed liquids. Above the inflexion point, a curvature of the $\pi(A)$ curve changes sign. This point is a manifestation of pretransitional effect before the next transition to 3D solid or disorganized collapse.

The curves of $\mu_{\perp}$-A recorded during compression and decompression are very similar to the ones of the compound B described in section 4.1.3. Big domains of liquid phase coexisting with gas phase cause a strongly distorted signal of surface potential and incorrect results of dipole moment calculations. Better results were obtained after passing the point where surface pressure starts to increase. From this "take-off" point, the two curves of compression and decompression mostly overlap, showing the very weak changes of slope at the points A = 0.35 nm^2/molecule and A_c = 0.23 nm^2/molecule. The points correspond to the beginning of the transition to solid phase and to the collapse of solid phase, respectively.

4.1.5. Collective rotations

The collective molecular precession driven by water molecules transfer through the Langmuir monolayer doped with chiral additives for the first time was described by Tabe and Yokoyama.[59] Observation of this phenomenon is possible because of liquid-crystalline properties of the studied molecules. Its self-assemble at the air/water interface creating a monolayer of smectic-C* type. Chirality of the molecules is a necessary condition for rotation. The rotation is a result of mechanical balance between driving force of the molecular precession and the viscous torque proportional to a rotational viscosity, usually denoted as γ_1. Experimental study of temperature dependence of rotational viscosity, γ_1(T), of Langmuir monolayer is the main goal of this part of my work and will be described in section 4.1.7.

An observation of molecular rotation was possible, despite the low resolution of BAM (8.3 μm/pixel), because it occurs in a liquid – crystalline phase uniformly ordered on macroscopic scale. A polarized laser-light of BAM is incident on the surface covered by the monolayer and is reflected or extinguished if the orientation of the molecules is, respectively, parallel or perpendicular to the incidence plane. With our setup, it is impossible to distinguish between n and – n orientation of ordering vector, so the colour variations from black to white to black mean a rotation by the angle π.

Only two of the studied chiral compounds are able to rotate (the compounds B and C) and the other two are not (the compounds A and D). The ability of the compounds for rotation depends on location of the chirality centre with respect to the air – water interface. Figure 26 presents schematic drawing of the molecular organization of monolayers with the indication of chirality centre. The explanation of the reasons why two of the compounds studied here are able to rotate and the other two are not is given as follows. A driving force for molecular rotation comes from a linear flux of water molecules evaporating from the surface and hitting the chiral group. *Only when the chiral group of the ferroelectric liquid crystal in Langmuir monolayer is not attached to the interface and stays in the air does the system exhibit the collective rotations.* Unfortunately, even raising the temperature of a water subphase and changing the humidity of an atmosphere over the monolayer from saturated vapour to dry argon, I was not able to put in motion the molecules of the compounds A and D. In a case of compound A, analyzing the molecular structure and relating it to its isotherm, one can see that the force making the molecules to move is not strong enough when the molecules are lying flat, attached to the water surface with two polar groups. It is obvious that during detachment to tilted orientation, it is easier to detach the carboxylic group with a long hydrocarbon chain. In such situation the chiral group remains immersed in water, as depicted in Figure 26, and cannot work as a molecular motor.

As a result, for compound A, I did not observe any rotation in any conditions. For compound D the BAM image 1 of Figure 23 recorded at high area per molecule (after film spreading and solvent evaporation) shows that molecules of this compound are aggregated in islands of 2D solid phase. The molecules are closely packed because at the increase of surface pressure they occupy the area of 0.23 nm^2/molecule. It means that the molecules are more or less vertical and their chiral groups are immersed in the water subphase, making the rotation impossible.

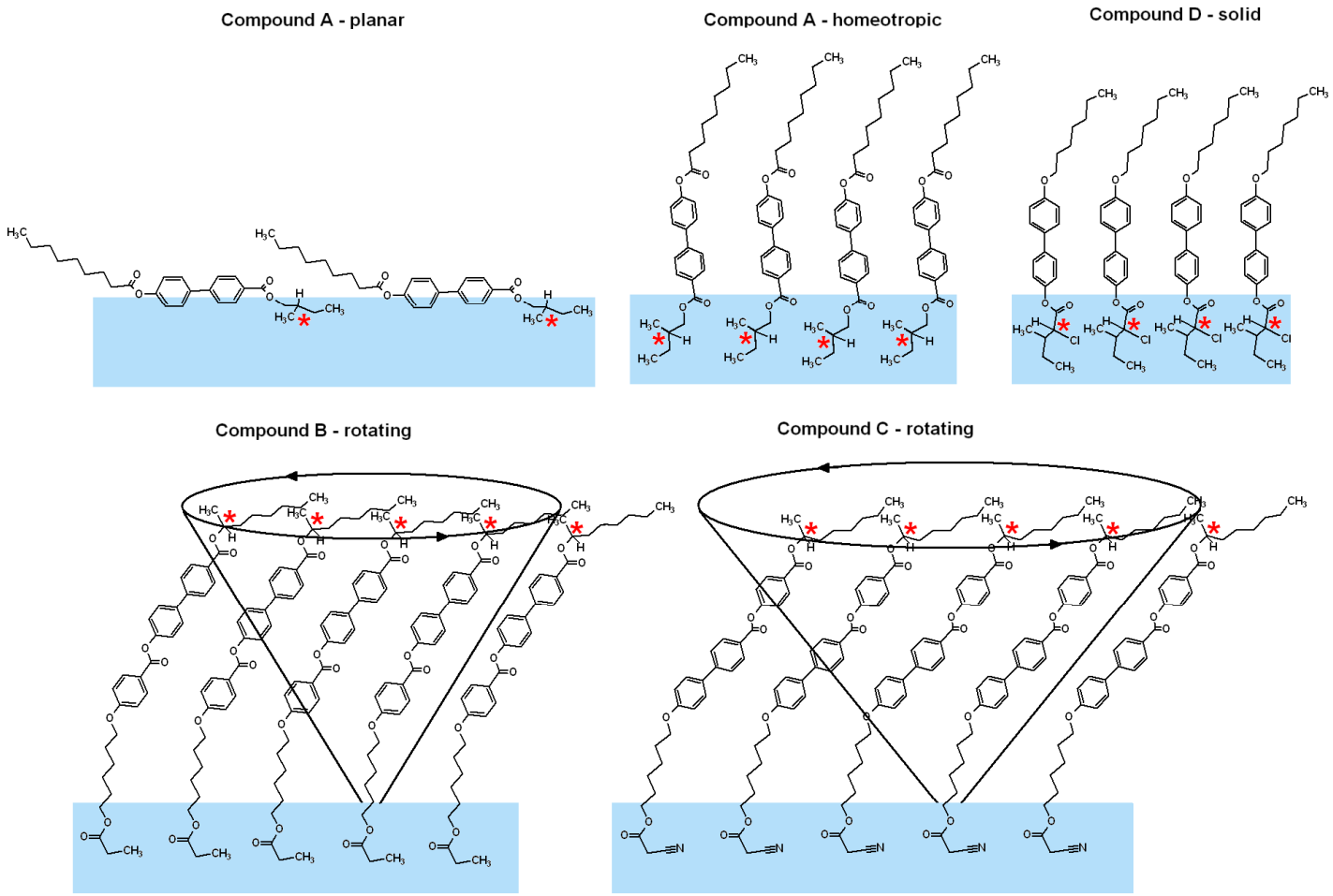

Figure 26 Schematic drawing of the molecular organization at water/air interface for particular compounds in different phases. Red star marks the chiral centre.

In the case of monolayers created by the compounds B and C, the molecules in the rotating phase are strongly tilted, and this tilt forces the in – plane orientation and ordering.

The molecules of these two compounds are attached to water surface by their polar groups. The chiral groups, at the opposite ends of the elongated molecules, remain well above the interface. The linear flow of water across the Langmuir monolayer drive the propeller – like chiral molecules to rotation, which results in the oscillatory pattern. In Figure 27 , the images of typical textures observed in the monolayers of the compounds B and C are presented.

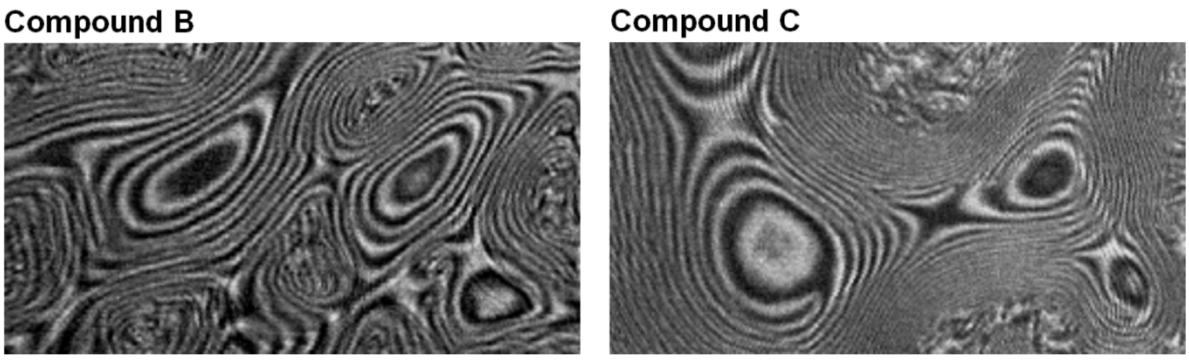

Figure 27 Examples of the textures of rotating phases most frequently observed in compounds B and C at water/air interface. The images show the areas (2.08×1.00) mm^2.

This texture is continuously changing, dark areas turn bright and opposite. It means that a vector order parameter, i.e. a director of molecular orientation characterizing the local ordering in the monolayer is rotating. Figure 28 shows the rotation of the ordering director as a sequence of 5 images taken with 6 seconds delay between the images obtained at temperature 23°C. This figure presents BAM images at different times, showing left-handed (anticlockwise) rotation. This rotation is related to the molecular chirality. In Langmuir monolayers of dipalmitoyl phosphatidylcholine (DPPC) Krüger and Lösche[76] observed right- and left-handed spiral structures for L-DPPC and D-DPPC, respectively. The pattern visible on the images is a defect created around a dust particle.

Figure 28 Sequence of the images taken with time delay 6 s indicating the changes of the tilt azimuth

Figure 29 shows a big domain in the monolayer of compound B with a periodic variation of molecular orientation. Changes in molecular orientation are visible as alternate dark and bright stripes similar to the interference fringes. A panel below the image of the domain shows the image analysis in which a saturation of black colour is measured along the long axis of the domain as a function of its real dimension. A structure of the domain is in continuous motion. The colours are varying from black to white and again to black, which gives an effect of growing fringes moving outside from the center of the domain.

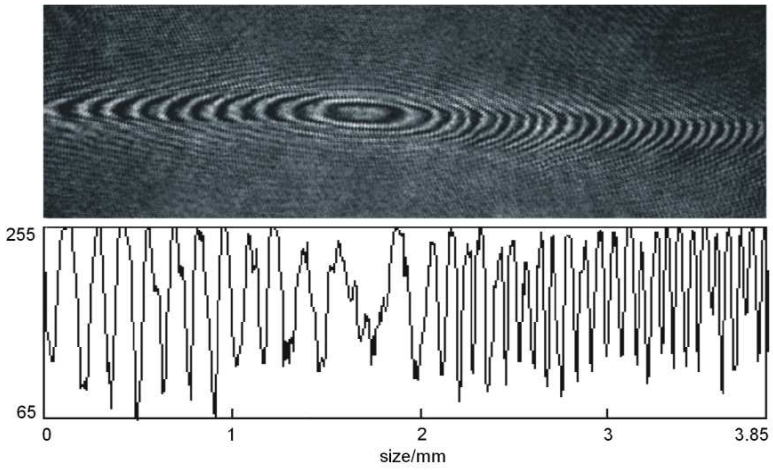

Figure 29 Big elongated domain of rotating molecules of compound B and a profile of fringes drawn against real size of the domain.

A plot below the image of Figure 29, the result of image analysis, allows to measure a pitch of the director twist. Because the distance between two neighbouring minima (or maxima) of light intensity corresponds to the director rotation by the angle π, the pitch of twist is 316 μm

and 154 μm, respectively, on the left side and right side of a center of the domain. The pitch of twist is three orders of magnitude greater than the pitch of cholesteric phase or SmC*. It means that the twist of ordering director is not directly related to chirality of the molecules. It is a result of linear flow of water molecules that drives the chiral molecules to rotation, as suggested by Tabe and Yokoyama.[59]

4.1.6. Langmuir isotherms of the compound C monolayers at various temperatures

In detailed studies of the rotation phenomenon, I performed the quantitative measurements correlating the frequency of rotation with temperature of the subphase.

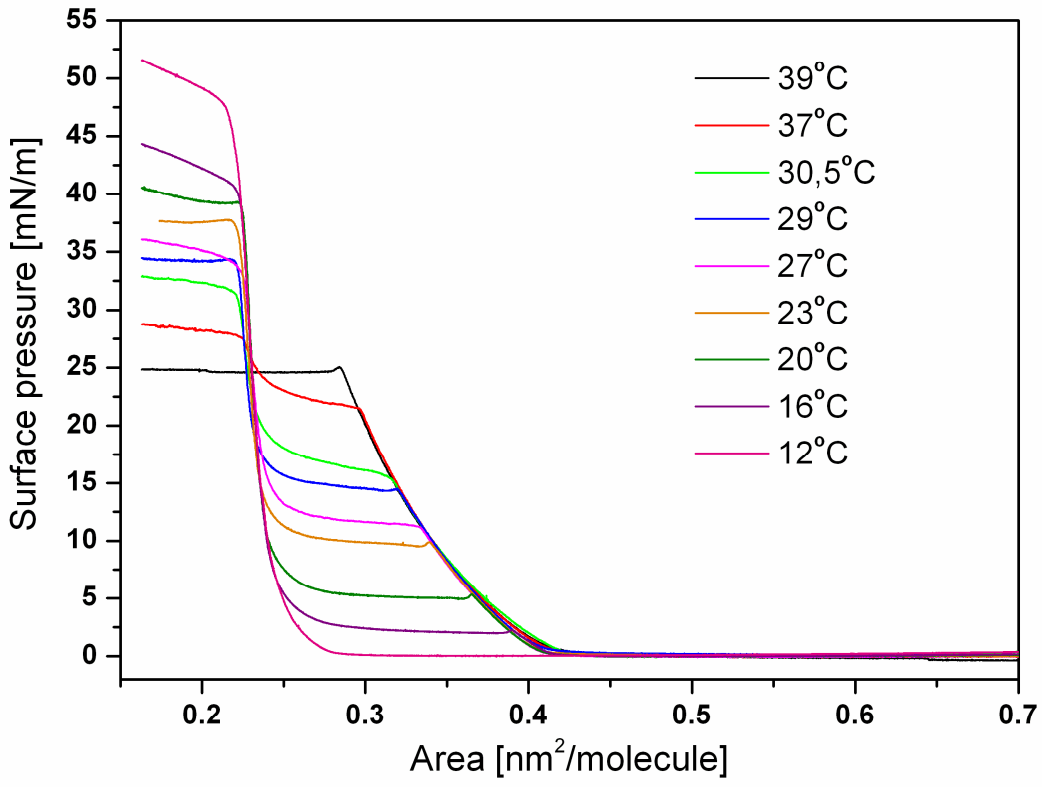

Figure 30 Isotherms of ferroelectric liquid crystal C monolayers on water at various temperatures. Note the increasing surface pressure of the plateau regions also increases with temperature. At 12℃ no clear plateau is visible

To provide the same conditions of an atmosphere over the monolayer, the chamber containing the experimental setup was flushed with dry argon. The rate of rotation was examined under variety of water temperatures, in the range of 12 – 39°C, with simultaneous isotherms measurement. The experimental surface pressure (π) - area per molecule (A) isotherms of the compound C monolayers at the air – water interface at various temperature are shown in Figure 30.

It is clear from the Figure 30 that the cusp point moves to higher surface pressure and lower molecular area with increasing temperature. The most of the $\pi - A$ isotherms show a cusp point followed by a plateau indicating a first – order phase transition from a liquid to a condensed phase.[77-79] At higher temperatures, the monolayer collapses at lower surface pressure. Thus, at temperature above ca. 37°C, it is not possible to observe the transition to a uniform solid phase prior to collapse. On the other hand, at very low temperature, the plateau region with coexistence of two phases (rotating and solid phase with untilted molecules) disappears. At 12°C the molecules create a solid phase without transitional liquid rotating phase. BAM images confirm this conclusion. Figure 31 shows the images which were taken at π = 0 mN/m region at 12°C and at plateau region at 39°C. The image A shows the “islands” of 2D solid (bright) in coexistence with gas phase (dark). The image B shows the rotating phase (dark and bright stripes) in coexistence with 3D aggregates created after collapse.

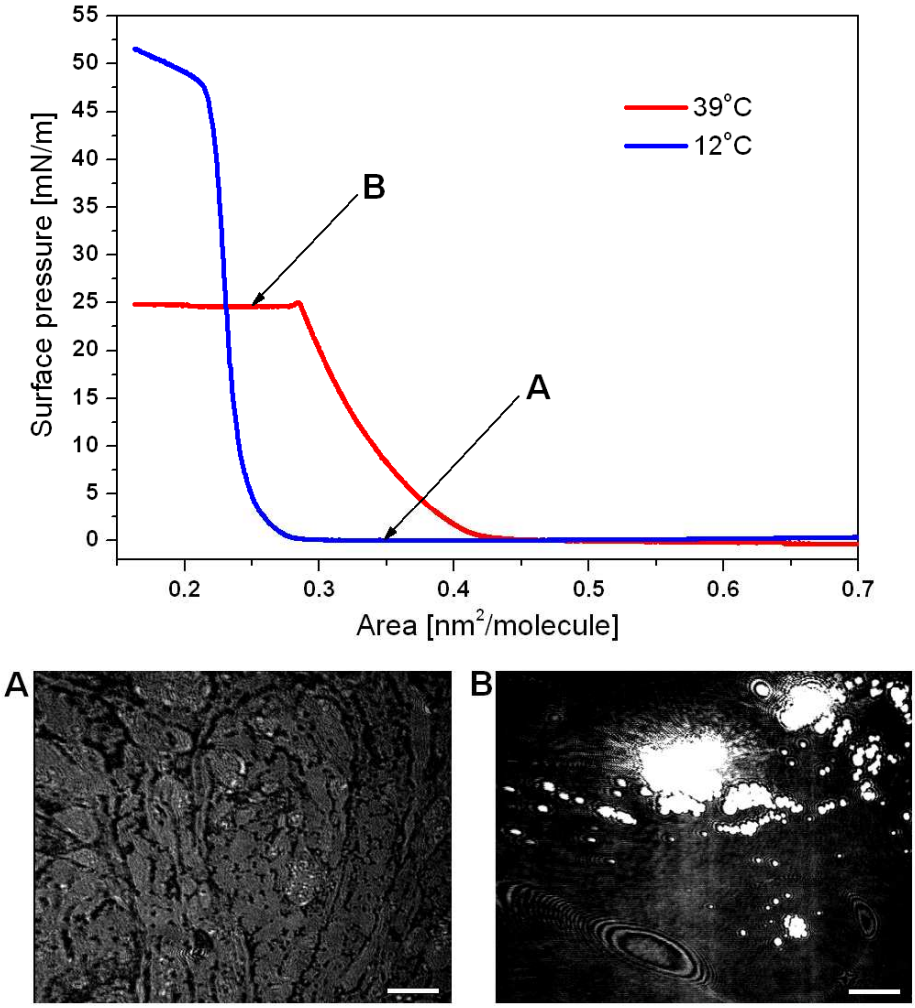

Figure 31 Surface pressure (π) - area per molecule (A) isotherm of the ferroelectric liquid crystal at the air/water interface at 12°C and 39°C . The letters A and B indicate the positions of BAM images shown below the plot; white bar of length 500 μm on images shows the scale.

4.1.7. Dependence of collective rotation frequency on temperature

Tabe and Yokoyama[59] examined the monolayer behaviours of chiral compounds spread on glycerol – water mixture surface. They demonstrated that precession speed is a linear function of relative humidity on the glycerol – water mixture. Humidity is measured by the relative water vapour pressure from the saturated pressure on mixture, to which the rate of water transfer across the monolayer is proportional. They observed that right-handed monolayer exhibit clockwise precession. In contrast, left-handed monolayer, with opposite

chirality, showed only an anticlockwise precession with exactly the same period as right-handed equivalent. Moreover, they demonstrated that for transmembrane water transfer from air to glycerol the direction of rotation is changing from clockwise to anticlockwise and vice versa.

Gupta at al.[60] studied pattern evolution as a function of relative humidity in the air above the monolayer. They demonstrated that when humidity increases, the spiral rotation rate decreases. The rotation rate decreases sharply above 70% and approaches zero at 90% relative humidity. They explained these results as follows: the increase in humidity decreases the concentration gradient of water across the interface, which lowers the evaporation rate and thus reduces the driving force for rotation.

In my studies of the rotation phenomenon, I performed the quantitative measurements correlating the frequency of rotation with temperature of the subphase. The rate of rotation was examined under variety of water temperatures, in the range of 12 – 39°C. To provide the same conditions of an atmosphere over the monolayer, the chamber containing the experimental setup was flushed with dry argon. The rate of rotation was examined at the first isotherm slope region when the homogenous rotating liquid phase appears. The molecular rotation (by angle 2π) as a function of water temperature is presented in Figure 32.

It is clear from the Figure 32 that the rate of monolayer rotation increases with decreasing temperature. The rotation slows down from 3 seconds at 39°C to almost 8 minutes at 12.6°C. To measure the slowest possible rate of rotation I decreased the temperature. I observed that at 12.6°C the rotating phase vanishes leaving uniform texture which corresponds to solid phase with untilted molecules.

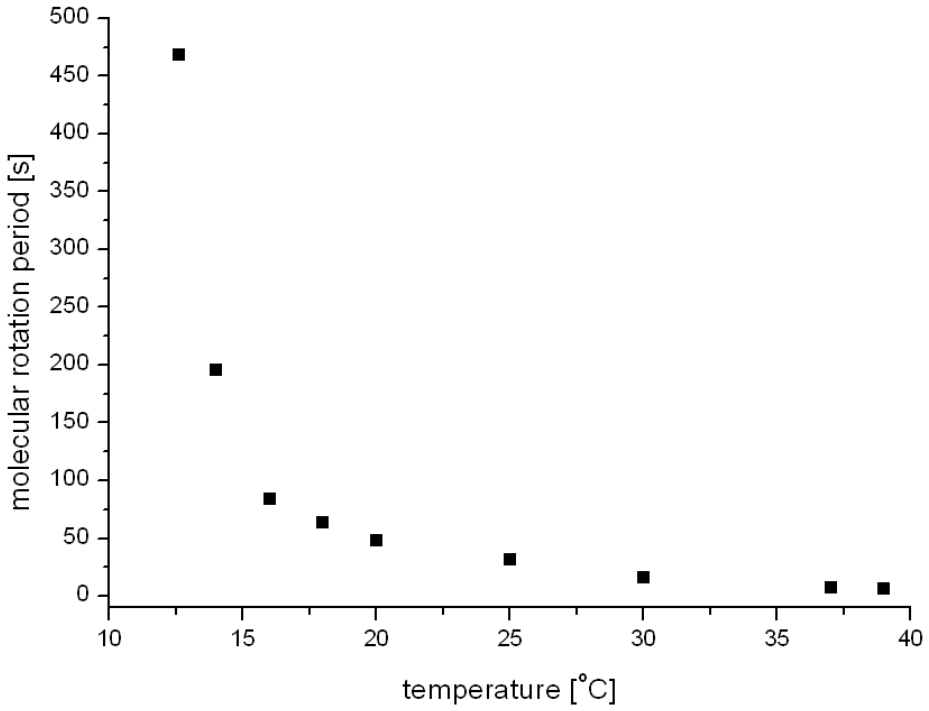

Figure 32 The rotation period (by angle 2π) as a function of water temperature.

The BAM images taken during disappearance of oscillatory pattern are shown in Figure 33. I conclude that the slowing down of collective rotation of chiral molecules at the air-water interface is connected with 2D phase transition to solid phase.

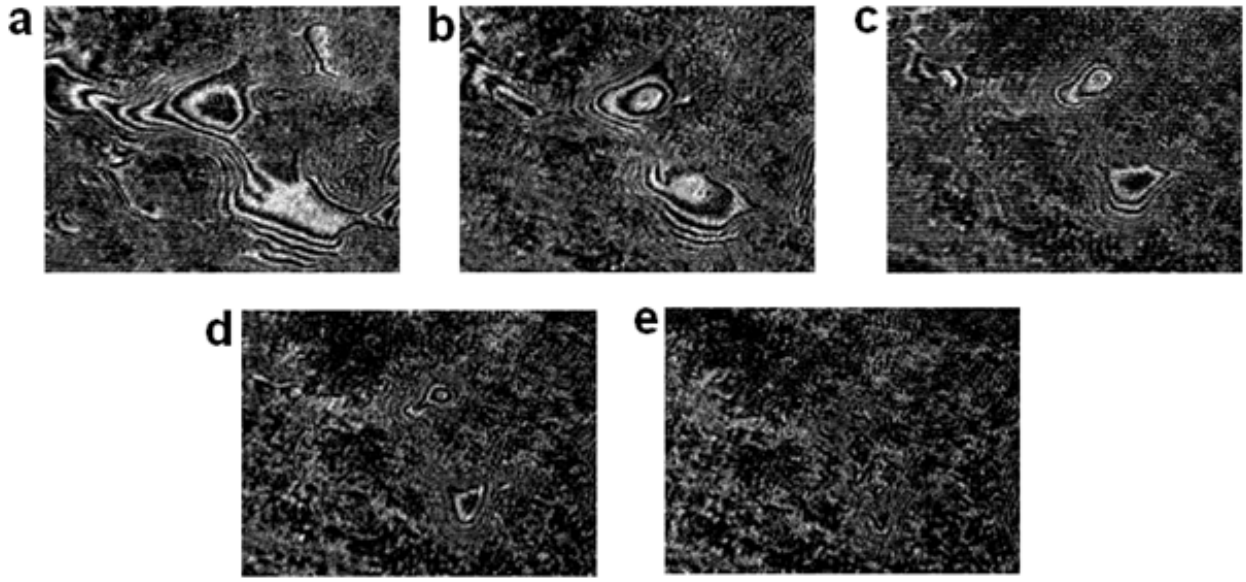

Figure 33 Sequence of the images taken with time delay 1 min showing a disappearance of oscillatory pattern. At 12,6℃ rotating phase vanishes leaving uniform texture which corresponds to solid phase with untilted molecules.

Surface torque, Γ_s, being a driving force causing precession of the director in the monolayer, is defined as a product of force, *f*, acting on the chiral group and a projection of a distance between polar and chiral groups on the plane of water surface, *r*, and multiplied by number density of the molecules in the monolayer, i.e. divided by *A* being a molecular area measured during measurements of Langmuir isotherms: $\Gamma_s = f \cdot r/A$. Continuous precession of the director at constant angular velocity is a result of balance between driving torque and viscous torque which can be written as $\Gamma_s = \gamma_s \cdot \omega$, where γ_s is the surface viscosity.[80] Surface viscosity is an important component which strongly affects the values of rotational viscosity usually measured in thin samples confined between two glass plates. Surface viscosity has to be taken into account as a correction to measured values of γ_1.[81] Both surface quantities, Γ_s and γ_s , are related to the bulk properties through the relations: $\Gamma = \Gamma_s/d$ and $\gamma_1 = \gamma_s/d$, where d is a thickness of the layer. The surface viscosity, γ_s, as measured in a monolayer and the rotational viscosity, γ_1, measured in bulk phase are the same physical properties after scaling through relation $\gamma_1 = \gamma_s/d$ because γ_s is not affected by interactions with interfaces, i.e. water at the bottom and air at the top. The cyano-group of studied ferroelectric liquid crystal anchored to water surface is very small and viscosity of air is also negligible.

The bulk torque, Γ, must be proportional to the momentum flux of evaporating water molecules. This flux is proportional to a pressure of saturated water vapour, p_{sat}.[82] The water evaporation occurs at vapour pressure difference Δp described as $\Delta p = p_{sat} - p_w$, where p_w is a partial pressure of water vapour in humid atmosphere over the Langmuir film. The balance between the driving torque and the viscous torque can be written as:

$$\Gamma = \nu \cdot \Delta p = \gamma_1 \cdot \omega \qquad (7)$$

where: ν is a chemical Lehmann coefficient, $\Delta p = p_{sat} - p_w$ is explained above, γ_1 is a rotational viscosity, and $\omega = d\varphi/dt$ is an angular velocity. The chemical Lehmann coefficient,

ν, is a material constant dependent mainly on the chiral strength of the chiral molecule, which is here understood intuitively as a parameter similar to the Lehmann rotatory power (LRP) defined for bulk chiral phases. Figure 34 shows the measured values of rotation frequency (angular velocity) as a function of temperature and a fit matching this data with theoretical analysis.

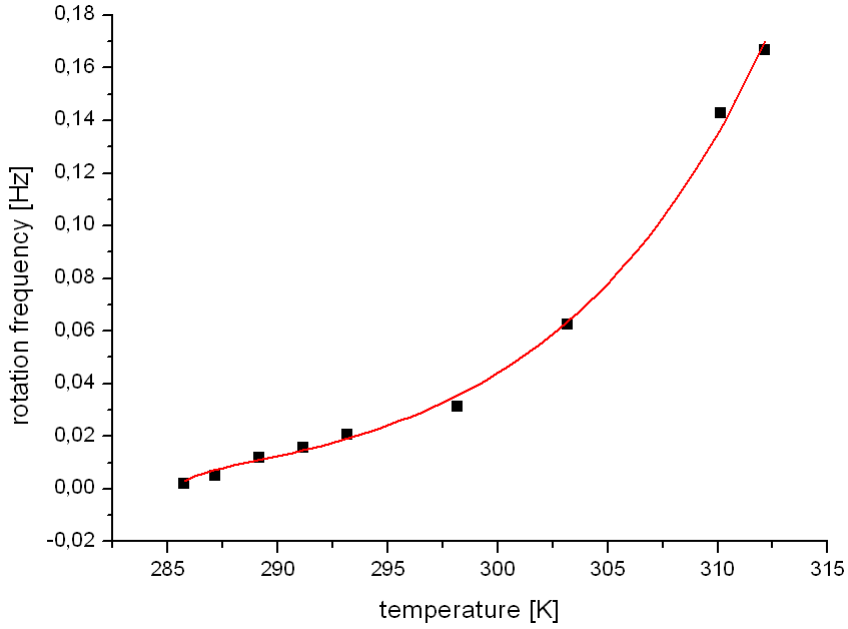

Figure 34 The rotation frequency ω as a function of temperature. The points represent the experimental data and the line shows the fit to equations (8), (9) and (10).

To analyze the data of $\omega(T)$ I used equation (7) with Δp substituted by p_{sat}. The collective rotation measurements were carried out in an atmosphere of dry argon, therefore I set p_w=0 Pa. In the equation:

$$\omega = \frac{\nu\, p_{sat}}{\gamma_1} \qquad (8)$$

the variables p_{sat} and γ_1 have to be replaced by their theoretical dependencies on temperature. According to the Clausius-Clapeyrone equation[8], saturated water vapour pressure p_{sat} is given by:

$$p_{sat} = p_0 exp\left(\frac{\Delta H}{RT_0} - \frac{\Delta H}{RT}\right) \qquad (9)$$

where ΔH is the enthalpy of water vaporization, T is the temperature, R is the gas constant.

The rotational viscosity γ_1 is described by the Vogel-Fulcher-Tamman (VFT) equation[83-85] commonly used to describe bulk viscosity of glass forming liquids close to the glass transition. In the case of monolayer I did not observed real glass transition, which usually occurs in a metastable state below the temperature of solidification. For that reason I introduced in the exponent of VFT equation the additional term (T-T_c), which contains information about temperature of the transition to solid phase, T_c. The equation used in analysis reads:

$$\gamma_1 = \gamma_0 exp\left(\frac{A(T-T_c)}{T-T_g}\right) \qquad (10)$$

where: γ_0 is a material dependent parameter, A is dimensionless parameter, T_g is the asymptotic temperature at which the viscosity diverges (hypothetic glass transition), and T_c is the experimentally established temperature of phase transition to solid state.

Equation (8) with substituted Equations (9) and (10) was used to fit the experimental data of angular velocity as a function of temperature. The calculated curve obtained as a result of fitting procedure is shown in Figure 34. The fit of experimental data to Equations (8), (9) and (10) seems relatively good – I can not expect better fits with visible scattering of experimental data, but the values of obtained parameters did not have reasonable values. Especially, the calculated value of ΔH which is the enthalpy of water evaporation had value two times bigger than the one known from thermodynamic tables. For this reason further fits were performed with more reasonable procedure. Since the theoretical Clausius-Clapeyron equation is not very precise I introduced to numerical results the calculated values of saturated vapor pressure of water. I used the Equation (11) suggested by National Institute of Standards and Technology in Washington[86] as the most precise in the temperature range I am interested in. The Equation has the form:

$$\ln p = 16.16629 - \frac{3736.276}{T-49.577} \qquad (11)$$

in which: p is in kPa and T is in K.

With the values of p_{sat} calculated for each temperature from Eq. (11) I calculated from Eq. (8) the values of the ratio γ_1/v as a function of temperature. This values behave the same way as rotational viscosity because v is constant. I fitted the values of γ_1/v as a function of temperature using VFT model given by Eq. (10) with experimental value of T_c = 285.0 K and treating γ_0, A, and T_g as adjustable parameters. This fitting gave very reasonable values of parameters A = -3.564 ± 0.138 and T_g = (282.16 ± 0.55) K and it has to be mentioned that this values are not affected by multiplication factor v.

The real temperature dependence of γ_1 (still with accuracy to small multiplication factor) was found by scaling of the ratios γ_1/v to typical value of rotational viscosity of nematic liquid crystals far from any phase transition. For scaling I took the average value of γ_1 = 0.1 Pa·s given in literature [87,88] as the value of rotational viscosity of the monolayer of compound C at temperature T = 296 K. This scaling gave the value of parameter γ_0 = (1.436 ± 0.164) Pa·s. The rotational viscosity as a function of temperature is shown in Figure 35 .

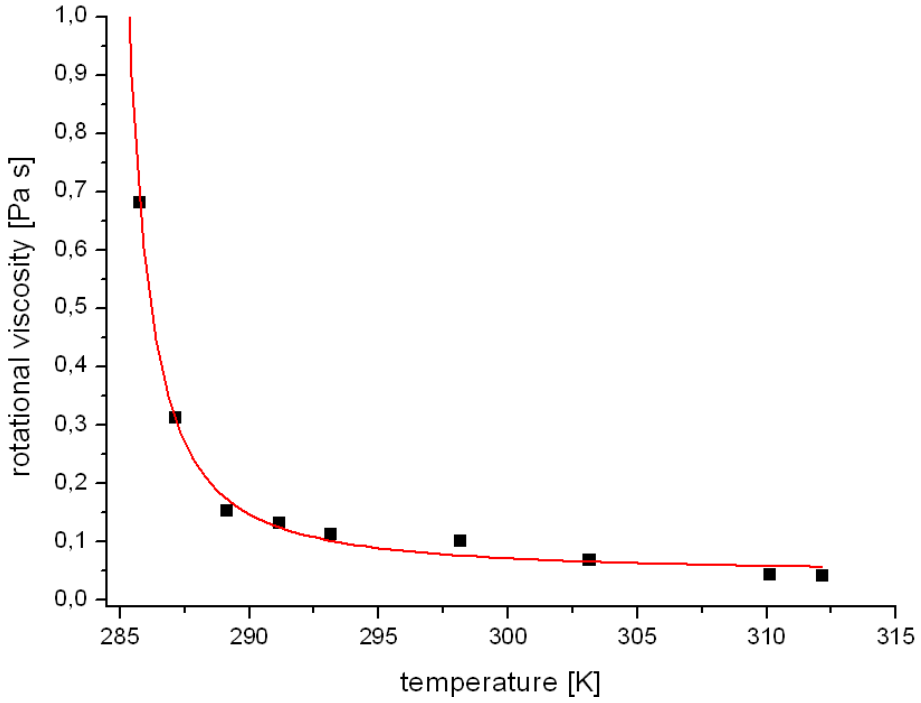

Figure 35 The rotational viscosity γ_1 as a function of temperature. The points represent the experimental data and the line shows the fit to equations (8), (10) and (11).

In conclusion, the authors[59-61] have shown that evaporation of subphase across a chiral liquid crystalline monolayer can drive collective molecular precession. In case of rotating 2D liquid phase of ferroelectric liquid crystal frequency of vector order-parameter rotation between the transition to solid phase at approx. 12°C and the collapse of the monolayer at 39°C was measured. Spreading the monolayer of compound C on water surface at temperature 12°C even at low concentrations does not give uniform 2D gas phase and big rafts of solid aggregates are visible on BAM images. In the proximity of the transition to solid phase close to 12°C the time of one revolution of the vector order parameter diverges. It is equivalent to the divergence of rotational viscosity. It was shown that in Langmuir monolayer the frequency of rotation can be extremely low (of the order of 10^{-4} Hz), i.e. 14 orders of magnitude lower than typical molecular rotations. This unusual slowing down of collective rotation is caused by proximity of two dimensional phase transition of smectic–C* phase to solid phase. It was found that the temperature dependence of rotational viscosity, γ_1, can be easily measured from BAM observations of molecular precession in Langmuir films provided that only one value of γ_1 is known from other independent measurement.

4.2. Bolaamphiphilic liquid crystals at the air – water interface

In this part of thesis I present the studies of 11 compounds from the new family of amphiphiles with an unusual head – group topology, known as bolaamphiphiles. Molecules of different shapes (X-, T-, and anchor) were studied and compared. Figure 36 schematically presents the shapes of the compounds under investigation.

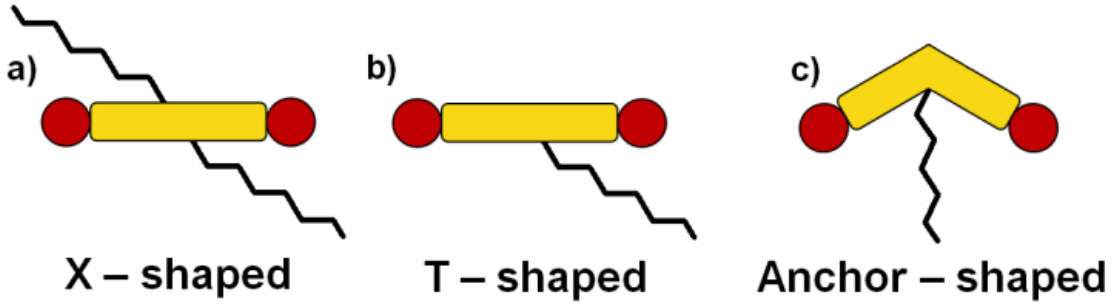

Figure 36 Schematic illustration of the shapes of the bolaamphiphilic compounds; yellow=rigid aromatic cores, red=polar glycerol groups, black curve=semiperfluorinated and alkyl chains.

The bolaamphiphilic compounds under investigation were synthesized in the group of Professor Carsten Tschierske from the Martin-Luther-University Halle-Wittenberg, Halle, Germany. The shape of the molecules, combined with the segregation of the lateral chains into distinct compartments, determines the bulk properties of the compound. This concept of polyphilic bolaamphiphiles led to a wide variety of different highly complex liquid crystalline soft-matter structures as described by the group of Professor Tschierske.[89-93] The temperatures of the phase transitions observed for particular bolaamphiphilic liquid crystal in bulk phases are collected in Table 4. The chemical structures of these compounds will be given in following sections.

Table 4 Mesophases and transition temperatures of the investigated compounds. Abbreviations: Cr = crystalline solid, Iso = isotropic liquid, Col_{squ} = square columnar phase, Col_{hex} = hexagonal columnar phase, Col = columnar phase with unknown lattice, M_1, M_2 = mesophases with unknown structure, g = glassy state.

Compound	Temperatures of the phase transitions / ºC
X1	$Cr \xrightarrow{83℃} M_1 \xrightarrow{65℃} Iso$
X2	$Cr \xrightarrow{70℃} Col_{squ} \xrightarrow{94℃} Iso$
X3	$Cr \xrightarrow{20℃} g \xrightarrow{50℃} Col_{hex} \xrightarrow{67℃} Iso$
X4	$Cr \xrightarrow{64℃} Col_{squ} \xrightarrow{92℃} Iso$
X5	$Cr \xrightarrow{113℃} Iso$
X6	$Cr \xrightarrow{93℃} Col_{hex} \xrightarrow{110℃} Iso$
T1	$Cr \xrightarrow{87℃} Col_{hex} \xrightarrow{229℃} Iso$
T2	$Cr \xrightarrow{99℃} M_2 \xrightarrow{180℃} Col \xrightarrow{218℃} Iso$
A1	$Cr \xrightarrow{113℃} Iso$
A2	$Cr \xrightarrow{63℃} Col_{hex} \xrightarrow{190℃} Iso$
A3	$Cr \xrightarrow{315℃} Col_{hex} \xrightarrow{132℃} Iso$

4.2.1. X-shaped bolaamphiphiles and reversible aggregation of compounds with partially fluorinated chains

In this part of thesis I present the study of the Langmuir monolayers of six compounds belonging to the group of X – shaped bolaamphiphiles. The chemical structures of these compounds are shown in Figure 37.

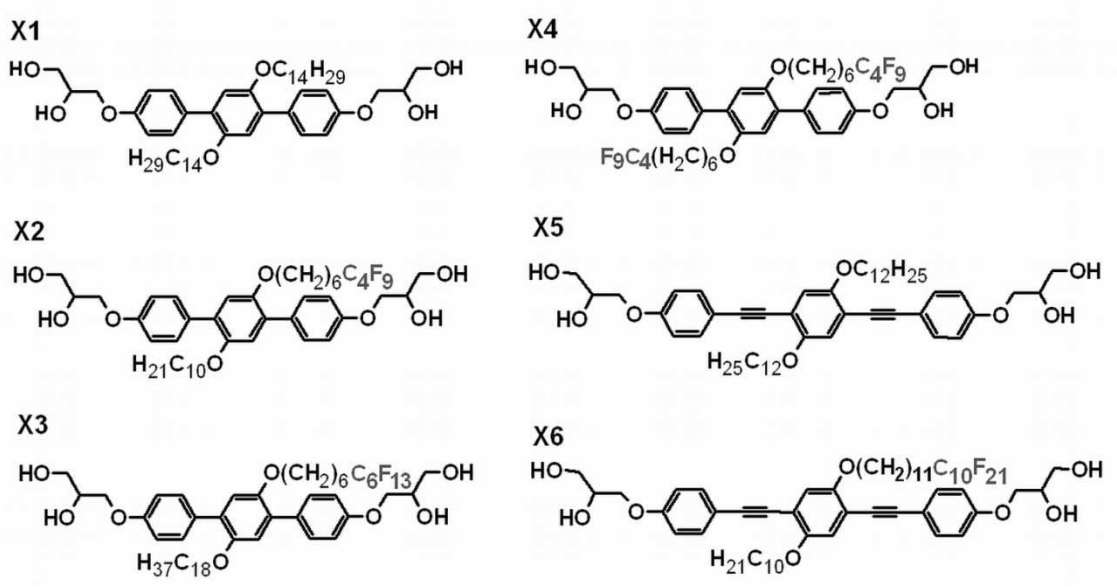

Figure 37 Chemical structures of the X – shaped bolaamphiphiles.

There are two types of rigid cores with different length. Compounds X1 to X4 with terphenyl cores terminated with two glycerol moieties and compounds X5 and X6 with significantly longer rigid cores due to the two additional ethinyl groups introduced between the benzene rings. The study of the Langmuir monolayers of the bolaamphiphiles with shortest rigid cores is given in the first instance.

The isotherms of compounds X1 to X4 are presented in Figure 38. For semi – perfluorinated compounds X2, X3 and X4 the curves of $\pi - A$ in both directions almost overlap, therefore the decompression runs are not shown in Figure 38.

The isotherms presented in Figure 38 exhibit the broad plateaus. In all cases the plateaus are reached at π = 20-25 mN/m, corresponding to an area of A = 1.10 to 1.30 nm^2/molecule. This area corresponds roughly to the area required by the aromatic rigid core with polar head groups laying on the water surface (2.2 nm x 0.45 nm + some extra space for the oxygens carrying the lateral chains). Comparing the isotherms of compounds X3 and X4, it follows that the area A seems to be additionally affected by the number of fluorinated segments. It can be assumed that before the plateau is reached the polar terminal groups of

compounds X1-X4 interact strongly with the water surface causing that these molecules are laying flat on the air/water interface.

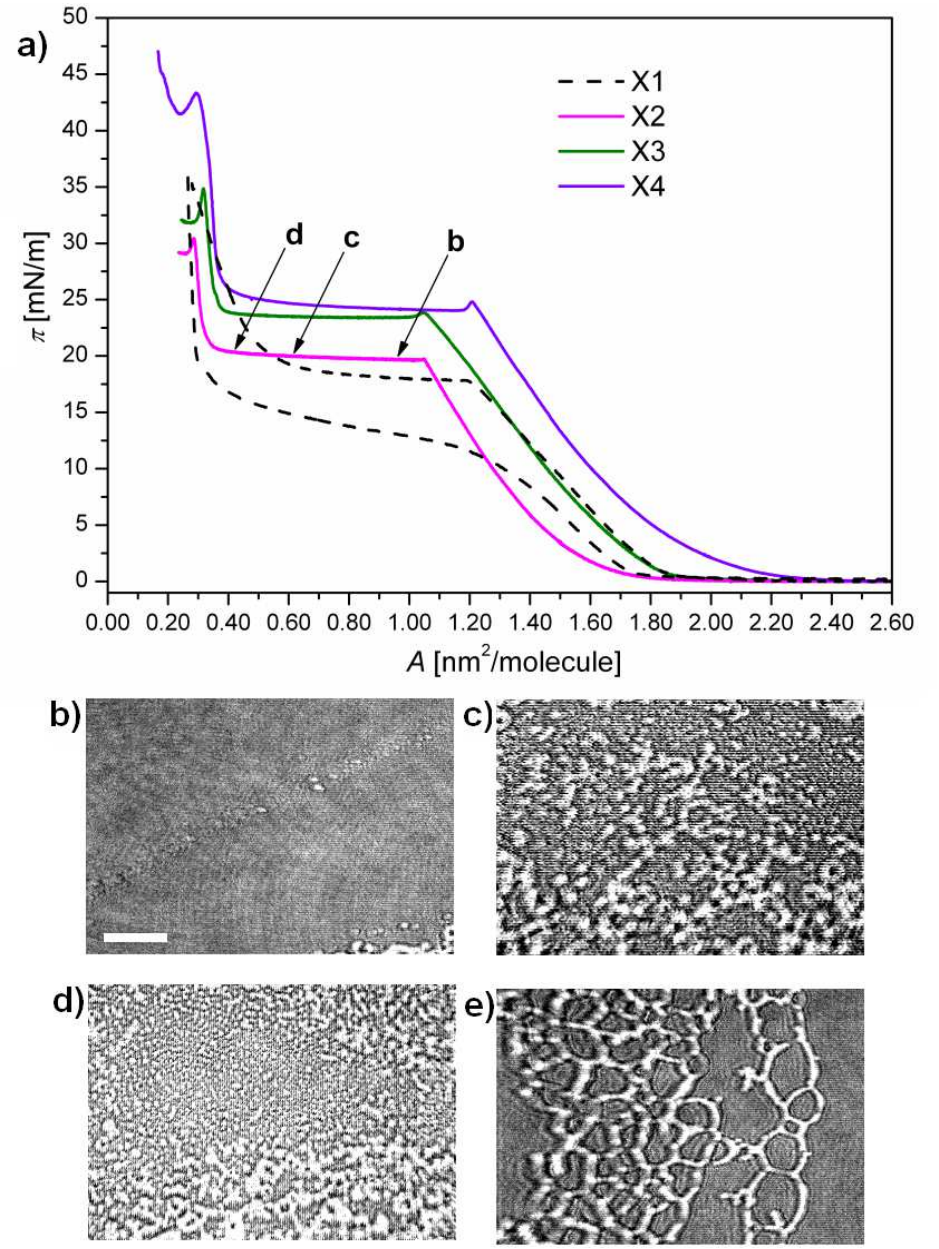

Figure 38 Isotherms and BAM images for X-shaped compounds: a) shows the hysteresis loop (compression and decompression) for the dialkylsubstituted compound X1 (dashed lines) and the compression runs (only) for semi-perfluorinated compounds X2, X3 and X4; b) - d) are the BAM images recorded at conditions marked with the same letters on the isotherm of compound X2: b) shows first domains of the trilayer appearing at the beginning of the plateau, c) and d) correspond to the increasing area covered by the trilayer during compression; e) (not marked on the isotherm) shows the remains of the trilayer in coexistence with the monolayer observed during decompression of compound X2 (not shown) at the right end of the plateau; white scale bar in image b) shows length of 400 μm.

As the plateau is reached the bolaamphiphilic cores become densely packed with the lateral chains arranged on top and covering these layers. Therefore, the molecular area at this kink is mainly determined by the size of the bolaamphiphilic cores (aromatics, glycerols and ether oxygens carrying the lateral chains) and the effect of the flexible lateral chains is smaller. Only in the case of two fluorinated chains (compound X4) large diameter of these chains seems to influence the required surface area. Additionally, enlargement of the fluorinated parts of the side chains enhances the stability of these layers due to an increase of hydrophobicity (it results from comparison of surface pressure value at plateau, for compounds X2 and X4). A second rise of the isotherms starts at A = 0.30-0.40 nm^2/molecule. The ratio of the areas per molecule at both ends of the plateau is very close to 3. It suggests that trilayer formation is setting in at the beginning of the plateau.

The most important feature of the isotherms of compounds X2 – X4 with fluorinated segments is their reversibility and reproducibility in spite of the compression to complete collapse of the film. Among the four compounds X1 – X4 only those with fluorinated chains (X2 – X4) show perfectly reversible π-A isotherms. The reversibility manifests as the perfectly overlapping isotherms what means that compounds X2 – X4 have no tendency for aggregation. Only bolaamphihiples with fluorinated lateral chains give these perfectly reversible isotherms, whereas for non-fluorinated compounds such as X1 this process is irreversible (hysteresis loop in Figure 38a for compound X1).[94]

Figure 39 schematically presents compression of monolayer to aggregates after complete collapse and two ways of their disintegration during decompression: perfectly reversible process with recovered monolayer and irreversible process with disordered aggregates after decompression.

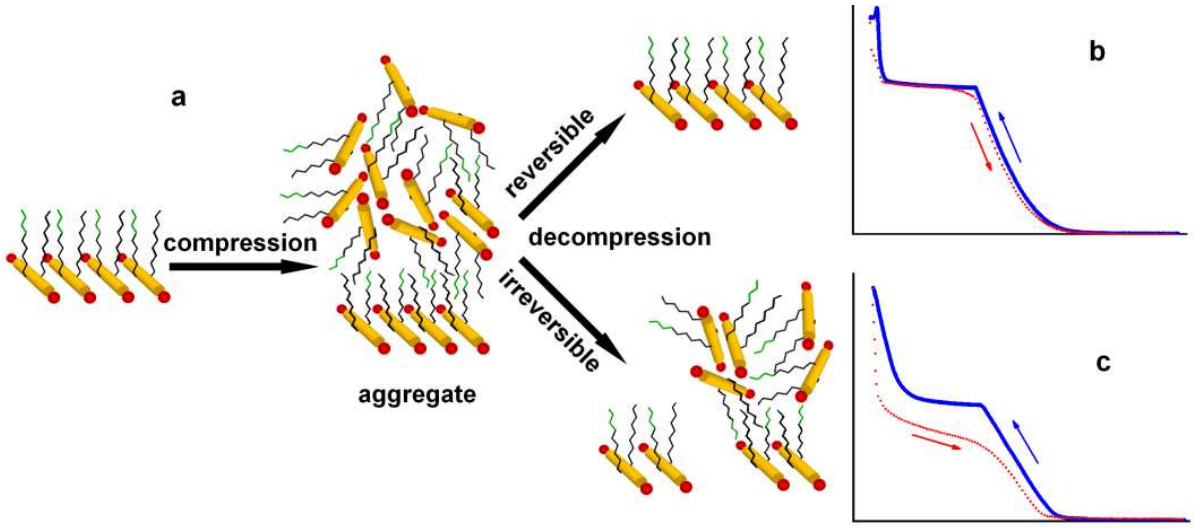

Figure 39 Sketch showing compression/decompression of monolayer (a) and perfectly reversible process in spite of the compression to complete collapse of the film observed for compounds X2 – X4 (b) and typical irreversible process with a monolayer coexisting with disordered aggregates after decompression observed for compound X1.

Isotherms recorded for compounds X2 – X4 showing compression and decompression runs are presented in Figure 40. Compounds X2 and X3 contain one partially fluorinated chain. They exhibit perfect reversibility (plateaus appear at the same surface pressure in both directions).

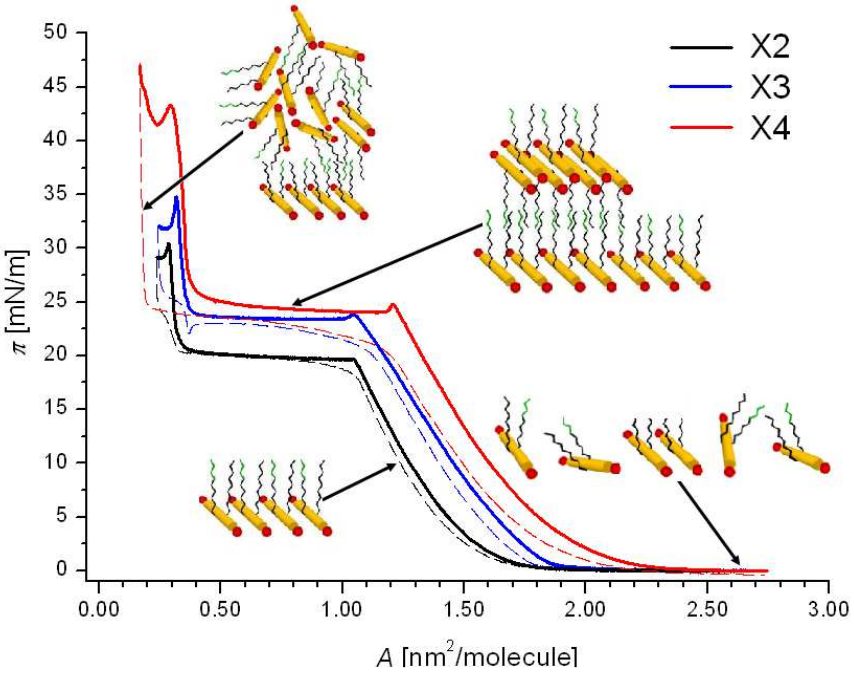

Figure 40 Reversible isotherms of three partially fluorinated bolaamphiphiles: solid and dashed lines correspond to compression and decompression runs, respectively.

Compound X4 with the highest degree of fluorination (two fluorinated segments) shows a small hysteresis loop but exhibits higher stability of the film and excellent reproducibility (the same isotherms in subsequent cycles, not shown in this plot).

The isotherms are perfectly reproducible in repeated cycles for fluorinated compounds with all runs overlapping even for the highest possible compression/decompression rate of 1.50 nm^2 $molecule^{-1}$ min^{-1} (usually experiments were carried out at much lower velocities of approximately 0.05 nm^2 $molecule^{-1}$ min-1). Three cycles for compound X2 are shown in Figure 41.

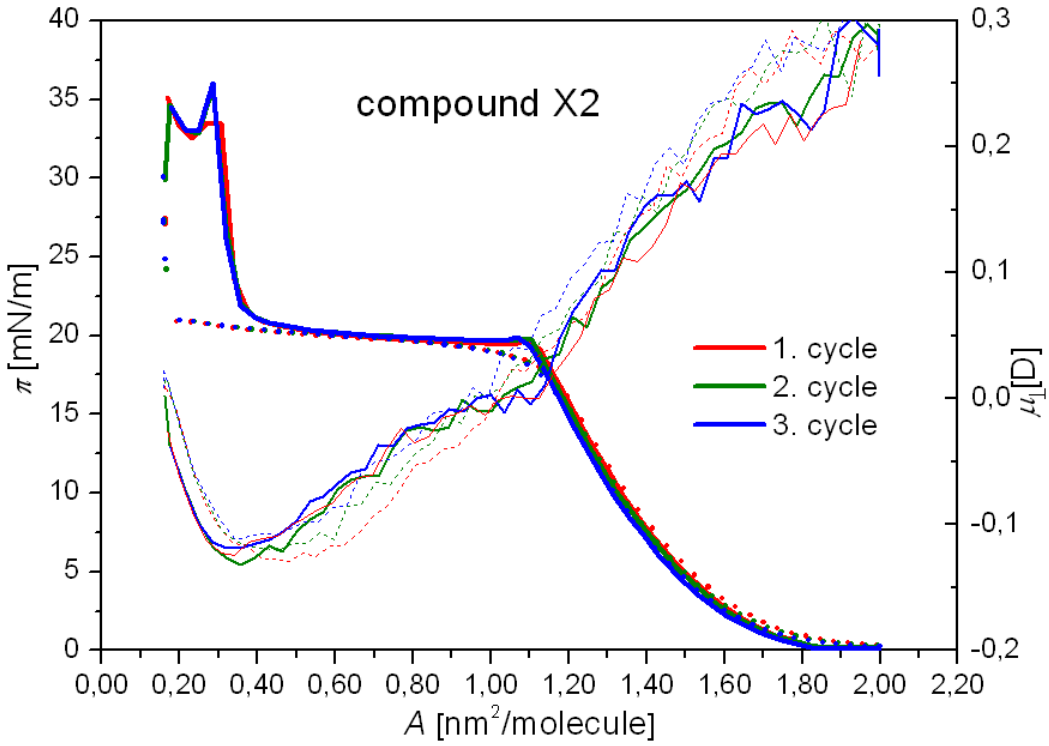

Figure 41 Reversible isotherm of compound X2 (three cycles) giving the same surface pressure at the plateau: solid and dotted lines correspond to compression and decompression runs, respectively

Difference can be observed for the isotherm obtained for the non-fluorinated compound X1. The reversibility is reduced for this compound and isotherm (presented in Figure 42) shows a strong hysteresis. Consecutive cycles systematically shift towards smaller values of area per molecule being the result of irreversible aggregation.

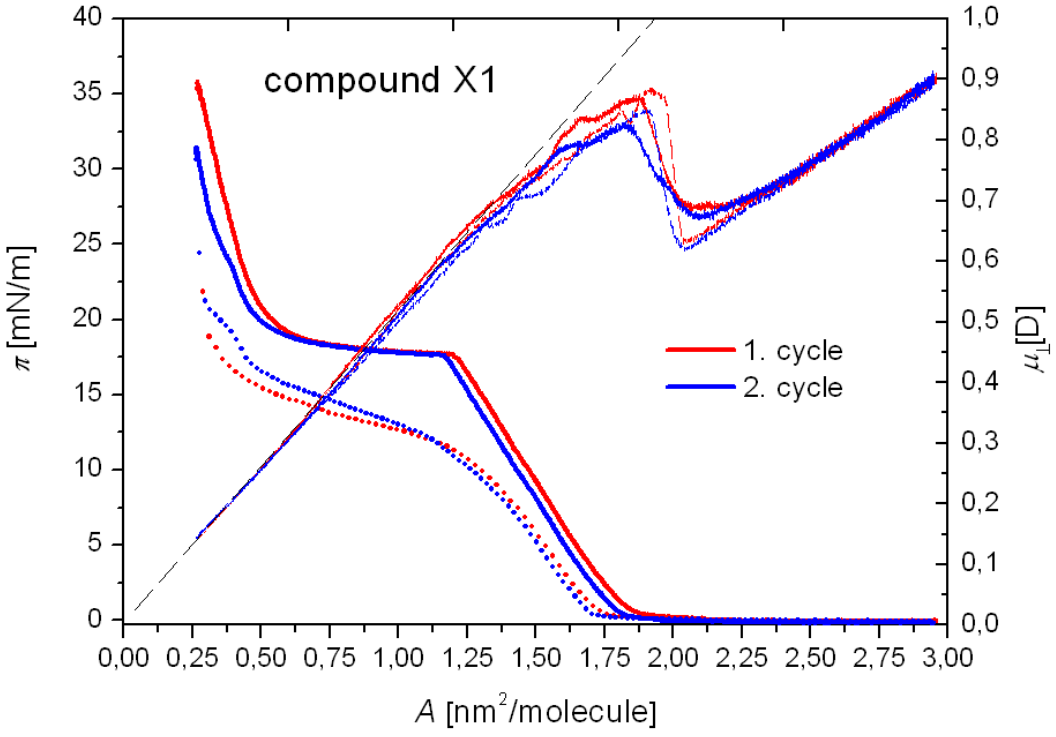

Figure 42 Two cycles of compression/decompression runs for non – fluorinated compound X1.

Whether the introduction of fluoride to the molecule belonging to the group of rod-like liquid crystal prevents the chaotic aggregation has been examined in the following part. For this purpose, the Langmuir monolayers of two compounds of the rod-like shape were created at the air-water interface. One of the compound is the non-fluorinated 8OCB liquid crystal, and the second is its partially fluorinated analogues, denoted as F6H2OCB. The structural formulas of these compounds are shown in Figure 43.

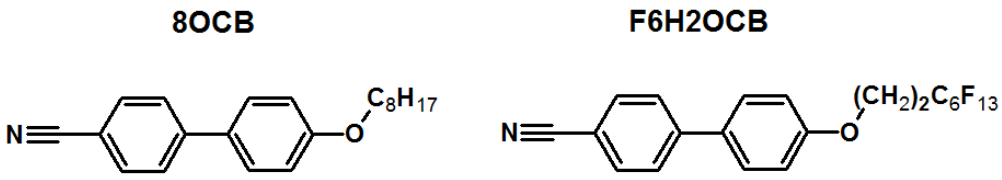

Figure 43 The chemical structures of rod-like liquid crystal molecules; non-fluorinated compound 8OCB and partially fluorinated compound F6H2OCB.

Figure 44 compares the π-A isotherms for the compounds 8OCB and F6H2OCB. Although the structures of these compounds are very similar the isotherms are radically different.

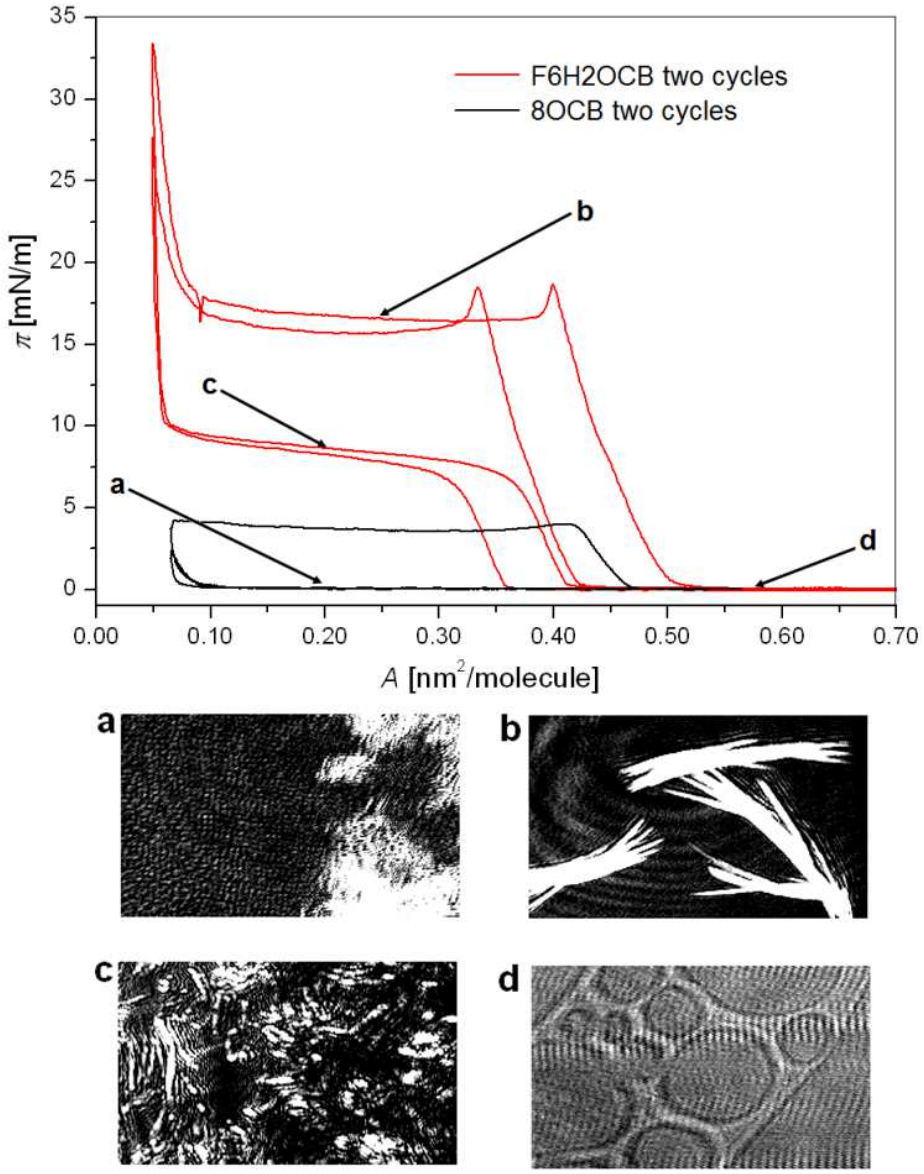

Figure 44 Isotherms and BAM images for the compounds 8OCB and F6H2OCB; a) - d) are the BAM images recorded at conditions marked with the same letters on the isotherms: a) the aggregates formed by the compound 8OBC after compression beyond collapse and still remaining during second compression; b) coexistence of monolayer and aggregates formed by the compound F6H2OCB; c) aggregates disappearing during decompression; d) coexistence of liquid and gas phases (2D foam) recovered after decompression to π = 0.

During compression of the compound 8OCB first pressure increase appears at molecular area A = 0.47 nm^2/molecule. This area corresponds to typical value for well-known monolayer of rod-like 8CB molecules.[95,96] Thus the compound 8OCB creates the monolayer at the air-water interface. This monolayer is unstable and collapses at the surface pressure π = 4 mN/m. After the collapse, tree-dimensional aggregates are formed. These aggregates do not disintegrate even after complete separation of the barriers and remain during second compression (as it is shown in image a in Figure 44). The second compression of the compound 8OCB does not cause any increase of surface pressure (except for very small areas, too small to be regarded as a monolayer) which means that this non-fluorinated compound creates an irreversible aggregates.

From the isotherm obtained for the fluorinated compound F6H2OCB follows that the partial replacement of hydrogen by fluorine in the aliphatic chain increases the stability of the monolayer to the surface pressure π = 19 mN/m. This replacement also significantly improves the reproducibility of the monolayer in the second cycle of compression and expansion. Despite the fact that the aggregates are formed during first compression (image b on Figure 44), decompression leads to decomposition of these aggregates (image c on Figure 44). After expansion to the zero surface pressure molecules of F6H2OCB create two-dimensional foam (coexistence of liquid and gas phases).

Additional information about the self assembly of compounds X1-X4 comes from the curve of the vertical component of the dipole moment. Simultaneously with the surface pressure the surface potential was measured using the Kelvin-electrode method. The $\mu_\perp$-A dependence is shown in Figure 42 for compound X1, in Figure 41 for compound X2 and in Figure 45 for compounds X3 – X4.

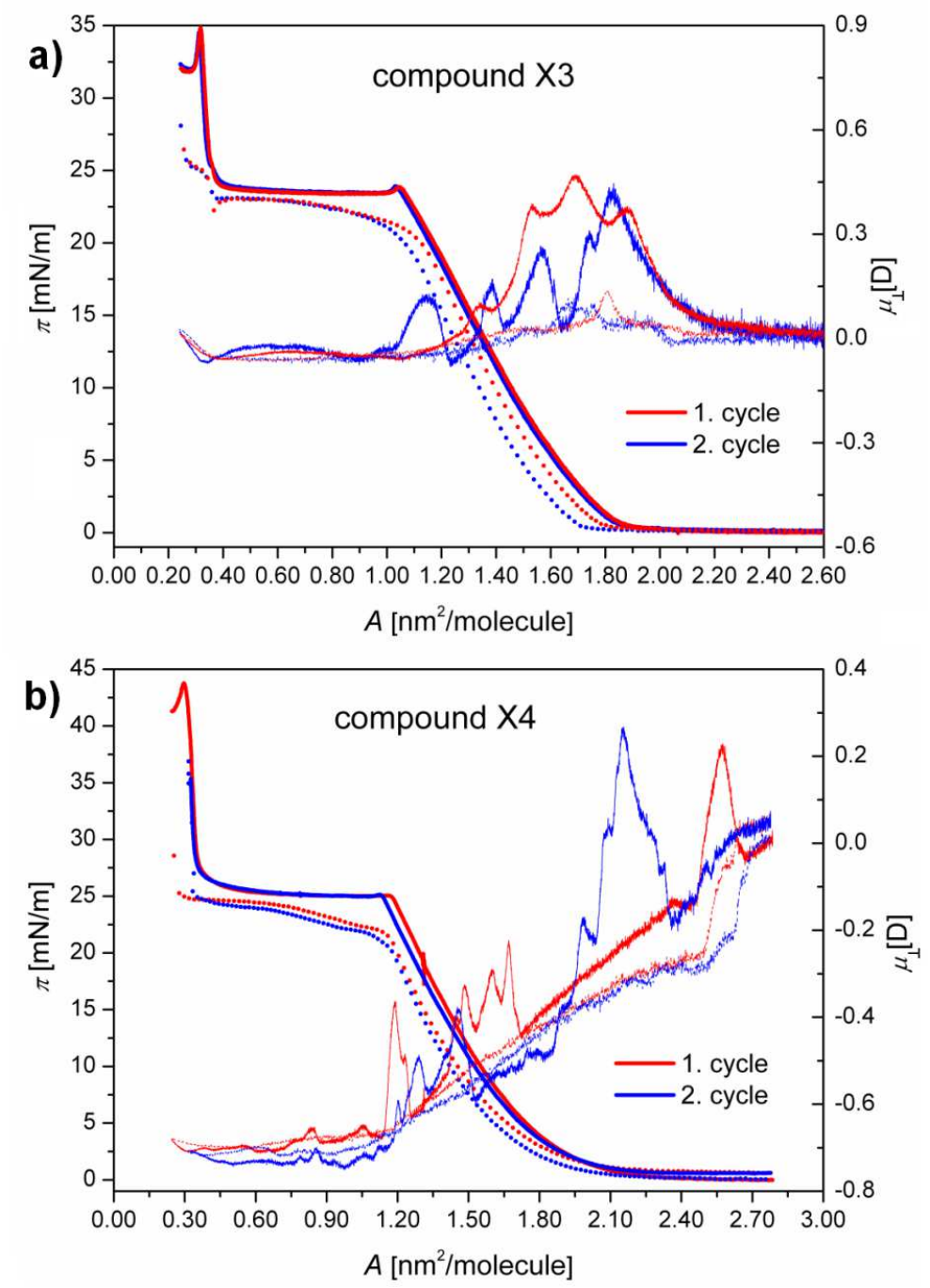

Figure 45 Results of surface pressure and surface potential measurement for compounds a) X3 and b) X4.

In the case of X – shaped molecules, for which the rigid cores with the polar groups are lying flat on water surface, an important contribution to the molecular dipole moment comes usually from the terminal C – H or C – F bonds of the lateral chains. In partially fluorinated compounds, the dipole moment of fluorinated parts is oriented in opposite

direction with respect to the dipole moment of non-fluorinated chains.[97] During compression of compounds with fluorinated chains $\mu_{\perp}$ decreases. It indicates the rising up of the fluorinated parts of the chains. An opposite effect i.e. an initial increase of $\mu_{\perp}$-A is observed in the non –fluorinated compound X1 (Figure 42). This could be interpreted in the following way: at the onset of the plateau the molecules are packed in a 2D film with maximum density. On further compression (in the plateau region) the molecules are removed from the surface by ‘‘escape into the third dimension’’ during formation of the triple layer. The dipole moments of the molecules in the second and third layers compensate because they are oriented in opposite directions. For compound X2 the decrease of $\mu_{\perp}$ continues after reaching the plateau region, but with reduced slope of $\mu_{\perp}$-A. It means that the dipole moments of the molecules in the second and third layers are not fully compensated. Such compensation of $\mu_{\perp}$ is observed for compound X3 and for compound X4 with two fluorinated chains as can be seen in Figure 45 (the curve of $\mu_{\perp}$-A in a plateau region is almost horizontal). A broad peak in the $\mu_{\perp}$-*A* curve observed for compound X3 upon compression of the monolayer shows that during the rise of the isotherm the longer hydrogenated chains are rising up first, causing the increase of the dipole moment. Upon further compression the contribution of vertically aligned fluorinated chains increases and causes the decrease of the $\mu_{\perp}$-A curve. In the plateau region no further change of the dipole moment is observed. These observations i.e. compensation of $\mu_{\perp}$ in the plateau region support the idea of well-organized trilayer formation. In this trilayer a double layer (bilayer of antiparallelly organized molecules) is organized on top of the surface layer.

For trilayer formation a reversible “roll-over” mechanism was proposed firstly for rod-like amphiphilic liquid crystals (aromatics perpendicular or tilted to the surface)[98-103]. Then it was proposed for T-shaped facial amphiphiles[104,105] having an arrangement of rod-like aromatics parallel to the surface as also found for the bolaamphiphiles X1 – X4. More

recently, trilayer formation was also reported for semi-perfluorinated hydrocarbons,[106] amphiphiles with bulky aromatic end groups[107] and for mixed monolayers formed by co-assembly of cationic lipids with anionic porphyrins.[108] For these co-assembled monolayers it was suggested that trilayer formation takes place in a kind of "lifting" process. The reversibility of the isotherms was explained by line tension of the trilayer domains coexisting with residues of monolayer.[109]Though these two modes (roll-over or lifting) of reorganization at the monolayer to trilayer transition are difficult to distinguish.

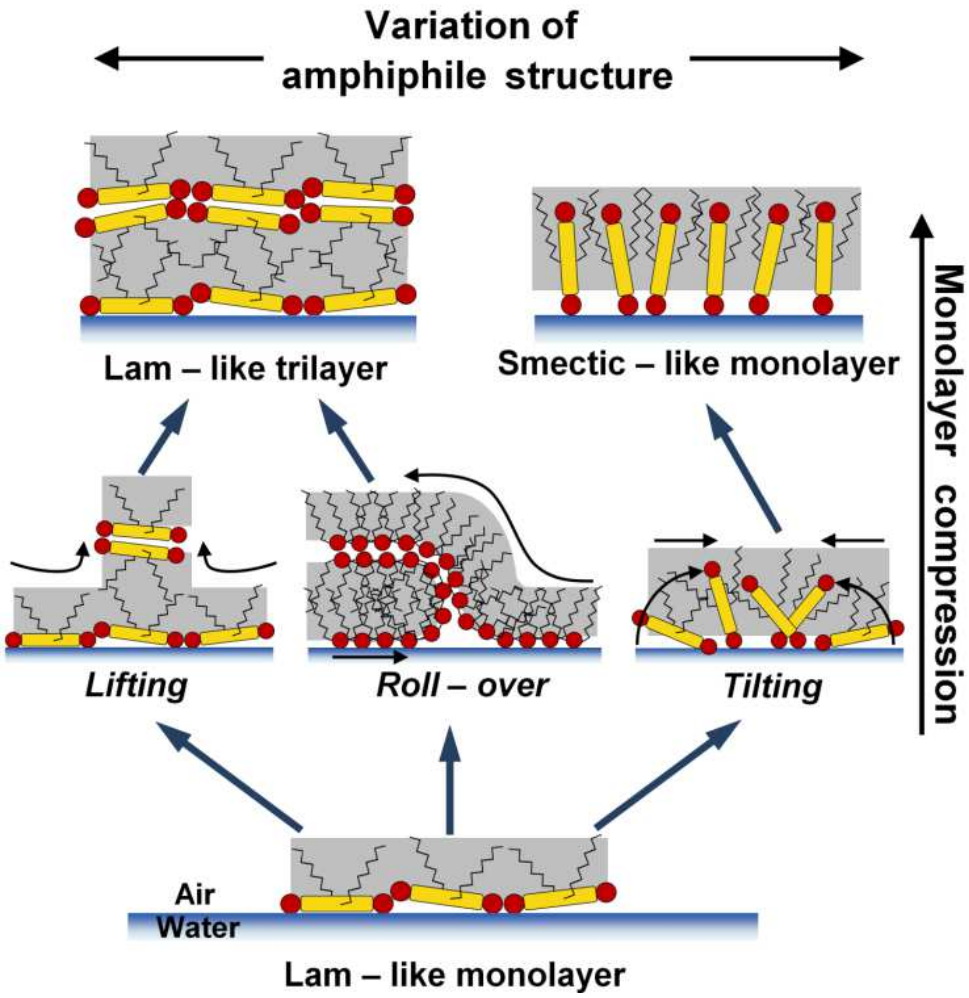

Figure 46 Schematic sketch of the bolaamphiphilic molecules arrangement in the monolayer (Lam-like monolayer) and after monolayer compression (Lam-like trilayer and smectic-like monolayer). Different types of transformations leading from Lam-like monolayer to trilayers (lifting and roll-over) and to smectic-like monolayer (tilting).

Formation of trilayer by lifting and roll-over mechanism schematically is presented in Figure 46. Generally, in my studies, the monolayers of gaseous and expanded liquid

phases with aromatic cores lying flat on the water surface were found for all bolaamphiphilic compounds at relatively low surface pressure.[110] This arrangement is denoted as a Lam-like monolayer in Figure 46. Lamellar phases (Lam phases) represent a special type of smectic liquid crystalline phases whereby the aromatic cores are arranged parallel to the smectic layers.[89,111-113] Figure 46 shows that upon further increase of the surface pressure, depending on the molecular structure, either triple-layer formation or monolayer structure was retained while the molecules changed their orientation to a tilted or vertical orientation (this situation will be described later).

The BAM images (presented in Figure 38) in the plateau region show the coexistence of two liquid phases of very different thickness. This is in line with the proposed formation of closely packed and well defined trilayers. Also indicates the fluidity of these layers. This fluidity seems to be responsible for the reversibility. It might be caused by the lateral attachment of the chains which is highly unfavourable for crystalline packing of both the aromatics as well as the chains. The relatively short fluorinated segments seem to further distort the packing of the lipophilic molecular segments. Hence, these short fluorinated segments increase the flexibility of the layers allowing fast reorganization of the molecules during compression and expansion.

The trilayer formation was verified by X – ray reflectivity (XRR) measurements of transferred films, measured by Jan Paczesny. In my dissertation I will refer to his experimental results (exactly to film thickness obtained from his measurements) so as to additionally support the proposed Langmuir film structure. For compounds X2 and X3 the monolayers was transferred at the surface pressure below the plateau (at π = 15 mN/m). The expected trilayer was transferred well above the plateau, but below the next singularity in the isotherm (at π = 30 mN/m). The layer transferred before the plateau region has a thickness of d_1=1.43 nm in case of compound X2, and d_1=1.65 in case of compound X3.

These values are in good agreement with a monolayer structure where the terphenyls lie flat on the surface and the two lateral chains are organized on top of the layer formed by the bolaamphiphilic cores. The film transferred at surface pressure π = 30 mN/m has a thickness of d_2=4.07 nm for compound X2, and d_2=4.76 for compound X3. Values of the layer thickness obtained for these compounds correspond to approximately three times the thickness of the monolayer film transferred at π = 15 mN/m. This ratio confirms that a well-defined trilayer is formed in the plateau region (d_2 : $d_1 \approx 3$). The same conclusion can be drawn for compounds X1 and X4. When the trilayer films of the X – shaped compounds are compressed further the well defined and ordered multilayers with a thickness of 5- and 7-layer are created.[114]

The study of the Langmuir monolayers of the bolaamphiphiles with longer rigid cores is given below. Compounds X5 and X6 consist of linear rigid cores which are significantly longer than in compounds X1 – X4, due to the two additional ethinyl groups introduced between the benzene rings. A comparison of the shorter compound X3 with the longer compound X6 is shown in Figure 47a. The isotherms of compounds X5 and X6 showing two compression/expansion cycles for each compound are presented in Figure 47b. The BAM images acquired for X6 at the most interesting parts of compression and decompression cycles are shown in Figure 47c and 44d.

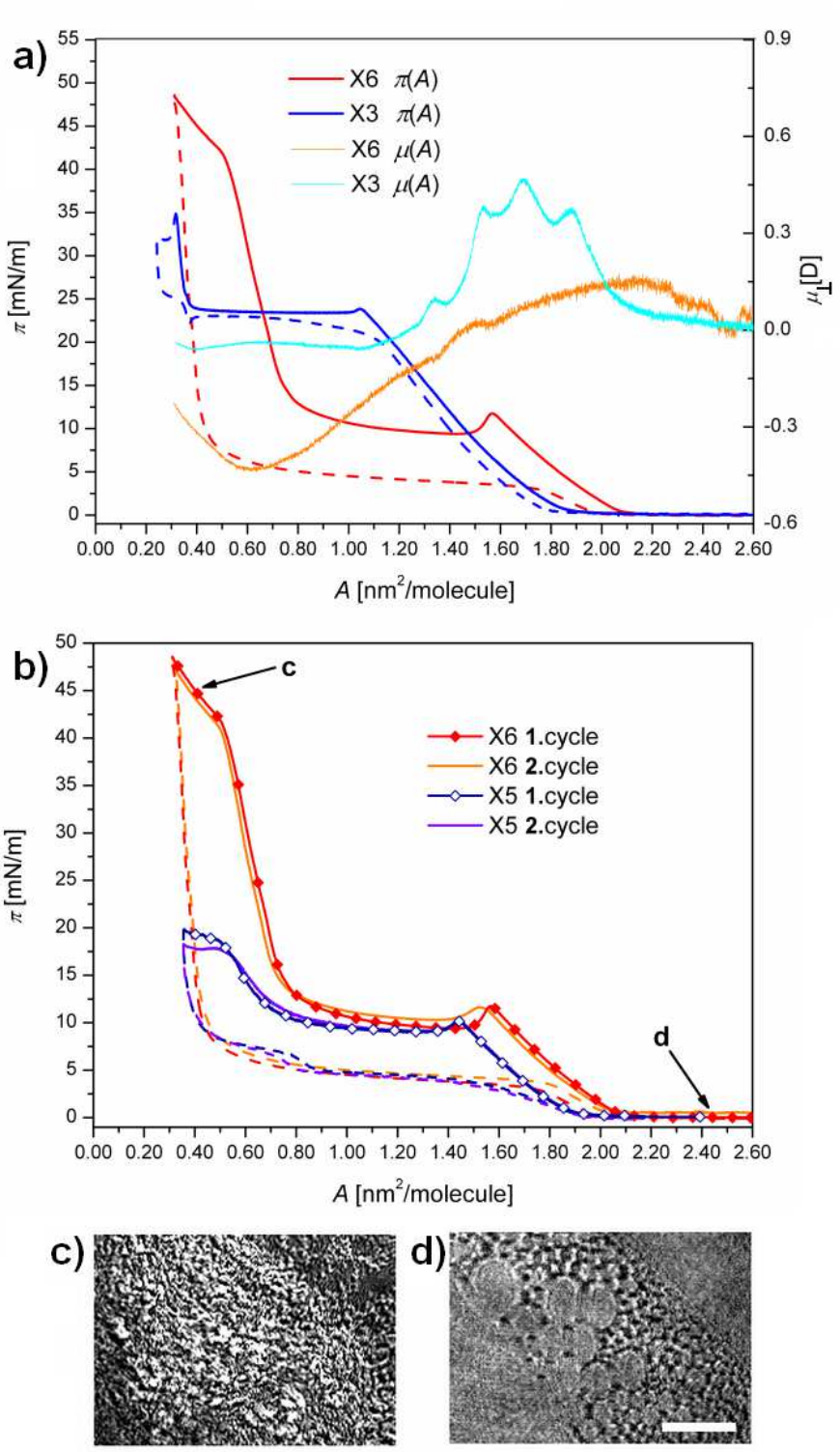

Figure 47 The comparison of two pairs of compounds, a) with different rigid cores and b) with different degree of fluorination in one lateral chain; a) the isotherms of compression (solid lines) and decompression (dashed lines) runs and the curves of vertical component of molecular dipole moment for X3 and for X6; b) two cycles of compression/decompression runs of two compounds with phenylene ethinylene based rigid core and different side chains are shown for comparison; c) shows the aggregates of X6 after compression beyond collapse and d) shows the coexistence of liquid and gas phases (2D foam) recovered after decompression; white scale bar in image d) shows length of 400 μm.

The isotherm cycle of compound X6 exhibits strong hysteresis (in spite of the presence of a partially fluorinated chain), which makes it distinct from compound X3 showing completely reversible isotherms. In addition to a reduced reversibility, also the shape of the isotherms of compounds X5 and X6 (compared in Figure 47b) is different from those of compounds X1 – X4. Compound X6 contains one partially fluorinated chain which is much longer than the hydrocarbon chain. The compound X5 has two relatively short hydrocarbon chains of the same length. The isotherms of both compounds are rather similar, but the film of the fluorinated compound X6 is more stable and it can be compressed to much higher surface pressure than the non-fluorinated compound X5. Though both compounds exhibit strong hysteresis (no reversibility), the reproducibility is still very good. The second compression curve nearly exactly follows the first one.

Analysis of the areas per molecule (A_1 and A_2) at both ends of the plateau for X6 resulted in a relation $A_1 \approx 2 \cdot A_2$ at $\pi \approx 10$ mN/m which is not compatible with trilayer formation and would suggest formation of bilayer. The film of X6 was transferred onto silicon wafers at $\pi = 8.5$ mN/m and at $\pi = 15.0$ mN/m using Langmuir-Blodgett technique. XRR measurements were performed (by Jan Paczesny) on these samples to estimate the thickness of the films. Values of the layer thickness obtained for compound X6 are equal to $d_1 = 1.57$ nm for the monolayer and $d_2 = 3.51$ nm for the layers transferred in the plateau region. The single layer thickness d_1 is very similar to that one measured for compound X3 ($d_1 = 1.65$ nm) whereas d_2 is much smaller than the related value of X3 ($d_2 = 4.76$ nm). The very different ratios $d_2 : d_1$ measured for X3 and X6 confirm that while compound X3 with a shorter terphenyl-based aromatic core creates a trilayer, the X-shaped compound X6 with a longer π – conjugated core forms a different structure in the plateau region.

Another difference between compounds X1 – X4 and X5 – X6 was found for the surface pressure at the first break in the π-A isotherms. This surface pressure is much lower

for compound X6 than observed for compounds X1-X4, although X6 has the longest fluorinated tail. Apparently, the surface pressure required for the trilayer formation is not reached for the Langmuir films of X6 and a different process, requiring less energy takes place. This is also manifested by the different shape of the $\mu_{\perp}$-*A* isotherm (Figure 47a) in the plateau region.

In the light of the results obtained from analysis of the areas per molecule, $\mu_{\perp}$-*A* isotherm and the film thickness, there is a second possible explanation for e.g. reducing the area per molecule at the air – water interface. Namely reorganization of the molecules within the monolayer. At low surface pressure compound X6 behaves like the X – shaped amphiphiles X1 – X4. The compound X6 adopts an arrangement parallel to the surface with both glycerol units attached to the water surface. However, for compound X6 this arrangement seems to be less stable at increased surface pressure, so that no trilayer is formed. Instead, a reorganization of the molecules by tilting, as observed in Figure 46 takes place. Additional information was gained from the comparison of the shapes of dipole moment curves recorded for compounds X3 and X6 (Figure 47a). If a monolayer-bilayer transition takes place in the plateau region the dipole moments of the molecules in the lower and upper layers should perfectly compensate. The $\mu_{\perp}$-*A* curve in this part should be a straight line extrapolated to the coordinate $\mu_{\perp}(A = 0) = 0$. In contrast, for compound X6 with a longer rod – like core the dipole moment curve continuously decreases after the first kink in the π-*A* isotherm. The dipole moment curve decrease continues until the second kink is reached (Figure 47a). Since $\mu_{\perp}$-*A* becomes negative at the first kink it indicates that there is a significant contribution of fluorinated chains organized, on average, perpendicularly to the surface. It supports the idea that for compounds X5 and X6 (compared in Figure 47b) no triple- or double layer is formed in the plateau region. I conclude that the monolayers are

retained and a reorganization of the molecules to a randomly tilted or vertical orientation of the aromatic cores takes place (like presented in Figure 46).

The distinct behaviour of compounds X1 – X4 on the one hand and X5 – X6 on the other hand can be explained by the distinct effect caused by the longer aromatic cores on the self-assembly behaviour. As the distance between lateral chains and polar groups is larger in compounds X5 and X6 with longer aromatic cores the influence of the lateral chains on the interaction of the polar groups with the water surface is reduced. Moreover, in compound X6 the disturbing effect of the shorter non-fluorinated alkyl chains is smaller and the glycerol group adjacent to this chain is less distorted than the glycerol group adjacent to the longer fluorinated chain. Therefore, upon film compression the shorter alkyl chains can be easily removed from the water surface and one of the polar groups (the one besides the shorter chain) becomes less distorted than the other one. Hence, the amphiphilic character of the molecules changes: at low surface pressure they behave as symmetric bolaamphiphiles (like compounds X1 – X4) retaining an orientation parallel to the surface which is stable up to π = 10 mN/m (Figure 46). However, at higher surface pressure after the first kink in the isotherm, they behave as non-symmetric bolaamphiphiles. Starting from this point a rearrangement takes place in the monolayers to an orientation tilted or perpendicular to the air water interface (Figure 46). The long semi-perfluorinated chain in compound X6 allows the formation of a separate sublayer of segregated perfluoralkyl chains, which significantly stabilizes these monolayers. However, the presence of a long fluorinated chain seems not to be required, because the symmetric alkyl substituted compound X5 shows a very similar isotherm. It is very likely that the same kind of molecular reorganization as proposed for X6 takes place for X5, too.

4.2.2. T-shaped bolaamphiphiles

The chemical structures of two compounds belonging to the group of T – shaped bolaamphiphiles are shown in Figure 48.

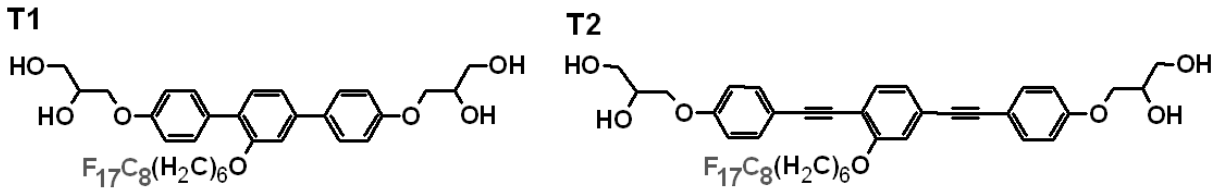

Figure 48 Chemical structures of the T – shaped bolaamphiphiles.

The chemical structures of T-shaped bolaamphiphiles are different from the X-shaped molecules because they posses only one semi – perfluorinated lateral chain. Also the π-A isotherms of compounds T1 and T2 are completely different from those recorded for the X – shaped molecules. T – shaped compounds give isotherms without plateaus. The isotherms have only one kink close to the end of the isotherms close to A = 0.40 nm^2/molecule.

The isotherms of T – shaped compounds was recorded at temperature 23ºC. The π-A curves are presented in Figure 49 together with the BAM images of the monolayer in particular stages of compression. Comparison of the isotherms of compounds T1 and T2 (Figure 49a) shows that the increase of surface pressure ("take-off" point) occurs at a little bit higher area per molecule for T2 compound. But surprisingly, the areas occupied by these two molecules at higher surface pressures, as estimated from the π-A isotherms, are nearly identical for both compounds (A = 0.39 nm^2/molecule), though they have a very different length. The compound T1 has a p-terphenyl core (L = 2.48 nm as measured between the ends of the primary OH groups in a most extended conformation). The compound T2 with two additional ethinyl groups has a longer core (L = 2.95 nm).

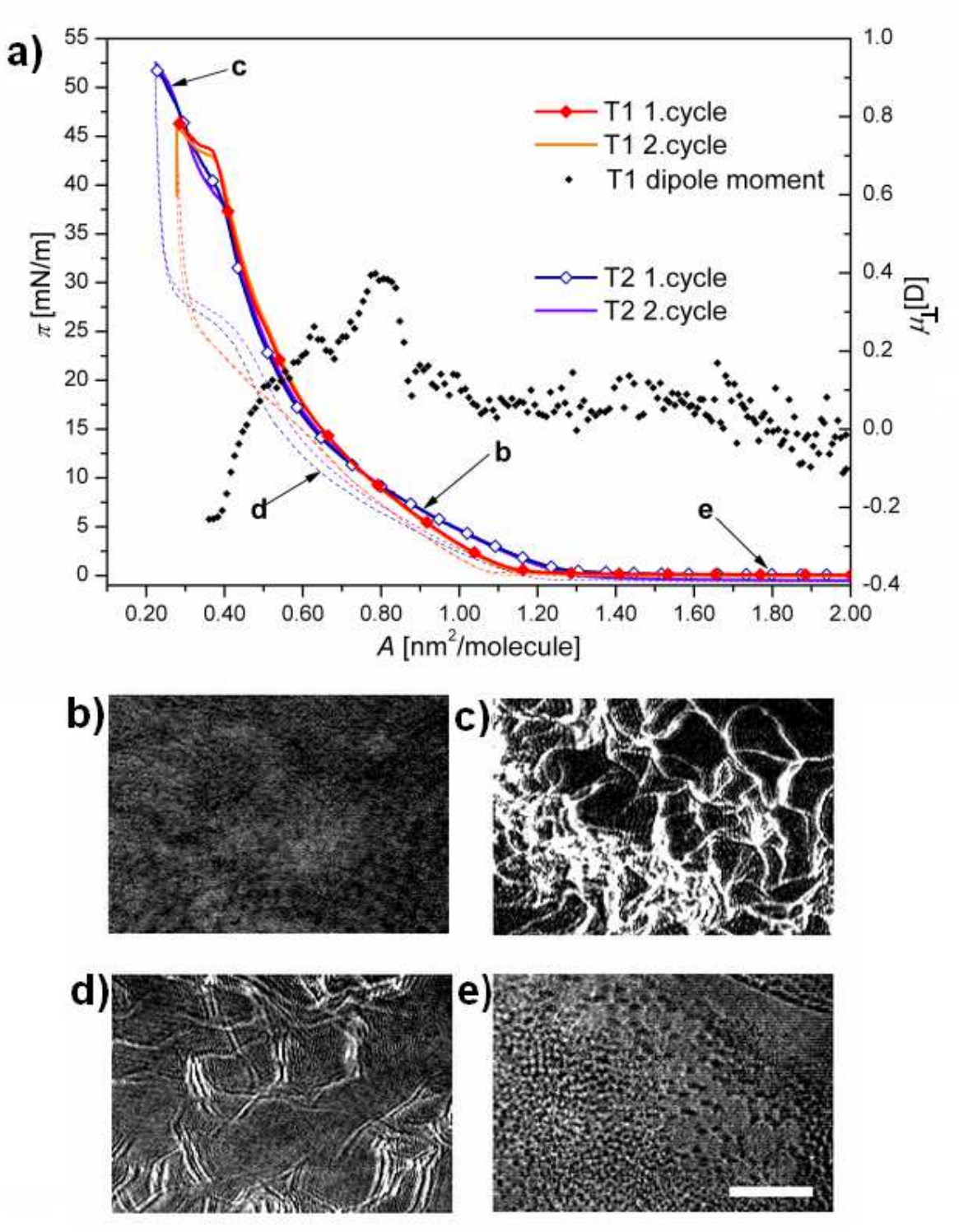

Figure 49 The $\pi(A)$ isotherms of compounds T1 and T2: two cycles of compression (solid lines) and decompression (dashed lines) as well as the dipole moment changes for compound T1 are shown in graph a). The BAM images for compound T2 are given as examples: letters b - e mark the conditions at which the BAM images, also marked as b) - e), were recorded; b) the uniform monolayer during compression, c) the aggregates formed after compression beyond collapse, d) aggregates disappearing during decompression, e) coexistence of liquid and gas phases (2D foam) recovered after decompression to π = 0; white scale bar in image e) shows length of 400 μm.

Surface potential (ΔV) measurements, presented as a vertical component of dipole moment changes, $\mu_{\perp}$-A is shown in Figure 49a for compound T1 as an example. When the surface pressure exceeds π = 10 mN/m a sudden decrease of the dipole moment appears. The decrease of $\mu_{\perp}$-A is most probably caused by rising up of the fluorinated lateral chains. It provides a negative dipole moment. Upon compression above π = 10 mN/m the fluorinated chains should adopt an orientation more or less perpendicular to the surface. This is not in line with a trilayer formation where the symmetric bilayer on top of the monolayer should not significantly contribute to the dipole moment. This behavior of the dipole moment upon compression is the same as observed for the X – shaped molecules X5 and X6. The value of films thickness transferred onto silicon wafers at π = 33 mN/m gave d = 2.70 nm and d = 2.76 nm for compounds T1 and T2, respectively. These values are significantly smaller than expected for trilayers, but very close to the length of the rigid bolaamphiphilic moiety (T1: L = 2.48 nm; T2: L = 2.95 nm as estimated from CPK model).

Hence, the explanation of the organization of the T – shaped molecules T1 and T2 at the air – water interface is proposed as follows. At the beginning of compression the molecules are organized with the rod-like cores and the lateral chains parallel to the air-water interface (like in Figure 46). Upon further compression the molecules remain in a liquid-like state and reorganization takes place by detachment of one of the polar groups from the water surface. One of the glycerol groups retains contact to the water surface whereas the other one at the opposite end of the bolaamphiphilic molecule is detached from the surface. The molecules adopt a randomly tilted on average vertical configuration of the rod-like cores. The reorganization of the molecules T1 and T2 by tilting is similar to that observed for the the X – shaped molecules X5 and X6. The cross section of one molecule estimated from the isotherm in Figure 49a is equal to approx. 0.39 nm^2. This value seems to be consistent with the proposed organization of the molecules on average perpendicular to

the air-water interface. The cross section of the fluorinated part of the chain[115] is 0.285 nm^2 and the cross section of the terphenyl moiety is less than 0.20 nm^2. Hence, there is enough space for an on average vertical or slightly tilted arrangement of the rigid cores with the partially fluorinated lateral chains organized in the space between the rod-like cores.

The topology of connection of the lateral chain to the rigid aromatic core could be responsible for this kind of behaviour. In the "T-shaped" molecules the lateral chain is actually attached at an angle of 60° to the aromatic core. This configuration provides a rod-like shape rather than a true T-shape for these molecules (Figure 36). The lateral chain is closer to one of the polar glycerol groups and restricts the interaction of this polar group with the water surface. As a consequence, both polar groups are non-equivalent. This non-equivalence seems to allow an easy detachment of one of the polar group from the water surface, this one which is closer to the lateral hydrophobic chain. The second polar group at the opposite end of the rod – like core stays in water subphase. As a result, upon compression, the aromatic cores adopt a tilted or even vertical orientation with respect to the water surface.

The π-*A* isotherms of compounds T1 and T2 show strong hysteresis during compression/decompression cycles. The compression runs show perfect reproducibility because in a second and the subsequent cycles identical compression curves were obtained (for clarity only two cycles for each compound are shown in Figure 49). Examples of BAM images, recorded during compression/decompression runs of compound T2 confirm reversible aggregation of the molecules. Reversible aggregation does not mean reversibility of the isotherm in a meaning presented in discussion of X1 – X4 compounds. Here, 3D aggregates appear only after the kink (Figure 49c) and disintegrate during decompression (Figure 49d) to disappear completely after decompression to π = 0 mN/m. Disintegration occurs during decompression at surface pressures of approximately 15 mN/m and 25 mN/m

for T1 and T2, respectively, but this very slow process is visible as inflection points on the curves of decompression. Reversible aggregation manifests just as a reproducibility of the isotherms (repeatable subsequent cycles). The reappearing liquid phase forms a two-dimensional foam at π = 0 mN/m, as shown in Figure 49e.

4.2.3. Anchor-shaped bolaamphiphiles

The compounds A1 – A3 (presented in Figure 50) as distinct from other bolaamphiphilic molecules posses different arrangement of benzene rings. These molecules resemble a shape of an anchor because a single aliphatic chain is attached to a bent rigid core at the central phenyl ring inside an angle created by the arms of the core.

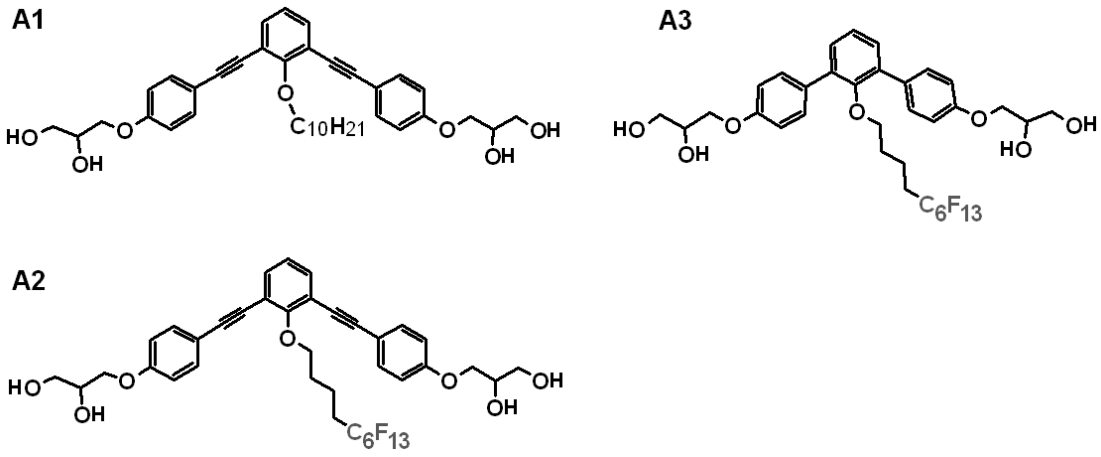

Figure 50 Chemical structures of the Anchor – shaped bolaamphiphiles.

All compounds A1, A2 and A3 exhibit isotherms with broad plateaus similar to compounds X1-X6. Figure 51 presents the comparison of isotherms of compounds A1 and A2, because these bolaamphiphiles have the same rigid cores and the same length of aliphatic chains. The only difference between them is that the chain in compound A1 is fully hydrogenated whereas compound A2 contains a fluorinated C_6F_{13} segment at the end of the chain.

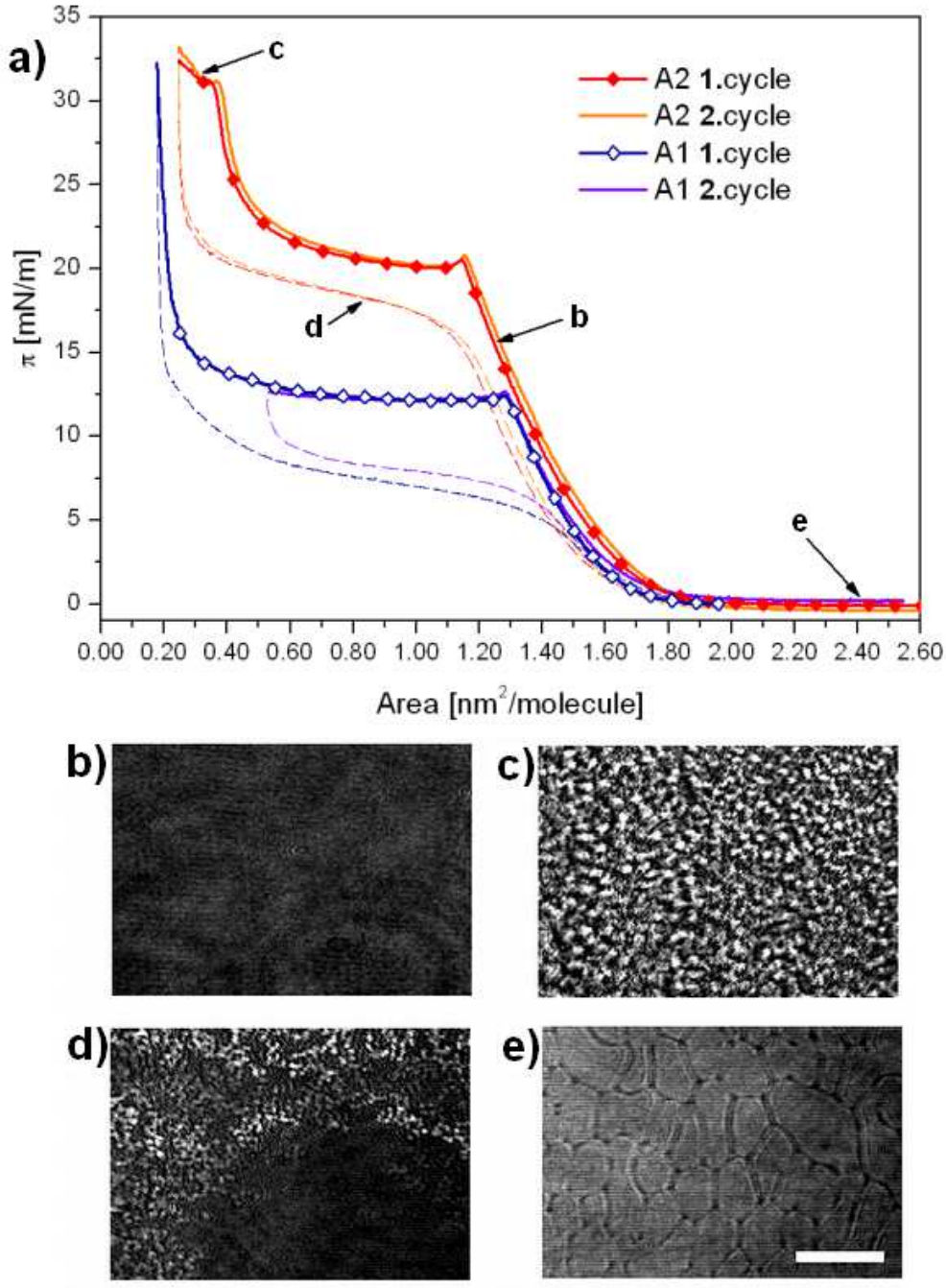

Figure 51 Isotherms of compounds A1 and A2: two cycles of compression (solid line) and decompression (dashed lines) are shown in (a); letters b - e mark the conditions at which the BAM images for compound A2 (also marked as b - e) were recorded; image b shows the uniform monolayer during compression of homogenous liquid phase; image c shows the aggregates formed after compression beyond collapse; image d shows aggregates disappearing during decompression; image e shows coexistence of liquid and gas phases (2D foam) recovered after decompression to $\pi = 0$; white scale bar in image e shows length of 400 μm.

The first increase of surface pressure ("take-off" point) occurs at a the same area per molecule for compound A1 as well as compound A2. It means that the molecules are arranged identically in case of both monolayers. Extrapolation of the compression curves to

$\pi = 0$ gives the molecular area $A_0 = 1.70$ nm^2. It allows for a conclusion that the bent aromatic cores lay flat on the water surface with the bent parallel to the surface. The molecules are fixed on the surface by the two glycerol groups and the ether oxygen carrying the lateral chain.

The films of compound A2 were transferred onto silicon wafers at π = 20 mN/m (before reaching the plateau) and at π = 30 mN/m (before the second transition). Values of the layer thickness are equal to d_1 = 1.43 nm and d_2 = 3.71 nm, respectively. The value of d_1 = 1.43 nm is also in good agreement with the thickness of a model monolayer formed by the aromatic cores lying flat on water with the disordered fluid semi – perfluorinated chains covering these aromatics.

The area at the beginning of the plateau is amount to 1.16 nm^2/molecule. This value is smaller than the area required by the X-shaped amphiphile X6 comprising a similar, but linear core. The difference between areas of A2 and X6, measured at the same surface pressure π = 9.4 mN/m, is about 0.2 nm^2/molecule, which agrees well with the additional space required by the second OCH_2 group of compound X6. The second increase of the surface pressure at the end of the plateau of compound A2 starts at an area of 0.43 nm^2/molecules and ends at A = 0.4 nm^2/molecule. Hence, the comparison of the areas per molecule at both ends of the plateau leads to a ratio which is equal to 2.7. This value allows for a conclusion that the molecules of compound A2 create trilayer in the plateau region.

The trilayer formation in the plateau region is in line with the ratio d_2 : d_1 = 2.6 (d_1 = 1.43 nm and d_2 = 3.71 nm) obtained from thickness measurement. The fact that the ratio d_2: d_1 is a bit smaller than exactly three could be explained by some intercalation of the lateral chains in the formed trilayer structure.

There is a second possibility of molecular reorganization at the plateau region Namely a reorganization of the molecules in the monolayers by adopting, on average, a

perpendicular organization similar to compounds X5 and X6. The value of monolayer thickness expected for vertical alignment (estimated from CPK model) would give d = 2.7 nm, which is much smaller than the thickness d_2 = 3.71 nm obtained from X – ray reflectivity measurement. Therefore, it allows to conclusion that in the plateau region of the isotherm of compound A2 a trilayer formation occurs. The proposed trilayer formation is also in line with the surface potential measurements. The isotherms of surface pressure π, and vertical component of dipole moment $\mu_\perp$ are shown in Figure 52.

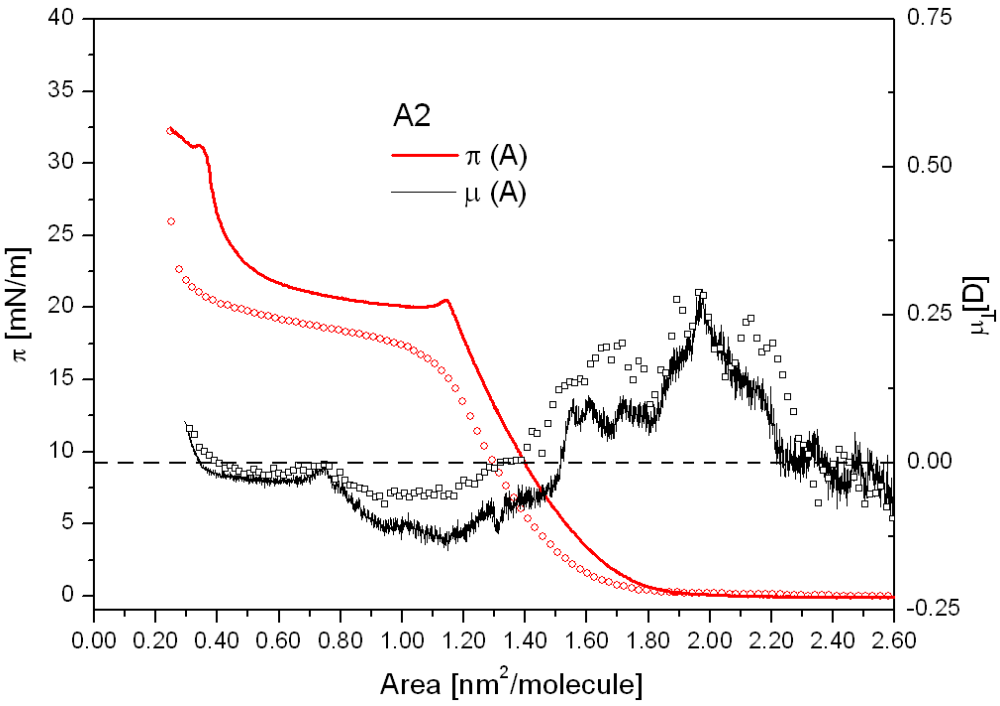

Figure 52 Isotherms of surface pressure, π, and vertical component of dipole moment, $\boldsymbol{\mu}_\perp$, *vs.* molecular area, *A*, for anchor-shaped compound A2: lines correspond to compression and open symbols to decompression runs.

In the case of a transition to a monolayer with molecules organized perpendicularly to the surface a decrease of the dipole moment, as observed for compounds T1/T2 and X5/X6 would be expected due to the negative contribution of the terminal C – F bond of vertically aligned R_F segments. The surface potential measurement, in case of compound A2, indicate a increase of dipole moment in the plateau region. Therefore I reject

reorganization of the molecules in the monolayers by adopting a vertical alignment and assume a trilayer formation.

The BAM image in Figure 51c shows a rough surface of the film after breakdown of the trilayer at the second kink in the isotherm curve. During decompression the trilayer cannot be recovered, so in the image in Figure 51d the coexistence of the trilayer with aggregates and the monolayer can be observed. The shape of the domains and the fact that their size diminishes during expansion allows to conclude that the trilayer is still in the liquid state. It is one of the reasons why the isotherm, although irreversible (because of small hysteresis), is perfectly reproducible in subsequent compression.

For compound A1 with a non-fluorinated n-alkyl chain the second increase of surface pressure occurs at an area per molecule much smaller than for A2 (Figure 51a). This area is smaller than the value estimated from CPK model for single molecule in monolayer. The surface pressure increase at non-realistic value of molecular area is typically observed for completely disordered films, suggesting that disorganized aggregates are created also in this case. In this region the curve of dipole moment is a nearly straight line going through zero, what means that all dipole moments compensate because of completely random aggregation. Figure 53 presents the isotherms of surface pressure π, and vertical component of dipole moment $\mu_{\perp}$.

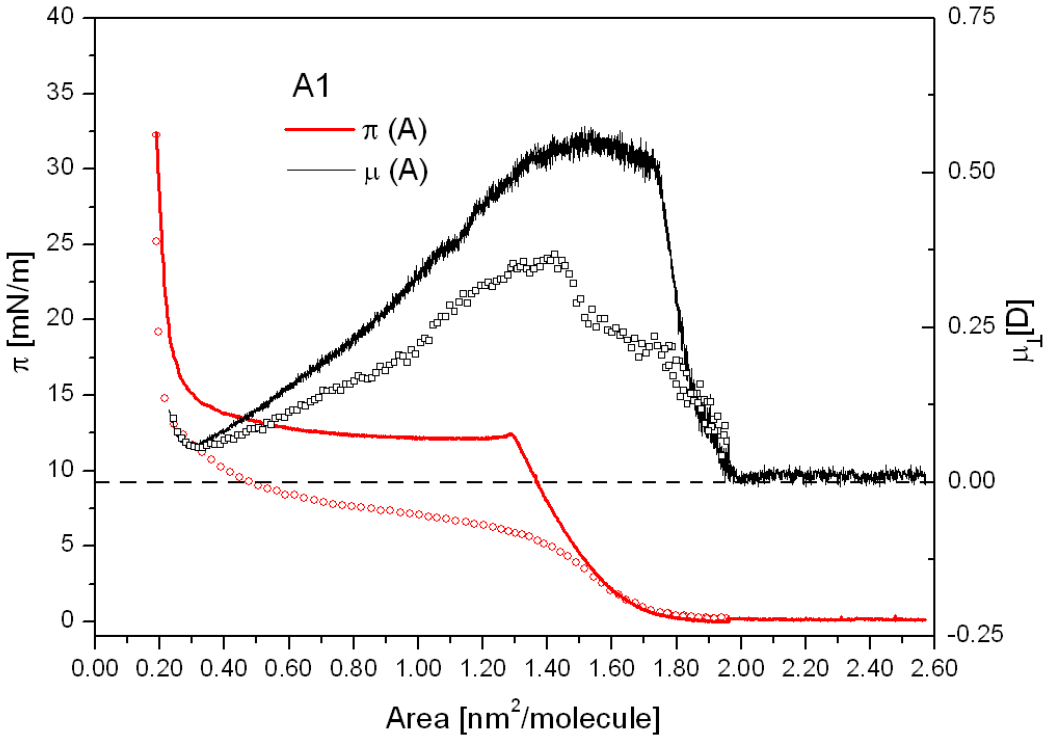

Figure 53 Isotherms of surface pressure, π, and vertical component of dipole moment, $\boldsymbol{\mu}_{\perp}$, *vs.* molecular area, *A*, for anchor-shaped compound A1: lines correspond to compression and open symbols to decompression runs.

Hysteresis between compression and decompression runs is here much stronger than in the case of A2. The second compression perfectly overlaps with the first one showing a perfect reproducibility, too. It means that the aggregation is reversible after decompression of the film to "zero" pressure and the aggregates need time for disintegration.

As it is shown in Figure 51a, the surface pressure at which the monolayers lose their stability is higher for the fluorinated compound A2. This observation shows that partial fluorination makes the interaction with the water surface stronger. Comparison of the isotherms of compounds A1 and A2 (Figure 51a) shows also that the partial fluorination of the lateral chain in the case of anchor-shaped molecules increases its tendency for self organization into trilayers, but it is not affecting the reproducibility in this case.

Compound A3 has the same fluorinated lateral chain as compound A2, but its rigid core consists of a m-terphenyl moiety, so this part of the molecule is smaller than the cores

of compounds A1 and A2. The isotherms of surface pressure π, and vertical component of dipole moment $\mu_{\perp}$, as a function of area per molecule *A*, measured at temperature 23ºC, are shown in Figure 54.

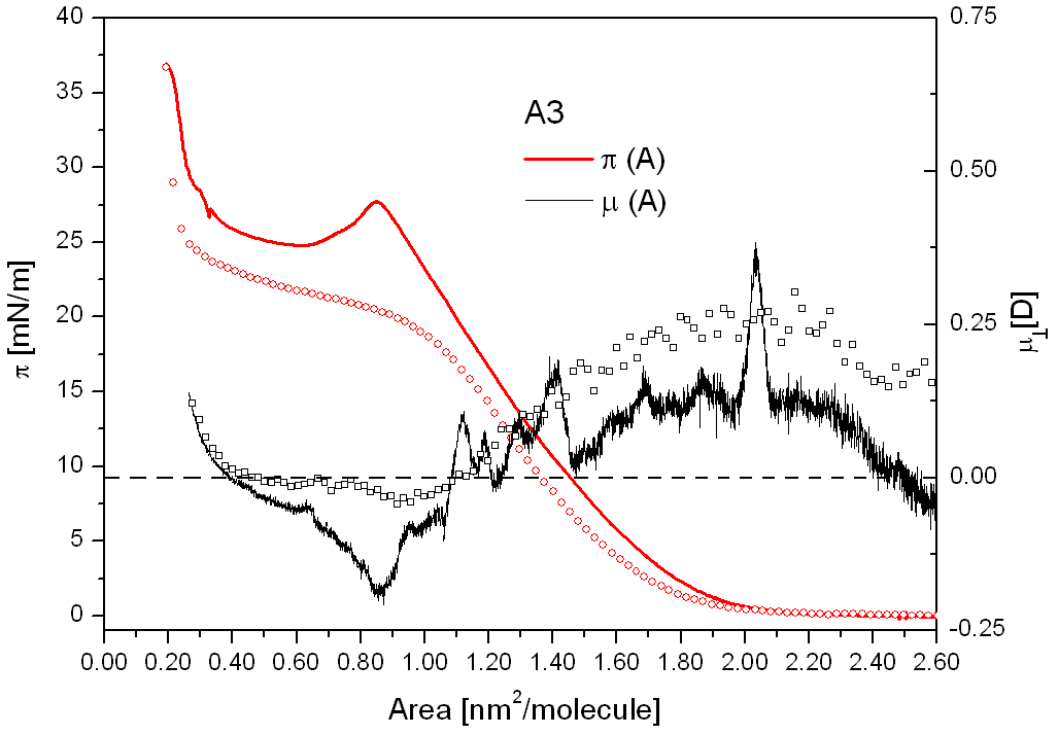

Figure 54 Isotherms of surface pressure, π, and vertical component of dipole moment, $\boldsymbol{\mu}_{\perp}$, *vs.* molecular area, *A*, for anchor-shaped compound A3: lines correspond to compression and open symbols to decompression runs.

Compound A3 has a compression isotherm very similar to the one of compound A2, but with reduced molecular areas at the transition. It shows that this compound also creates a trilayer during compression.

The fact that anchor shaped compounds form Langmuir films similar to the X-shaped molecules, but distinct from those of T-shaped molecules, could partly be due to the equal distance of the lateral chain from both polar groups in the anchor shaped bolaamphiphiles. As a consequence, both polar groups are equivalent and for that the easier detachment of one of the polar gropup from the subphase does not appear. In addition, the combination of bent shape and substitution inside the bay area between the rod-like wings distorts a parallel

alignment of these cores. Hence, the formation of vertical or tilted (to the air – water interface) arrangement of the rigid cores becomes more difficult. Therefore, upon film compression a Lam-like trilayer organization with the cores parallel to water surface becomes more favourable in this case.

5. Summary and conclusions

In my dissertation I present results for two groups of compounds, ferrorelectric and bolaamphiphilic liquid crystals, spread on water surface. Employing techniques such as Brewster angle microscopy, surface pressure and surface potential measurements, yielded the characterization of the structures of the Langmuir films in both cases.

In the first part of experimental section I present the results of my study of monolayers of four ferroelectric liquid crystals at the air-water interface. The studies show that only two them (the compounds B and C) create textures of circular stripe patterns, observed using Brewster angle microscopy. These patterns arise from collective rotation of molecules driven by water evaporation through the monolayer. The compounds B and C are attached to water surface by their polar groups, and the chiral groups, at the opposite ends of the elongated molecules, remain well above the interface. The other two ferroelectrics (the compounds A and D) have both groups (polar and chiral) at close proximity, and therefore the chiral group is also attached to the surface or even submerged in water. I conclude that necessary requirements for the molecules to be able to exhibit the collective rotations are:

(i) the nonpolar chiral group and the strongly polar group should be attached to the opposite ends of the rod-like core of the molecule;

(ii) the chiral group should not be immersed in a subphase;

(iii) the molecules in the monolayer should be tilted, but attached to the water surface with one terminal group, preferably at some distance from the chirality center.

Typical time of rotation of a single molecule is in the range $10^{-12} – 10^{-9}$ s.[3] I observed in Langmuir monolayer the time of rotation up to 500 seconds, fourteen orders of magnitude slower than the one for a single molecule.

The rate of rotation was examined under variety of water temperatures, in the range of 12 – 39°C. The experiments shows that the rotation frequency depends on subphase temperature and at low temperature, when the driving force for rotation is reduced, the speed of collective rotation decreases. In my dissertation I conclude that the slowing down of collective rotation upon decrease of temperature is caused by two–dimensional chiral smectic–C to solid–like phase transition.

In the second part of my work I present the studies of 11 compounds from the group of specific surfactants known as bolaamphiphiles. The molecules of different shape (X-, T-, and anchor shaped) were studied. Some of these compounds have a fluorinated lateral chains and some are non-fluorinated. The research shows that the bolaamphiphiles create on water surface stable and well organized Langmuir monolayers and multilayers. The most interesting feature of the compounds is that partially fluorinated bolaamphiphiles exhibit an unusual reversibility and reproducibility of Langmuir isotherms in spite of the compression to complete collapse of the film and even for the highest possible compression/decompression rate. The presence of fluorinated chain prevents from chaotic aggregation of the compound belonging to the group of rod-like liquid crystal. The studies of compound 8OCB with and without fluorinated fragment of chain show that the partial replacement of hydrogen by fluorine in the aliphatic chain significantly improves the reproducibility of the monolayer. The balance between rigidity and flexibility of the molecules, adjusted by partial fluorination and the shape of the molecules, seems to be the key factor to avoid irreversible aggregation of the molecules.

For all bolaamphiphilic compounds the densely packed monolayers were formed with the aromatic cores laying flat on the air/water interface. Further compression either leads to formation of well defined trilayers (layering transition) or by reorganization of the cores into, on average, vertical orientation. It seems that the degree of distortion of the polar groups attached to the ends of the rigid π-conjugated cores by the laterally attached hydrophobic chains is the key factor deciding which type of reorganization is observed in the monolayer. For X-shaped bolaamphiphiles with two relatively long lateral chains of approximately equal length, triple layer formation is dominating. If one chain is removed (T-shaped bolaamphiphiles) the two polar groups at the opposite ends become distinct and these bolaamphiphiles preferably organize with their anisometric cores perpendicular to the surface with the less hindered polar group acting as an anchor group. Even slight modification of the molecular structure of the two fundamental types of bolaamphiphiles (T-shaped and X-shaped) can change the self-assembly behaviour dramatically. For example, an elongation of the rigid core of X-shaped compounds reduces the degree of distortion of the polar groups by the lateral chains and gives rise to reorganization of the monolayers by changing the molecular orientation (compounds X5 and X6). On the other hand, bending the rod-like core of T-shaped molecules (leading to the anchor-shaped compounds) makes the two polar groups equivalent which favours formation of trilayer without changing the orientation of the molecules.

In summary, the most important results of my PhD thesis are:

- Evaporation of subphase across a chiral liquid crystalline monolayer can drive collective molecular precession.
- *Only when the chiral group of the ferroelectric liquid crystal in the Langmuir monolayer is not attached to the water interface and stays in the air the system exhibit collective rotation.* This is original conclusion not found in previous papers.

- In Langmuir monolayer the time of rotation is unusually much slower than for single molecule, lasts even 8 minutes.
- Additional slowing down of collective rotation at low temperatures is caused by two – dimensional chiral smectic – C to solid – like phase transition.
- X –, T – and anchor – shaped bolaamphiphiles create on water surface stable and well organized Langmuir monolayers and multilayers.
- *The compounds with fluorinated segments give perfectly reversible and reproducible isotherms in spite of the compression to complete collapse of the film. Partial fluorination of the lateral chains prevents the monolayers from chaotic aggregation.*
- Depending on shape and degree of fluorination compression leads to transition with trilayers formation (layering transition) or to reorganization into vertical orientation.

6. References

[1] K.S. Birdi. Lipid and biopolimerr monolayers at liquid interfaces. Plenum, 1989.

[2] V. M. Kaganer, H. Möhwald, P. Dutta. Structure and phase transitions in Langmuir monolayers. *Rev. Mod. Phys.* **1999**, *71*, 779.

[3] J. A. Janik, M. Godlewska, T. Grochulski, A. Kocot, E. Sciesinska, J. Sciesinski, W. Witko. Molecular Reorientation in Liquid Crystals. *Mol. Cryst. Liq. Cryst.,* **1983**, *98*, 67-81.

[4] H. Stegemeyer, Guest Ed. Liquid Crystals. Darmstadt: Steinkopf, New York: Springer, 1994.

[5] P. Oswald, P. Pierański, Nematic and Cholesteric Liquid Crystals, Taylor & Francis Group, 2005.

[6] S. Chandrasekhar, Liquid Crystals, Cambridge University Press, 1977.

[7] P. J. Collings, Liquid Crystals, Adam Hilger, Bristol, 1990.

[8] R. Hołyst, A. Poniewierski, A. Ciach. TERMODYNAMIKA DLA CHEMIKÓW, FIZYKÓW I INŻYNIERÓW. Wydawnictwo Uniwersytetu Kardynała Stefana Wyszyńskiego, Warszawa 2005.

[9] S. Singh. LIQUID CRYSTALS: FUNDAMENTALS. World Scientific, 2002.

[10] C. Tschierske. Liquid crystal engineering – new complex mesophase structures and their relations to polymer morphologies, nanoscale patterning and crystal engineering. *Chem. Soc. Rev.*, **2007**, *36*, 1930-1970

[11] U. Beginn. Thermotropic columnar mesophases from N–H· · ·O, and N· · ·H–O hydrogen bond supramolecular mesogenes. *Prog. Polym. Sci.* **2003**, *28*, 1049–1105

[12] R. J. Bushby, O. R. Lozman. Discotic liquid crystals 25 years on. *Current Opinion in Colloid & Interface Science*, **2002**, *7*, 343-354.

[13] F. Seitz, D. Turnbull. Solid State Physics. Vol. 4. Academic Press, 1957.

[14] K.M. Rabe, Ch.H. Ahn, J.-M. Triscone. Physics of ferroelectrics: a modern perspective. Springer, 2007.

[15] J.A. Gonzalo, B. Jiménez. Ferroelectricity: The Fundamentals Collection. Wiley-VCH, 2005.

[16] R.B. Meyer, L. Liebert, L. Strzelecki, P. Keller. Ferroelectric liquid crystals. J. Physique Lett. **1975**, *36*, 69-71

[17] R.B. Meyer. Ferrorelectric Liquid Crystals – A Rewiev. *Mol. Cryst. Liq. Cryst.*, **1977**, *40*, 33-48.

[18] P. J. Collings. Ferroelectric liquid crystals: The 2004 Benjamin Franklin Medal in Physics presented to Robert B. Meyer of Brandeis University. Journal of the Franklin Institute, **2005**, *342*, 599-608

[19] P. Oswald, P. Pierański, Smectic and Columnar Liquid Crystals, Taylor & Francis Group, 2006.

[20] N. A. Clark, S. T. Lagerwall. Submicrosecond bistable electrooptic switching in liquid crystals. *App. Phys. Lett*. **1980**, *36*, 899.

[21] B. Franklin. Of the Stilling of Waves by means of Oil. Extracted from Sundry Letters between Benjamin Franklin, LL. D. F. R. S. William Brownrigg, M. D. F. R. S. and the Reverend Mr. Farish. *Phil. Trans.* **1774**, *64*, 445.

[22] I. Langmuir. The constitution and fundamental properties of solids and liquids. II. Liquids. *J. Am. Chem. Soc.* **1917**, *39*, 1848-1906.

[23] G.L. Gaines, Jr. Insoluble Monolayers at Liquid-Gas Interfaces. Interscience Publishers, 1966.

[24] K. B. Blodgett. Films Built by Depositing Successive Monomolecular Layers on a Solid Surface. *J. Am. Chem. Soc.* **1935**, *57*, 1007-1022

[25] P. Alexandridis, B. Lindman. Amphiphilic Block Copolymers: Self-Assembly and Applications. Elsevier Science B.V.,2000.

[26] P. Dynarowicz-Łątka, A. Dhanabalan, O. N. Oliviera Jr. Modern physicochemical research on Langmuir monolayers. *Advances in Colloid and Interface Science*. **2001**, *91*, 221-293

[27] A. Ulman. An Introduction to Ultrathin Organic Films: From Langmuir-Blodgett to Self-Assembly. Academic Press, 1991.

[28] J.-H. Fuhrhop, T. Wang. Bolaamphiphiles. *Chem. Rev.* **2004**, *104*, 2901-2937.

[29] J.-H. Fuhrhop, D. Fritsch. Bolaamphiphiles Form Ultrathin, Porous, and Unsymmetric Monolayer Lipid Membranes. *Acc. Chem. Res.* **1986**, *19*, 130-137

[30] J.-M. Kim, D. H. Thompson. Tetraether Bolaform Amphiphiles as Models of Archaebacterial Membrane Lipids: Synthesis, Differential Scanning Calorimetry, and Monolayer Studies. *Langmuir* **1992**, *8*, 637-644.

[31] A. Gambacorta, A. Gliozzi, M. De Rosa. Archaeal lipids and their biotechnological applications. World J. Microbiol. Biotechnol. **1995**, *11*, 115-131

[32] A. Jacquemeta, V. Viec, L. Lemiegrea, J. Barbeaua, T. Benvegnua. Air/water interface study of cyclopentane-containing archaeal bipolar lipid analogues. *Chemistry and Physics of Lipids* **2010**, *163*, 794-799

[33] Q. Lu, M. Liu. Spontaneous two-dimensional crystallization and photochemical reaction of a novel bolaamphiphilic naphthol ester in the spreading Langmuir film at the air/water interface and transferred Langmuir-Blodgett film. *Thin Solid Films* **2003**, *425*, 248-254

[34] J.-H. Fuhrhop, H.-H. David, J. Mathieu, U. Liman, H.-J. Winter, E. Boekemat. Bolaamphiphiles and Monolayer Lipid Membranes Made from 1,6,19,24-Tetraoxa-3,2

1 -cyclohexatriacontadiene-2,5,20,23-tetrone. *J. Am. Chem. Soc.* **1986**, *108*, 1785-1791

[35] T. Hutter, Ch. Linder, E. Heldman, S. Grinberg. Interfacial and self-assembly properties of bolaamphiphilic compounds derived from a multifunctional oil. *Journal of Colloid and Interface Science* **2012**, *365*, 53-62

[36] A. Meister, M. J. Weygand, G. Brezesinski, A. Kerth, S. Drescher, B. Dobner, A. Blume. Evidence for a Reverse U-Shaped Conformation of Single-Chain Bolaamphiphiles at the Air-Water Interface. *Langmuir* **2007,** *23*, 6063-6069

[37] L. Tamam, T. Menahem, Y. Mastai, E. Sloutskin, S. Yefet, M. Deutsch. Langmuir Films of Chiral Molecules on Mercury. *Langmuir* **2009**, *25*, 5111–5119

[38] J. Richard, A. Barraud, M. Vandevyver, A. Ruaudel-Teixier. Two-step transfer of conducting Langmuir films from a glycerol subphase. *Thin Solid Films* **1988**, *159*, 207-214

[39] G. Roberts. Langmuir-Blodgett Films. Plenum 1990

[40] J. Ignes-Mullol, J. Claret, R. Reigada, F. Sagues. Spread monolayers: Structure, flows and dynamic self-organization phenomena. *Physics Reports* **2007**, 448, 163-179.

[41] J.T. Davies, E.K. Rideal. Interfacial Phenomena. Academic Press, New York, 1961.

[42] D. Vollhardt, V.B. Fainerman. Progress in characterization of Langmuir monolayers by consideration of compressibility. *Advances in Colloid and Interface Science* **2006**, *127*, 83-97

[43] W.D. Harkins. The Physical Chemistry of Surface Films, Reinhold Publishing Co., New York, 1952.

[44] A. W. Adamson. Chemia fizyczna powierzchni. PWN, Warszawa 1963

[45] Lord Kelvin. Contact Electricity of Metals. *Phil. Mag*., **1898**, *46*, 96-98

[46] R.H. Tredgold, G.W. Smith. Surface potential studies on Langmuir-Blodgett multilayers and adsorbed monolayers. *Thin Solid Films* **1983**, *99*, 215-220

[47] S. Henon, J. Meunier. Microscope at the Brewster angle: Direct observation of first-order phase transitions in monolayers. *Rev. Sci. Instrum.* **1991**, *62*, 936-939

[48] D. Hoenig, D. Mobius. Direct visualization of monolayers at the air-water interface by Brewster angle microscopy. *J. Phys. Chem.* **1991**, *95*, 4590–4592

[49] D. Mobius. Light microscopy of organized monolayers. Curr. Op. Coll. Interface Sci., **1996**, *1*, 250-256.

[50] F. Schreiber. Structure and growth of self-assembling monolayers. *Progress in Surface Science*, **2000**, *65*, 151-256.

[51] R. Bilewicz, T. Sawaguchi, R.V. Chamberlain II, M. Majda. Monomolecular Langmuir-Blodgett Films at Electrodes. Electrochemistry at Single Molecule "Gate Sites". *Langmuir*, **1995**, *11*, 2256-2266

[52] R. Bilewicz, M. Majda. Monomolecular Langmuir-Blodgett Films at Electrodes. Formation of Passivating Monolayers and Incorporation of Electroactive Reagents. *Langmuir*, **1991**, *7*, 2794-2802

[53] A. Ulman. Formation and Structure of Self-Assembled Monolayers. *Chem. Rev*., **1996**, *96*, 1533-1554.

[54] A. Kumar, H.A. Biebuyck, G.M. Whitesides. Patterning Self-Assembled Monolayers: Applications in Materials Science. *Langmuir*, **1994**, *10*, 1498-1511.

[55] K.B. Blodgett, I. Langmuir. Built-Up Films of Barium Stearate and Their Optical Properties. *Phys. Rev*., **1937**, *51*, 964-982

[56] P. Martin, M. Szablewski. Langmuir-Blodgett Troughs. Operating Manual 6th Edition. Nima Technology LTD, 2001.

[57] I. Langmuir, V. J. Schaefer. Activities of Urease and Pepsin Monolayers. *J. Am. Chem. Soc.* **1938**, 60, 1351

[58] T. Furuno, H. Sasabe, R. Nogata, T. Akaike. Studies of Langmuir-Blodgett films of poly(1-benzyl-L-histidine)-stearic acid mixtures. *Thin Solid Films,* **1985**, 133, 141-152.

[59] Y. Tabe, H. Yokoyama. Coherent collective precession of molecular rotors with chiral propellers. *Nat.Materials.* **2003**, *2*, 806-809

[60] R. K. Gupta, K. A. Suresh, S. Kumar. Spatiotemporal patterns in a Langmuir monolayer due to driven molecular precession. *Phys. Rev. E* **2008**, *78*, 041703

[61] P. Milczarczyk – Piwowarczyk, A. Żywociński, K. Noworyta, R. Hołyst. Collective rotations of ferroelectric liquid crystals at the air/water interface *Langmuir* **2008,** *24*, 12354-12363

[62] D. Svenšek, H. Pleiner, H. R. Brand. Phase winding in chiral liquid crystalline monolayers due to Lehmann effects. *Phys. Rev. Lett.* **2006**, 96, 140601.

[63] J.-L. Gallani, C. Bourgogne, S. Nakatsuji. Layering transitions and schlieren textures in Langmuir films of two organic radicals. *Langmuir* **2004**, 20, 10062–10067.

[64] J.-L. Gallani, S. Mery, Y. Galerne, D. Guillon. Organization of a polar molecule at the air−water interface. *J. Phys. Chem. B* **2004**, 108, 11627-11632.

[65] H. C. Berg. Molecular motors: Keeping up with the F1-ATPase. *Nature (London),* **1998**, *394*, 324.

[66] R. D. Vale, R. A. Milligan. The Way Things Move: Looking Under the Hood of Molecular Motor Proteins. *Science,* **2000**, *288*, 88.

[67] M. A. Greeves. Stretching the lever-arm theory. *Nature (London),* **2002**, **415**, 129.

[68] Z. Raszewski et al. Influence of quadrupolar ordering factor on supermolecular structure in ferroelectric Sm C. *Mol. Cryst. Liq. Cryst.* **1999**, *328*, 255-263.

[69] J. Dziaduszek, R. Dąbrowski, K. Czupryński, N. Bennis. Ferroelectric compounds with strong polar cyano group in terminal position. *Ferroelectrics* **2006**, *343*, 3-9.

[70] K. Skrzypek, M. Tykarska. The induction of antiferroelectric phase in the bicomponent system comprising cyano compound. *Ferroelectrics* **2006**, *343*, 177-180.

[71] M. Tykarska, K. Skrzypek. The enhancement and induction of antiferroelectric phase. *Ferroelectrics* **2006**, *343*, 193-200.

[72] R. Hołyst, A. Poniewierski, P. Fortmeier, H. Stegemeyer. Coupling of polarization and dislocation in ferroelectric smectic liquid-crystal films. *Phys. Rev. Lett.* **1998**, *81*, 5848-5851.

[73] J.-L. Gallani, S. Mery, Y. Galerne, D. Guillon. Organization of a polar molecule at the air-water interface. *J. Phys. Chem. B* **2004**, *108*, 11627-11632.

[74] E. K. Mann, S. V. Primak. Stability of two-dimensional foams in Langmuir monolayers. *Phys. Rev. Lett*. **1999**, *83*, 5397-5400.

[75] J. B. Rosenholm, P. Ihalainen, J. Peltonen. Thermodynamic characterization of Langmuir monolayers of thiolipids - A conceptual analysis. *Colloids Surf, A* **2003**, *228*, 119-130.

[76] P. Krüger, M. Lösche. Molecular chirality and domain shapes in lipid monolayers on aqueous surfaces. *Phys. Rev. E* **2000**, *62*, 7031-7043.

[77] A. Miller, W. Knoll, H. Möhwald. Fractal growth of crystalline phospholipid domains in monomolecular layers. *Phys. Rev. Lett.* **1986**, *56*, 2633-2636.

[78] A. Miller, H. Möhwald. Diffusion limited growth of crystalline domains in phospholipid monolayers. *J. Chem. Phys*. **1987**, *86*, 4258-4265.

[79] A. Artoti, E. Leontidis, E. Maltseva, G. Bresezinski. Effects of hofmeister anions on DPPC Langmuir monolayers at the air-water interface. *J. Phys. Chem. B* **2004**, *108*, 15238-15245.

[80] P. Dhar, Y. Cao, T.M. Fischer, J.A. Zasadzinski. Active Interfacial Shear Microrheology of Aging Protein Films. *Phys. Rev. Lett.* **2010**, *104*, 016001

[81] P. Oswald, A. Dequidt, A. Żywociński. Sliding planar anchoring and viscous surface torque in a cholesteric liquid crystal. *Phys. Rev. Lett.* **2008**, *77*, 061703

[82] R. Hołyst, M. Litniewski. Evaporation into vacuum: Mass flux from momentum flux and the Hertz–Knudsen relation revisited. *J. Chem. Phys*. **2009**, *130*, 074707.

[83] H. Vogel. Das Temperaturabhangigkeitgesetz der Viskosität von Flüssigkeiten. *Physik Z.*, **1921**, *22*, 645-646

[84] G.S. Fulcher. Analysis of recent measurements of the viscosity of Glasses. *J. Am. Ceram.* Soc., **1925**, *8*, 339–355

[85] G. Tamman, W. Hesse. Abhängigkeit der Viskosität von der Temperatur bie unterkühlten Flüssigkeiten. Z. *Angorg. Chem.*, **1926**, *156*, 245-257

[86] W. Wagner, A. Pruss. International Equations for the Saturation Properties of Ordinary Water Substance. Revised According to the International Temperature Scale of 1990. Addendum to J. Phys. Chem. Ref. Data **16**, 893 (1987). *J. Phys. Chem. Ref. Data*, **1993**, **22**, 783-787.

[87] H. Kneppe, F. Schneider, K. Sharma. Rotational viscosity γ_1 of nematic liquid crystals. *J. Chem. Phys*. **1982**, *77*, 3203-3208.

[88] P. Oswald. About the Leslie explanation of the Lehmann effect In cholesteric liquid crystals. *EPL* **2012**, *97*, 36006.

[89] C. Tschierske. Liquid crystal engineering – new complex mesophase structures and their relations to polymer morphologies, nanoscale patterning and crystal engineering. *Chem. Soc. Rev*. **2007**, *36*, 1930-1970.

[90] G. Ungar, C. Tschierske, V. Abetz, R. Holyst, M.A. Bates, F. Liu, M. Prehm, R. Kieffer, X. Zeng, M. Walker, B. Glettner, A. Zywocinski. Self-Assembly at Different

Length Scales: Polyphilic Star-Branched Liquid Crystals and Miktoarm Star Copolymers. *Adv. Funct. Matter*., **2011**, *21*, 1296-1323.

[91] C. Tschierske, C. Nurnberger, H. Ebert, B. Glettner, M. Prehm, F. Liu, X.-B. Zeng, G. Ungar. Complex tiling patterns in liquid crystals. *IntarfaceFocus*, doi:10.1098/rsfs.2011.0087

[92] R. Kieffer, M. Prehm, B. Glettner, K. Pelz, U. Baumeister, F. Liu, X.-B. Zeng, G. Ungar, C. Tschierske. X-Shaped polyphilics: liquid crystal honeycombs with single-molecule walls. *Chem. Commun*., **2008**, *33*, 3861-3863.

[93] B. Glettner, F. Liu, X.-B. Zeng, M. Prehm, U. Baumeister, G. Ungar, C.Tschierske,. Liquid-Crystal Engineering with Anchor-Shaped Molecules: Honeycombs with Hexagonal and Trigonal Symmetries Formed by Polyphilic Bent-Core Molecules. *Angew. Chem. Int. Ed.*, **2008**, *47*, 6080-6083.

[94] P. Nitoń, A. Żywociński, R. Hołyst, R. Kieffer, C. Tschierske, J .Paczesny, D. Pociecha, E. Górecka. Reversible aggregation of X-Shaped bolaamphiphiles with partially fluorinated lateral chains at the air/water interface. *Chem. Commun*., **2010**, *46*, 1896 – 1898

[95] T. Martyński, J. Miyake. Molecular Organization in Langmuir Films of a Dichroic Azo Dye-Liquid Crystal Mixture. I. Thermodynamic Data and BAM Observations. *Z. Naturforsch*., **2003**, *58a*, 23-32.

[96] T. Martyński, A. Biadasz, D. Bauman. Molecular Organization in Langmuir Films of Dichroic Azo DyeLiquid Crystal Mixtures. II. Surface Potential Measurements. *Z. Naturforsch*., **2003**, *58a*, 97-102.

[97] M. Broniatowski, P. Dynarowicz – Łątka. *Iso*-branched semifluorinated alkanes in Langmuir monolayers. *J. Colloid Interface Sci.* **2006**, *299*, 916-923.

[98] M. N. G. de Mul, J. A. Mann Jr., Multilayer Formation in Thin Films of Thermotropic Liquid Crystals at the Air-Water Interface. *Langmuir* **1994**, *10*, 2311-2316.

[99] M. Ibn-Elhaj, H. Möhwald, M. Z. Cherkaoui, R. Zniber. Effect of Intermolecular and Interfacial Interactions on the Three- and Two-Dimensional Structure and Phase Behavior of Three-Block Liquid-Crystalline Siloxane Derivatives. *Langmuir* **1998**, *14*, 504-516.

[100] M. Ibn-Elhaj, H. Riegler, H. Möhwald, M. Schwendler, C. A. Helm, X-ray reflectivity study of layering transitions and the internal multilayer structure of films of three-block organosiloxane amphiphilic smectic liquid crystals at the air-water interface. Phys. Rev. E **1997**, *56*, 1844-1852.

[101] B. Rapp, H. Gruler, Phase transitions in thin smectic films at the air-water interface. Phys. Rev. A **1990**, *42*, 2215-2218.

[102] M. C. Friedenberg, G. G. Fuller, C. W. Frank, C. R. Robertson. Formation of Bilayer Discs and Two-Dimensional Foams on a Collapsing/Expanding Liquid-Crystal Monolayer. *Langmuir* **1994**, *10*, 1251-1256.

[103] M. Badis, M. H. Guermouche, J.-P. Bayle, M. Rogalski, E. Rogalska, Organization of Four Thermotropic Liquid Crystals of Different Polarities on Model Liquid and Solid Surfaces. *Langmuir* **2004**, *20*, 7991-7997.

[104] J. A. Schröter, R. Plehnert, C. Tschierske, S. Katholy, D. Janietz, F. Penacorada, L. Brehmer. Monolayer Properties of a New Family of Amphiphiles with an Unusual Head-Group Topology. *Langmuir* **1997**, *13*, 796-800.

[105] R. Plehnert, J. A. Schröter, C. Tschierske. Influence of the Position of the Hydrophilic Group on the Monolayer Properties of Rigid Amphiphiles with Laterally Attached Headgroups. *Langmuir* **1999**, *15*, 3773-3781.

[106] C. de Garcia Lux, J.-L. Gallani, G. Waton, M. P. Krafft. Compression of Self-Assembled Nano-Objects: 2D/3D Transitions in Films of (Perfluoroalkyl)Alkanes—Persistence of an Organized Array of Surface Micelles. *Chem. Eur. J.* **2010**, *16*, 7186-7198.

[107] J. J. Haycraft, C. A. DeVries, H. Garcia Flores, A. Lech, J. P. Hagen, C. J. Eckhardt. Experimental investigation of the reversible collapse of a capped amphiphile Langmuir monolayer. *Thin Solid Films* **2007**, *515*, 2990–2997.

[108] M. Perez-Morales, J. M. Pedrosa, M. T. Martın-Romero, D. Möbius, L. Camacho. Reversible Trilayer Formation at the Air-Water Interface from a Mixed Monolayer Containing a Cationic Lipid and an Anionic Porphyrin *J. Phys. Chem. B* **2004**, *108*, 4457-4465.

[109] A. M. Gonzalez-Delgado, M. Perez-Morales, J. J. Giner-Casares, E. Munoz, M. T. Martın-Romero, L. Camacho. Reversible Collapse of Insoluble Monolayers: New Insights on the Influence of the Anisotropic Line Tension of the Domain J. *Phys. Chem. B* **2009**, *113*, 13249–13256.

[110] P. Nitoń, A. Żywociński, J. Paczesny, M. Fiałkowski, R. Hołyst, B. Glettner, R. Kieffer, C. Tschierske, D. Pociecha, E. Górecka, "Aggregation and Layering Transitions in Thin Films of X-, T-, and Anchor-Shaped Bolaamphiphiles at the Air–Water Interface", *Chemistry – A European Journal*, **2011,** *17*, 5861-5873

[111] N. M. Patel, M.R. Dodge, M.H. Zhu, R.G. Petschek, C. Rosenblatt, M. Prehm, C. Tschierske. Twist Elasticity and Anchoring in a Lamellar Nematic Phase. *Phys. Rev. Lett.*, **2004**, *92*, 015501

[112] M. Prehm, X.H. Cheng, S. Diele, M.K. Das, C. Tschierske. New Liquid Crystalline Phases with Layerlike Organization. *J. Am. Chem. Soc*. **2002**, *124*, 12072-12073

[111] N. M. Patel, M.R. Dodge, M.H. Zhu, R.G. Petschek, C. Rosenblatt, M. Prehm, C. Tschierske. Twist Elasticity and Anchoring in a Lamellar Nematic Phase. *Phys. Rev. Lett.*, **2004**, *92*, 015501

[112] M. Prehm, X.H. Cheng, S. Diele, M.K. Das, C. Tschierske. New Liquid Crystalline Phases with Layerlike Organization. *J. Am. Chem. Soc.* **2002**, *124*, 12072-12073

[113] M. Prehm, S. Diele, M.K. Das, C. Tschierske. Correlated Layer Structures: A Novel Type of Liquid Crystalline Phase with 2D-Lattice. *J. Am. Chem. Soc.* **2003**, *125*, 614-615.

[114] J. Paczesny, P. Nitoń, A. Żywociński, K. Sozański, R. Hołyst, M. Fiałkowski, R. Kieffer, B. Glettner, C. Tschierske, D. Pociecha, E. Górecka. Stable, ordered multilayers of partially fluorinated bolaamphiphiles at the air–water interface. *Soft Matter*, **2012**, DOI: 10.1039/C2SM00022A

[115] C. W. Brunn, E. R. Howells. Structures of Molecules and Crystals of Fluoro-Carbons. *Nature* **1954**, *174*, 549-551.